# Age-associated changes in lineage composition of the enteric nervous system regulate gut health and disease

Subhash Kulkarni[1#], Monalee Saha[1], Alpana Singh[1], Jared Slosberg[2], Sushma Nagaraj[1], Laren Becker[3], Chengxiu Zhang[1], Alicia Bukowski[1], Zhuolun Wang[1], Guosheng Liu[1], Jenna Leser[1,] Mithra Kumar[1], Shriya Bakhshi[1], Matthew Anderson[4], Mark Lewandoski[4], Elizabeth Vincent[3], Loyal A. Goff [2, 5, 6], Pankaj Jay Pasricha[1]

[1]Center for Neurogastroenterology, Department of Medicine, Johns Hopkins University – School of Medicine, Baltimore, MD 21205

[2]Department of Genetic Medicine, Johns Hopkins University – School of Medicine, Baltimore, MD 21205

[3]Division of Gastroenterology, Stanford University – School of Medicine, Stanford CA 94301

[4]Center for Cancer Research, National Cancer Institute, Frederick, MD 21702

[5]Department of Neuroscience, Johns Hopkins University – School of Medicine, Baltimore, MD 21205

[6]Kavli Neurodiscovery Institute, Johns Hopkins University – School of Medicine, Baltimore, MD 21205

[#]Address all correspondence to:

Subhash Kulkarni, Ph.D.

Assistant Professor

Department of Medicine

skulkar9@jh.edu

## Abstract

The enteric nervous system (ENS), a collection of neurons contained in the wall of the gut, is of fundamental importance to gastrointestinal and systemic health. According to the prevailing paradigm, the ENS arises from progenitor cells migrating from the neural crest and remains largely unchanged thereafter. Here, we show that the lineage composition of maturing ENS changes with time, with a decline in the canonical lineage of neural-crest derived neurons and their replacement by a newly identified lineage of mesoderm-derived neurons. Single cell transcriptomics and immunochemical approaches establish a distinct expression profile of mesoderm-derived neurons. The dynamic balance between the proportions of neurons from these two different lineages in the post-natal gut is dependent on the availability of their respective trophic signals, GDNF-RET and HGF-MET. With increasing age, the mesoderm-derived neurons become the dominant form of neurons in the ENS, a change associated with significant functional effects on intestinal motility which can be reversed by GDNF supplementation. Transcriptomic analyses of human gut tissues show reduced GDNF-RET signaling in patients with intestinal dysmotility which is associated with reduction in neural crest-derived neuronal markers and concomitant increase in transcriptional patterns specific to mesoderm-derived neurons. Normal intestinal function in the adult gastrointestinal tract therefore appears to require an optimal balance between these two distinct lineages within the ENS.

## Introduction

The enteric nervous system (ENS) is a large collection of neurons, glial, and precursor cells that resides within the gastrointestinal wall and regulates gut motility and secretion along with modulating epithelial and immune cell function[1,2]. During fetal development, the mammalian ENS is populated by neurons and glia derived from neural crest (NC)-derived precursors[3-9]. These precursors follow diverse migratory routes to colonize and innervate various parts of the gut before birth[10-12]. It is not clear, however, that this lineage persists in its entirety in the adult gut, as indicated by the observed lack of expression of fluorescent reporter protein in a subpopulation of adult enteric neurons in NC-lineage-traced mice[13,14]. Alternative sources of enteric neurons that have been proposed in the literature include the ventral neural tube (VENT)[15], or the Pdx1-expressing pancreatic endoderm[14], but the interpretation of these studies has been limited by the lack of robust lineage markers for non-NC derived neurons[16]. In addition, while prior studies have documented cellular changes to the ageing ENS[17], the developmental mechanisms behind these changes are unknown. Thus, confirmation of a second, distinct lineage of enteric neurons in adults is important for our understanding of the healthy post-natal development and aging of the ENS, as well as for the pathogenesis of acquired disorders of the ENS.

In this study, we found that while the early post-natal ENS is derived from the canonical NC-lineage, this pattern changes rapidly as the ENS matures, due to the arrival and continual expansion of a novel population of Mesoderm-derived Enteric Neurons (MENs) which represent an equal proportion of the ENS in young adulthood and with increasing age, eventually outnumber the NC-derived Enteric Neurons (NENs). We also found that, while the NEN population is regulated by glial derived neurotrophic factor (GDNF) signaling through its receptor RET, the MEN population is regulated by hepatocyte growth factor (HGF) signaling. Increasing HGF levels during maturation or by pharmacological dosing increase proportions of MENs. Similarly,

decrease in GDNF with age decrease NENs; and increasing GDNF levels by pharmacological dosing increase NENs proportions in the adult ENS to impact intestinal motility.

These results indicate for the first time that the mesoderm is an important source of neurons in the second largest nervous system of the body. The increasing proportion of neurons of mesodermal lineage is a natural consequence of maturation and aging; further, this lineage can be expected to have vulnerabilities to disease that are distinct from those affecting the NEN population. These findings therefore provide a new paradigm for understanding the structure and function of the adult and aging ENS in health, age-related gut dysfunction and other acquired disorders of gastrointestinal motility.

## Results

**Only half of all mid-age adult enteric neurons are derived from the neural crest.** We analyzed small intestinal longitudinal muscle-myenteric plexus (LM-MP) from adult (post-natal day 60; P60) Wnt1-cre:*Rosa26*-tdTomato mice, in which tdTomato is expressed by all derivatives of Wnt1$^{+}$ NC-cells[18]. In these tissues, while GFAP, a glial marker, was always co-expressed with tdTomato (Fig 1a), tdTomato-expression was absent in many myenteric neurons (Fig 1b, c). By careful enumeration, almost half of all myenteric neurons expressing the pan-neuronal marker HuC/D were found to not express the reporter (Fig 1d, percent tdTomato$^{+}$ neurons: 55.73 ± 2.404 SEM; percent tdTomato$^{-}$ neurons: 44.27 ± 2.404 SEM; enumerated from 2216 neurons from 6 mice). In these lineage-traced mice, myenteric ganglia were found to contain tdTomato$^{high}$ and tdTomato$^{low}$ neurons and due care was taken to image subsets (Suppl. Fig 1a). Both tdTomato$^{high}$ and tdTomato$^{low}$ neurons were classified as tdTomato$^{+}$ and only neurons that did not show any tdTomato-expression were classified as tdTomato$^{-}$ neurons. Immunofluorescence staining of small intestinal LM-MP tissue from adult Wnt1-cre:*Rosa26*-tdTomato mice using antibodies against tdTomato protein showed a consistent lack of reporter expression in a popula-

tion of myenteric neurons (Suppl. Fig 1b). This lack of reporter expression is not a function of tissue peeling or fixation, as the tdTomato$^{-}$ cells within the myenteric ganglia were also observed in freshly harvested unpeeled gut tissue, when imaged using a live tissue fluorescence microscope (Suppl. Fig 1c). In addition, we noticed that myenteric ganglia of the Wnt1-cre:*Rosa26*-tdTomato transgenic mouse show similar tdTomato aggregation in cells of the myenteric plexus from both freshly harvested and immediately fixed tissue (Suppl. Fig 1d, e). Since we previously showed ongoing neuronal loss in healthy ENS[19], we reasoned that cells that show hyper-aggregation of tdTomato are in advanced stages of cell death. Cells with hyper-aggregation of tdTomato showed a lack of staining for the nuclear marker DAPI (Suppl. Fig 1e), suggesting that these are indeed cells in the advanced stages of death, and given that they are not labeled with antibodies against HuC/D, their presence does not alter our estimation of tdTomato-expressing neurons (Suppl. Fig 1f). Thus, the absence of reporter expression in myenteric ganglia of freshly harvested tissue and the presence of tdTomato aggregation in both freshly harvested and fixed tissues shows that our observations are not caused due to any technical issues in tissue isolation and preservation.

Additional confirmation was provided by an analogous Wnt1-cre:*Hprt*-tdTomato lineage-traced mouse line, in which tdTomato was expressed from the *Hprt* locus in a Wnt1-cre-dependent manner (*Hprt* locus is X-inactivated in females, hence only adult male mice were used)[20]; and by the Pax3-cre:*Rosa26*-tdTomato lineage-traced mouse line, where *Rosa26*-tdTomato driven by the Pax3-cre transgene labels the derivatives of the neural tube and pre-migratory NC (Suppl. Fig 1g, h)[21]. Similar lack of reporter expression was previously observed in adult myenteric neurons from Sox10-cre NC-lineage-traced mice, and more recently in significant numbers of myenteric neurons from Wnt1-cre:*Rosa26*-H2B-mCherry mice, which expresses nuclear localized reporter mCherry in NC-lineage cells, further confirming our observations of the presence of non-NC-derived neurons in the adult ENS[13,22].

**Lineage-tracing confirms a mesodermal derivation for half of all adult myenteric neurons.** Alternative sources of enteric neurons proposed previously include the ventral neural tube[15], and the pancreatic endoderm[14], but the interpretation of these studies was limited by the lack of robust lineage markers[16]. Brokhman et al.[14] found evidence of labeled neurons in inducible Pdx1-cre, Foxa2-cre, and Sox17-cre lineage-traced mouse lines and inferred their derivation from pancreatic endoderm. However, in a Pdx1-cre lineage-traced mouse line, many neuroectoderm-derived neurons of the central nervous system have also been previously shown to be derived from Pdx1-expressing cells[23], suggesting that Pdx1 is not an exclusive endodermal marker. Foxa2 is expressed by mesoderm-derived cells in the heart[24] and Sox17 also labels mesoderm-derived cells, especially cells of the intestinal vasculature[25-28]. We therefore hypothesized that the mesoderm may be the true developmental source of the non-NC enteric neurons.

Mesoderm-derived cells during embryogenesis express Tek[24] and analysis of LM-MP tissues from adult male Tek-cre:*Hprt*-tdTomato lineage-traced mice revealed the presence of a population of tdTomato$^{+}$ neurons (Fig 2a). Since Tek is not expressed in the adult ENS (Suppl. Fig 2a), the presence of Tek-derived adult myenteric neurons suggested their mesodermal origin. We then used *mesoderm posterior 1* or Mesp1 as a definitive developmental marker for the mesoderm[29-33] to confirm the mesodermal derivation of the non-NC derived adult enteric neurons. Reporter expression in this mouse line has been previously studied in cardiac development, which we confirmed by observing its expression in the adult heart tissue (Fig 2b). Expression of tdTomato in vascular cells of both Tek-cre and Mesp1-cre mice was more pronounced than in myenteric neurons (Fig 2a, c) and in cardiac myocytes of Mesp1-cre mice (Fig 2b, Suppl. Fig 2b), which reflects the variable expression of the reporter gene in both the neural crest-lineage and mesoderm-lineage specific transgenic mouse lines (Fig 2b, c; Suppl. Figs 1a, 2c). Using an analogous Mesp1-cre:*Rosa26*-EGFP lineage-traced mouse line, in which EGFP was expressed from the *Rosa26* locus in a Mesp1-cre-dependent manner, we next confirmed the derivation of a

139 population of myenteric neurons from Mesp1-expressing mesoderm (Fig 2e, Suppl. Fig 2d, e).
140 Similar to our observations with the tdTomato reporter (Fig 2a-d), we observed lower expression
141 of the reporter EGFP in myenteric neurons as compared to vascular cells (Fig 2e; Suppl. Fig 2d,
142 e). Variable expression of CAG and other pan-cellular promoters in various cell-types and dur-
143 ing processes of maturation have previously been reported[34-37]. In addition, an earlier study by
144 Agah et al showed differing degrees of CAG-driven LacZ reporter activation in a cardiac-specific
145 transgenic cre mouse line, which were unrelated to copy number, suggesting insertional and
146 positional effects or, potentially, differential methylation[38]. These reports are consistent with our
147 observation and could potentially help explain the observed variable expression of CAG and
148 CMV promoter-driven reporter genes in our study.

149 Analysis of small intestinal LM-MP from P60 Mesp1-cre:*Rosa26*-tdTomato lineage-traced mice
150 showed that tdTomato-expression was observed in about half of all myenteric neurons (Fig 2f;
151 percent tdTomato$^+$ neurons: 50.28 ± 2.89 SEM; percent tdTomato$^-$ neurons: 49.72 ± 2.89 SEM;
152 enumerated from 484 neurons from 3 mice). Because of the variable expression of the reporter
153 gene in the transgenic mice described above, we also labeled Mesp1-cre:*Rosa26*-tdTomato$^+$
154 neurons with the S46 antibody, which was raised against the slow tonic myosin heavy chain
155 protein MHCst derived from avian embryonic upper leg muscle, and is expressed exclusively by
156 mesoderm-derived cell populations (Fig 2g)[39-42]. MHCst immunostaining was exclusively ob-
157 served in all Tek-cre:*Rosa26*-tdTomato$^+$ MENs (Suppl. Fig 2f). None of the 107 MHCst$^+$ intra-
158 ganglionic cells observed (35.67 ± 6.17 SEM MHCst$^+$ cells per mouse) across 3 Wnt1-
159 cre:*Rosa26*-tdTomato mice expressed tdTomato, suggesting that MHCst immunostaining was
160 exclusive to non-NC lineage neurons (Fig 2h, Suppl. Fig 3a). Thus, both lineage tracing and
161 protein biomarker expression provides strong support for their mesodermal origin (Fig 2g,
162 Suppl. Fig 3a). Along with our observations on Wnt1-cre:*Rosa26*-tdTomato mice (Fig 1c), our

results indicate that these two distinct lineages together account for all the adult small intestinal myenteric neurons.

In a prior report, Avetisyan et al. showed that the proteins RET, a receptor tyrosine kinase that transduces GDNF signaling in NC-derived enteric neuronal precursors, and MET, a receptor for hepatocyte growth factor (HGF), are expressed by different subsets of adult myenteric neurons[43]. MET is classically expressed by mesoderm-derived cells[44], and by using immunostaining of small intestinal LM-MP tissues from Wnt1-cre:*Rosa26*-tdTomato and Mesp1-cre:*Rosa26*-tdTomato mice, we found that the expression of MET was restricted to a subpopulation of adult MENs (Fig 3a, b). By contrast, RET expression was confined to NENs (Fig 3c).

We then studied whether MENs and NENs differed phenotypically. In the adult murine ENS, inhibitory enteric motor neurons express the nitric oxide-producing enzyme nitric oxide synthase 1 (NOS1); and enteric sensory neurons, called intrinsic primary afferent neurons (IPANs) express the neuropeptide calcitonin gene related peptide (CGRP)[9,43]. Immunostaining using antibodies against NOS1 (expressed by nitrergic neurons) and CGRP (sensory neuronal marker) expression in the LM-MP from P60 Wnt1-cre:*Rosa26*-tdTomato mice showed that both tdTomato$^+$ NENs and tdTomato$^-$ MENs express these two neuronal markers (Fig 3d, e). However, quantification of proportions in these two neuronal lineages shows that while the majority (~73%) of NOS1$^+$ inhibitory neurons are NENs (Fig 3f; of the 616 NOS1$^+$ neurons observed across 3 mice, NOS1$^+$ tdTomato$^+$: 72.94% ± 4.46 SEM; NOS1$^+$ tdTomato$^-$: 27.06% ± 4.46 SEM; $p = 0.0019$; Student"s t-test), the majority (~75%) of CGRP$^+$ neurons are MENs (Fig 3g; of the 146 CGRP$^+$ neurons observed across 3 mice, CGRP$^+$ tdTomato$^-$: 75.76% ± 0.63 SEM; CGRP$^+$ tdTomato$^+$: 24.24% ± 0.63 SEM; $p < 0.0001$; Student"s t-test). These results are in keeping with a previous

report that show low expression of NOS1 and abundant expression of CGRP by MET$^+$ neurons[43], previously not known to be derived from a different lineage. In addition, MENs also express Cadherin-3 (CDH3, Fig 3h, Suppl. Fig 3b), which is known to also mark a sub-population of mechanosensory spinal neurons[45]. Apart from their derivation from a distinct developmental lineage, the mean cell size of MENs was significantly larger than that of NENs (Suppl. Fig 4a; n = 143 neurons/group observed across 3 mice; Feret diameter (µm) MENs: 17.47 ± 0.50 SEM, NENs: 13.03 ± 0.36 SEM, p = 0.002; Student"s t-test).

**An expanded molecular characterization of MENs using unbiased single cell RNA sequencing (scRNAseq)-based analyses.** The distinct nature of the MENs and NENs was further ascertained by scRNAseq-based analyses on all cells isolated from ileal LM-MP. Unlike other studies that analyzed either FACS-sorted Wnt1-cre:*Rosa26*-tdTomato$^+$ ENS-cells or used classical NENs markers such as Snap25 to drive identification and/or enrichment of enteric neurons[46,47], we performed agnostic clustering of the scRNAseq data from tissues of two 6-month-old adult male C57BL/6 wildtype mice (Fig 4a; Suppl. Fig 4b, c). We identified clusters of NC-derived cells by exclusive expression of canonical NC markers Ret and Sox10 (which include the clusters of Ret-expressing NENs and Sox10-expressing Neuroglia); and the MENs cluster by its co-expression of the genes Calcb (CGRP), Met, and Cdh3 (Fig 4a, b). With cells from both samples pooled together, we compared 1,737 NC-derived cells across the NENs (77 cells) and Neuroglia (1660 cells) clusters with 2,223 cells in the MENs cluster. A list of top differentially expressed genes for every cluster are provided in Suppl. Table 2.

The neuronal nature of MENs was first established by testing our scRNAseq dataset for expression of genes known to be expressed by enteric or other neurons. We found detectable expression of genes Elavl2 (HuB), Hand2, Pde10a, Vsnl1, Tubb2b, Stmn2, Stx3, and Gpr88 in the MENs as well as in the NC-derived cell clusters (Fig 4b). While expression of Elavl2, Stmn2 and

Hand2 has been previously observed in enteric neurons[48,49], the expression of neuronal marker genes Pde10a (expressed by medium spiny neurons in the striatum[50]), Vsnl1 (expressed by hippocampal neurons[51]), Gpr88 (expressed by striatal neurons[52]), Stx3 (expressed by hippocampal neurons[53]), and Tubb2b (expressed by adult retinal neurons[54]) has not been studied. Using antibodies against these markers along with co-staining with ANNA1 antisera to mark all HuC/D$^{+}$ neurons, we visualized the expression of these neuronal markers in both tdTomato$^{+}$ NENs and tdTomato$^{-}$ MENs of the small intestinal myenteric plexus tissue from adult Wnt1-cre:*Rosa26*-tdTomato mice (Fig 4c, Suppl. Fig 3l-q). In addition, the MENs cluster was also enriched in previously characterized ENS markers, such as Ntf3 and Il18[2,55] (Fig 4b). We validated the MEN-specificity of these markers using immunochemical analyses (Fig 4c; Suppl. Fig 3b - k).

Examination of the MENs cluster yielded additional MENs-specific marker genes Slpi, Aebp1, Clic3, Fmo2, Smo, Myl7, and Slc17a9, whose expression by adult enteric neurons has not been previously described and which we also validated (Fig 4b, c; Suppl. Fig 3b - k). Next, we found that the mean UMI per cluster in MENs (n = 2223 cells, 4023.91 ± 85.35 SEM) was significantly greater than in Neuroglia (n = 1660 cells, 1137.93 ± 27.93 SEM, $p < 0.0001$) and while it was greater than in NENs (n = 77 cells, 3391.71 ± 386.52 SEM), this difference did not meet statistical threshold ($p = 0.11$, One way ANOVA).

These data help show the neuronal nature of MENs while distinguishing them from NENs at the molecular level. In addition, cells within the Neuroglia cluster showed expression of glial genes such as Sox10 as well as neuronal genes such as Ncam1, Hand2 and Stmn2, suggesting that NC-derived neurons may be present within both the NENs cluster as well as the Neuroglia cluster (Fig 4b).

**Detection of MENs in other murine and human datasets.** Recently, by performing single nuclei RNA sequencing (snRNAseq) on flow sorted Phox2b-expressing nuclei from the adult murine LM-MP tissue, May-Zhang et al[56] detected the presence of a cluster of neurons in the adult murine gut that expressed mesenchymal markers. We tested whether the MENs-expressed genes that we validated earlier (Fig 4c, Suppl. Fig 3) were also expressed by the „mesenchymal" neurons in the May-Zhang et al dataset. We found a high degree of similarity between the top genes expressed by the MENs cluster in our scRNAseq dataset and the „mesenchymal" neurons in the May-Zhang et al dataset (Table 1, Suppl. Fig 4d). Furthermore, examination of the top genes shows that this neuronal sub-population is significantly different from the other Calcb-expressing neuronal populations, which we presume to be the CGRP-expressing NENs (Table 1).

To confirm that the „mesenchymal" neurons identified by May-Zhang et al are MENs, we used an agnostic bioinformatics projection-based approach which we have previously published[57]. This approach allows us to learn latent space representations of gene expression patterns using single cell transcriptomic data, which include patterns that correspond to cell-type-specific gene expression signatures[57]. We can then project other single cell and bulk RNA transcriptomic datasets into these learned patterns to accurately quantify the differential use of these transcriptional signatures in target data across platforms, tissues, and species[57]. In this instance, gene expression patterns were learned on our murine single cell transcriptomic data using non-negative matrix factorization (NMF) dimensionality reduction and the data was decomposed into 50 distinct NMF-patterns[57,58] (Fig 5a). Four NMF patterns were identified that were specific to MENs (Fig 5a, b; Suppl. Fig 4e). We next projected the snRNAseq dataset from May-Zhang et al[56] into the four MEN-specific patterns and found that all these patterns specifically labeled the cluster of „mesenchymal" neurons in the May-Zhang et al dataset of the adult ileal ENS (Fig 5b). Further, upon clustering the projection weights from the four MEN-specific patterns, we identi-

258 fied a cluster of cells that showed higher usage of all four patterns, when compared to all the
259 other cells in the dataset (Suppl. Fig 4f). The genes that define this cluster of cells are similar to
260 the top-expressed genes that define our MENs cluster (Suppl. Fig 4g, Table 1). This approach,
261 together with the high similarities in the top-expressed genes, establishes that cluster of neu-
262 rons annotated as „mesenchymal" neurons by May-Zhang et al are indeed MENs.

263 In addition, our results are supported by a recent report by Elmentaite et al.[59] who performed
264 scRNAseq on dissociated single cells from the human gut at fetal, juvenile, and adult ages and
265 catalogued multiple intestinal cell-types to generate a comprehensive gut cell atlas. Canonical
266 enteric neurons, while adequately represented in the fetal ages, were not found in the juvenile
267 and adult ages which were dominated by mesenchymal and other cell types[59]. Given that our
268 scRNAseq approach of sequencing diverse cell types from the murine gut wall without any
269 marker-based pre-selection was similar to this approach in human tissue, we reasoned that
270 MENs would also be represented in Elmentaite et al"s description of mesenchymal cell clusters,
271 especially in the juvenile and adult ages. To detect putative MENs in this human gut cell atlas
272 data, we projected the entire human mesenchymal cell scRNAseq dataset into the four murine
273 MEN-specific NMF patterns and detected putative human MENs clusters (Suppl. Fig 4h). Since
274 our identification of MENs and the generation of MEN-specific NMF patterns was based on
275 post-natal healthy murine tissue, we next projected data from only post-natal healthy mesen-
276 chymal clusters into the four MEN-specific NMF patterns (Fig 5b). The four patterns identified a
277 population of cells within the post-natal intestinal mesenchymal cell clusters suggesting that
278 these cells are putative MENs in the human gut (Fig 5b). These putative MENs, which map to
279 Cluster 1 in our representation of the intestinal mesenchymal cells from the post-natal gut cell
280 atlas data (Fig 6a) were annotated previously by Elmentaite et al. as transitional stromal cells
281 (Fig 6b). We next tested whether these clusters expressed neuronal markers expressed by en-
282 teric neurons and found that the pan-neuronal marker Uchl1 as well as neuronal markers

283 Hand2, Stx3, Slc17a9, Pde10a and Tubb2b that we earlier showed to be expressed by MENs
284 (Fig 6c) were expressed by the putative MENs in the adult human gut.

285 We next hypothesized that the reason these cells were not annotated as enteric neurons was
286 due to the use of a NENs-restricted gene list. Apart from the NENs marker Ret, such gene lists
287 often contain the pre-synaptic gene Snap25, a component of the SNARE complex, which is
288 widely assumed to be a pan-neuronal marker in the adult ENS[46,47,60,61]. While we have previous-
289 ly observed the NENs-specific nature of RET, transcriptomic data suggests that MENs either do
290 not express Snap25 or do so in very small amounts (Suppl. Fig 4d). We tested the expression of
291 SNAP-25 by NENs and MENs in the myenteric ganglia of an adult Wnt1-cre:*Rosa26*-tdTomato
292 mouse and found that SNAP-25 expressing neurons expressed tdTomato, but not the MENs-
293 marker MHCst, suggesting the NEN-specific expression of this canonical marker for synaptic
294 neurons (Fig 7a). The low or lack of expression of Ret, Snap-25, Elavl3 and Elavl4 in MENs as
295 observed both by us and May-Zhang et al[56] (Suppl. Fig 4d) may help explain why these canoni-
296 cal gene lists missed the correct identification and annotation of MENs" neuronal nature in hu-
297 man datasets[47,59]. Next, we examined the expression of MENs markers MHCst, MET, and
298 SLC17A9 in LM-MP tissues from adult humans with no known gut motility disorder and found
299 them to be expressed by a population of myenteric neurons in normal adult human ENS (Fig 7b,
300 c; Suppl. Fig 5a, b). Thus, our bioinformatic approaches and immunofluorescence analyses of
301 MEN-specific markers in adult human gut together shows that the human gut similarly contains
302 a population of MENs.

303 We next tried sub-clustering the MENs cell cluster in our scRNAseq data to study whether indi-
304 vidual subclusters could be discriminated on the basis of MENs markers or other genes. How-
305 ever, these clusters did not yield meaningful information on specific marker genes that could be
306 used to define them (Suppl. Fig 6a, b).

**The proportion of mesoderm-derived neurons expands with age to become the dominant population in the aging ENS**. Since the ENS at birth consists solely of NENs[13], we next studied the birth-date and eventual expansion of the MEN lineage in the post-natal gut. Using Wnt1-cre:*Rosa26*-tdTomato mouse line, we enumerated the tdTomato$^-$ MENs in LM-MP at different ages and found a significant age-associated increase in MENs proportions (Fig 8a, b, c; One-way ANOVA, F = 117.6, DFn, DFd = 5, 12; $p < 0.0001$). At P11, MENs were found only in few isolated myenteric ganglia (Fig 8a) and together represented only ~5% of all myenteric neurons (tdTomato$^-$ neurons: 4.12% ± 2.98 SEM; n = 1327 HuC/D$^+$ neurons counted from 3 mice), suggesting that they originate shortly before this age. The proportion of MENs in myenteric ganglia rises sharply thereafter: by P22, they account for ~30% of all neurons (tdTomato$^-$ neurons: 29.63% ± 1.229 SEM; n = 742 neurons counted from 3 mice); and at P60 they represent ~45% of all neurons (tdTomato$^-$ neurons: 46.38% ± 4.62 SEM; n = 700 neurons counted from 3 mice). During the adult ages, the proportions of MENs in the adult ENS remains relatively stable as at P180, MENs continue to represent roughly half of all myenteric neurons (tdTomato$^-$ neurons: 57.29% ± 3.62 SEM; n = 586 neurons counted from 3 mice). However, MENs dominate the proportions of the aging ENS as at the very old age of 17 months (P510), the ENS is populated almost exclusively by MENs (Fig 8b; tdTomato$^-$ neurons: 95.99% ± 1.62 SEM; n = 996 neurons counted from 3 mice). Thus, the proportions of NENs and MENs in the myenteric ganglia can be used as a biomarker for deducing ENS age, as a healthy ENS dominant in NENs would be juvenile, one with roughly equal proportions would be adult, and an aging ENS is dominated by MENs.

We next tested whether the representation of MEN-specific transcriptomic signatures show a similar increase during the maturation and aging of the human gut. We tested whether the representation of the four MEN-specific NMF patterns (Fig 5a) increased with age in the human

transcriptomic data from Elmentaite et al[59]. We grouped the transcriptomic data from the wide-range of healthy post-natal specimens of the gut cell atlas into three groups: Juvenile (containing data on 2910 cells represented by 10 samples within the age range of 4 – 12 years), Adult (containing data on 3696 cells represented by 36 samples within the age range of 20 – 50 years), and Aging (containing data on 2848 cells represented by 37 samples within age range of 60 – 75 years) and tested whether the representation of the four MEN-specific patterns changed significantly between these age groups. Barring pattern 16 which showed a non-significant increase in projection weights between the Juvenile and Aging samples (One-way ANOVA, $F = 2.10$, DFn, DFd = 2, 8, $p = 0.18$), projection weights of MEN-specific pattern 27 (One-way ANOVA, $F = 16.08$, DFn, DFd = 2, 8, $p = 0.0016$), pattern 32 (One-way ANOVA, $F = 8.13$, DFn, DFd = 2, 8, $p = 0.01$) and pattern 41 (One-way ANOVA, $F = 9.818$, DFn, DFd = 2, 8, $p = 0.007$) all show significant age-associated increase in the human gut tissue (Fig 8d, every datapoint refers to mean projected pattern weight for cells within a defined age or age range). This suggests that analogous to the age-associated increase in MENs we observed in murine gut (Fig 8b), the proportions of MENs in the human gut also might increase with age. We also found that the representation of MENs cluster (Cluster 1) in the post-natal human gut cell atlas data expanded with maturation and age (Suppl. Fig 5c)

**GDNF and HGF levels regulate the populations of the neural crest-derived and the mesoderm-derived neurons, respectively, in the maturing ENS.** GDNF-RET signaling is responsible for proliferation and neurogenesis from NC-derived ENS precursor cells during development as well as for the survival of Ret-expressing enteric neurons[62-65]. Similarly, HGF signaling has been shown to be essential for the proliferation of mesoderm-derived cells[66]. Since the expression of the HGF receptor MET and the GDNF receptor RET is exclusive to MENs and NENs respectively, we studied the correlation between age and levels of HGF and GDNF in LM-MP (Fig 8e, f). Given that both GDNF, as well as HGF expression is found in the LM-MP

356 layer[43,67,68], we used LM-MP tissue to study how the levels of these two trophic factors change
357 in and around the ENS tissue during maturation. We found that in agreement with a previous
358 report[66], GDNF protein levels are markedly reduced between the P10 and the P30 ages and
359 remains reduced thereafter up to the P90 age (Fig 8g; n = 3 mice/age-group, F = 6.821, DFn,
360 DFd = 1, 7, p = 0.0348, One way ANOVA). In addition, expression of Gdnf transcripts show sig-
361 nificant reduction between the ages of P30 and P90 (Fig 8h; n = 6 mice/age-group, P30: 1.070
362 ± 0.179 SEM, P90: 0.539 ± 0.129 SEM, p = 0.037, Student"s t-test). On the other hand, HGF
363 expression increases progressively between P10 and P90 ages (Fig 8i, j: n = 3 mice/age-group,
364 Protein levels: F = 8.820, DFn, DFd = 1, 7, p = 0.02; mRNA levels: F = 36.98, DFn, DFd = 1, 16,
365 p < 0.0001, One way ANOVA). The ratio of HGF to GDNF expression in ileal LM-MP tissue
366 shows significant increase from the age of P10 to P90 in our data (Suppl. Fig 7a, F = 48.60,
367 DFn, DFd = 1, 7, p = 0.0002, One way ANOVA), and HGF expression is consistently more than
368 GDNF expression in the full thickness small intestinal tissue from adult and aging mice in the
369 Tabula muris data[69] (Suppl. Fig 7b). We then queried the plasma proteome levels from the
370 LonGenity cohort of 1,025 aging individuals and found that HGF levels correlated positively,
371 while GDNF and RET levels correlated negatively with age (Suppl. Fig 7c)[70], suggesting paral-
372 lels between our data from murine intestine and human plasma proteome data.

373 Since GDNF tissue levels are correlated with NENs proportions, we hypothesized that GDNF
374 signaling regulates NENs proportions in maturing and adult ENS. On administration of GDNF or
375 saline to cohorts of P10 Wnt1-cre:*Rosa26*-tdTomato mice over 10 days[62,71], we found that
376 GDNF treatment promoted the juvenile phenotype by enhancing the proportions of tdTomato$^{+}$
377 NENs (Fig 8k). GDNF supplementation reduced the proportion of tdTomato$^{-}$ MENs in P20 mice
378 to a level similar to that seen at the P10 age, while the MENs proportions in saline-treated con-
379 trol mice remained at a level expected of its age (Fig 8k; Controls: %MENs: 25.87 ± 4.37 SEM
380 of 1350 neurons from 3 mice; GDNF: %MENs: 3.86 ± 0.07 SEM of 1301 neurons from 3 mice; p

= 0.0072; Student"s t-test). Consistent with a previous report[62], the GDNF-driven expansion of NENs and associated contraction of MENs conserved the total neuronal numbers (Fig 8k; Controls: neurons/ganglia = 20.60 ± 4.00 SEM; GDNF: neurons/ganglia = 24.39 ± 6.96 SEM; p = 0.52; Student"s t-test).

Since HGF tissue levels increase with age, we hypothesized that increasing HGF signaling drives the expansion of MENs in the maturing gut. HGF administration to cohorts of P10 Wnt1-cre:*Rosa26*-tdTomato mice over 10 days promoted an increase in the tdTomato$^{-}$ MENs population in P20 mice to levels previously observed in P60 mice, while tissues from saline-treated control mice exhibited a MENs:NENs ratio that is expected at P20 (Fig 8l; Controls: %MENs: 27.40 ± 5.49 SEM of 1970 neurons from 5 mice; HGF: %MENs: 49.37 ± 5.52 SEM of 1704 neurons from 5 mice; p = 0.02, Student"s t-test). Similar to GDNF treatment, HGF treatment also did not cause any significant change in total neuronal numbers (Fig 8l; Controls: neurons/ganglia = 20.35 ± 2.22 SEM; HGF: neurons/ganglia = 18.21 ± 0.69 SEM; p = 0.38, Student"s t-test).

**Reduced GDNF-RET signaling accelerates ENS aging to cause intestinal dysfunction.** Since reduced GDNF or RET levels are associated with intestinal dysfunction in patients[61,72,73], we hypothesized that alterations in GDNF-RET signaling unrelated to those seen with normal aging, would cause dysfunction. To test this hypothesis, we studied lineage proportions and intestinal function in a mouse model of reduced RET signaling. Ret-null heterozygous mice, which have been previously used to study the effect of reduced RET signaling in the adult ENS, have normal ENS structure but altered gut physiology[62]. A similar mouse model with a Ret$^{CFP}$ allele has a CFP reporter inserted at its *Ret* locus rendering it null[74]. Ret$^{+/CFP}$ (or Ret$^{+/-}$) mice carrying a single copy of the Ret gene showed significant reduction in Ret transcript and RET protein expression in the murine gut[74]. In these mice, using antibodies against CFP/GFP, HuC/D, and

405 MHCst, we confirmed that the NENs marker Ret-CFP, and the MENs marker MHCst were ex-
406 pressed by different neuronal subpopulations (Fig 9a). Using the adult $Ret^{+/-}$ mice, we tested
407 the effect of partial Ret loss on ENS lineages at two adult ages: 9 weeks (~P60) and 16 weeks
408 (~P110). Using antibody against CFP/GFP to detect $CFP^{+}$ RET-expressing neurons, we found
409 that $Ret^{+/-}$ mice show a significant reduction in the proportions of Ret-$CFP^{+}$ NENs (Fig 9b; at 9
410 weeks: %$CFP^{+}$ neurons: 24.91 ± 5.42 SEM of 837 neurons from 3 mice; at 16 weeks: %$CFP^{+}$
411 neurons: 13.13 ± 0.98 SEM of 1227 neurons from 5 mice; p = 0.03, Student"s t-test). We ob-
412 served a corresponding significant increase in the proportions of $MHCst^{+}$ MENs with age in
413 $Ret^{+/-}$ mice (Fig 9c; at 9 weeks: %MENs: 58.74 ± 7.33 SEM of 644 neurons from 3 mice; at 16
414 weeks: %MENs: 82.84 ± 3.58 SEM of 935 neurons from 5 mice, One-way ANOVA, p = 0.014),
415 while control $Ret^{+/+}$ mice showed no significant age-associated change in the proportions of
416 MENs (Fig 9c; 9 weeks: %MENs: 43.27 ± 3.24 SEM of 780 neurons from 3 mice; 16 weeks:
417 %MENs: 54.48 ± 4.07 SEM of 1276 neurons from 5 mice, One-way ANOVA, p = 0.36), which is
418 consistent with our previous results that MENs proportions in wildtype animals are relatively
419 stable in this time window (Fig 8c). The expedited loss of NENs in $Ret^{+/-}$ mice confirms that de-
420 pletion of endogenous RET signaling in the adult ENS accelerates the aging-associated loss of
421 NENs.

422 Having previously shown that aging mice have intestinal dysmotility[75], we tested whether the
423 increased loss of NENs in the $Ret^{+/-}$ ENS, concomitant with the expansion of MENs accelerated
424 ENS aging, causes an early onset of aging-associated intestinal dysmotility. We studied whole
425 gut transit time (WGTT) in a cohort (n = 10) of adult $Ret^{+/-}$ mice and their littermate control (n =
426 8) $Ret^{+/+}$ mice over 7 weeks, between 9 and 16 weeks of age. While 9-week adult $Ret^{+/-}$ mice
427 were similar to control $Ret^{+/+}$ mice, WGTT between the two genotypes diverged with age. Con-

sistent with a prior report[62], 16-week old $Ret^{+/-}$ mice displayed significantly delayed intestinal transit compared to age-matched control $Ret^{+/+}$ mice (Fig 9d; WGTT (in min) $Ret^{+/+}$: 121.4 ± 4.01 SEM; $Ret^{+/-}$: 157.3 ± 14.62 SEM, p = 0.048; One way ANOVA).

**GDNF reverts aging in the ENS to normalize intestinal motility.** Along with others, we have previously shown that aging is associated with slowing of intestinal motility[76,77]. We hypothesized that this may be a consequence of the replacement of the juvenile NENs population by MENs and therefore GDNF supplementation, by restoring a more balanced MENs:NENs ratio, may prevent age related changes in motility. We studied 17-month-old male mice (at an age where NENs constitute only ~5% of all myenteric neurons; Fig 8c) before and after they received 10 days of intraperitoneal injection of GDNF or saline (n=5 for each cohort). While the two cohorts showed no significant difference in their intestinal transit times at baseline (WGTT (in min) Control: 192.8 ± 11.55 SEM; GDNF: 202.4 ± 7.60 SEM, p = 0.50, Student"s t-test), GDNF treatment caused significant improvement in intestinal transit (Fig 10a, WGTT (in min) Control: 175.0 ± 8.89 SEM; GDNF: 101.0 ± 8.91 SEM, p = 0.0004, Student"s t-test), reaching levels previously observed in healthy mice (Fig 9d).

GDNF treatment significantly reduced the proportions of $MHCst^{+}$ MENs (Fig 10b; Suppl. Fig 8a, b; Control: %MENs: 88.76 ± 1.48 SEM of 909 neurons from 5 mice; GDNF: %MENs: 74.12 ± 5.98 SEM of 799 neurons from 5 mice; p = 0.045; Student"s t-test) while increasing the numbers of $RET^{+}$ NENs (Fig 10c; Suppl. Fig 8c, d; Control: $RET^{+}$ neurons: 1.35 ± 0.05 SEM in forty-two 40X fields from 4 mice; GDNF: $RET^{+}$ neurons: 3.19 ± 0.56 SEM in forty-one 40X fields from 4 mice, p = 0.017; Student"s t-test). Consistent with our earlier observation, GDNF treatment did not change the average neuronal numbers in the ileal myenteric ganglia (Control: 17.56 ± 1.82 SEM neurons per ganglia, GDNF: 16.01 ± 1.22 SEM neurons per ganglia, p = 0.49, Student"s t-test).

**The two neuronal lineages in human disease.** In addition to the detection of MENs in the adult healthy gut by bioinformatic and immunofluorescence means (Fig 5, 6, 7), we next examined the relevance of the two neuronal lineages NENs and MENs in human disease. For this, we tested whether gut dysfunction associated with pathological reductions in NENs-signaling mechanisms are also associated with increased abundance of MENs. We mined previously generated and publicly available transcriptomic data from intestinal tissues of humans with normal gut motility (controls) and of patients with obstructed defecation (OD) associated with enteric neuropathy.[75]. In this dataset, Kim et al have previously shown that OD patients have significantly reduced intestinal expression of Gdnf and Ret[75]. Again, using our transfer learning tool *ProjectR*[57,78], which allowed us to query bulk-RNAseq data across species to estimate relative use of MENs-specific NMF-patterns generated earlier, we tested whether the usage of MENs-specific NMF-patterns was significantly altered between transcriptomes of OD patients and healthy humans (n = 3/group)[75]. This projection analysis indicated that 2 of the 4 MENs-specific NMF-patterns showed significantly higher usage in OD samples compared to controls (Fig 11a, Suppl. Fig 9; Student"s t-test, $p < 0.05$), providing evidence that the enteric neuropathy in these patients is associated with a relative increase in MENs-specific transcriptional signatures. We further queried the differential gene expression analysis performed by Kim et al and found that in addition to Gdnf and Ret (as reported by them) other important NEN genes (Snap25 and Nos1) were also significantly downregulated while the MEN marker genes identified in this study (Clic3, Cdh3, Slc17a9) (Fig 11b) were significantly upregulated.

## Discussion

Current dogma states that the adult ENS is exclusively derived from neural crest precursors that populate the gut during fetal development[79]. The results of this study indicate a much more complex system, one in which the fetal and early life “juvenile” ENS consisting of neural crest-derived enteric neurons (NENs) is incrementally replaced during maturation by mesoderm-

477 derived enteric neurons (MENs). Eventually, the aging ENS consists almost exclusively of the
478 neurons of the MEN lineage. Using a combination of floxed transgenic reporters bred into multi-
479 ple lineage fate mapping transgenic mice, this study also provides the first definitive evidence of
480 a significant mesodermal contribution to any neural tissue. Previously, the mesoderm and espe-
481 cially the Lateral Plate Mesoderm (LPM) was known to give rise to diverse cell-types within the
482 viscera, including several in the gut[80], and our study shows that cells of this embryonic deriva-
483 tion also give rise to ENS neurons. A previous report on a dual origin of the ENS described adult
484 enteric neurons from Foxa2$^{+}$ or Sox17$^{+}$ precursors[14] and inferred that these were endodermal in
485 origin. However, Foxa2 and Sox17 are also expressed by mesoderm-derived cells[24-27]. By con-
486 trast, using two NC-lineage-traced mouse lines (Wnt1-cre and Pax3-cre), two lineage-traced
487 mouse lines marking mesodermal derivatives (Tek-cre, and Mesp1-cre), and robust adult mes-
488 oderm markers, we identify a population of Mesp1-derived MHCst- and MET-expressing adult
489 enteric neurons, which makes up the entire non-NC-derived population of myenteric neurons.
490 These results provide robust evidence that the second source of adult enteric neurons is the
491 mesoderm, and not the endoderm.

492 In our single cell transcriptomic analysis, we used the markers Calcb, Met, and Cdh3 that we
493 had validated to identify and annotate the MEN cell cluster. When compared with the Ret and
494 Sox10-expressing cells within the various clusters of NC-derived cell populations, an additional
495 set of marker genes were found to be expressed widely or selectively within MENs. These
496 markers, which include both novel as well as established enteric neuronal markers[2,55,81], help
497 establish the neuronal nature of MENs and at the same time help differentiate them from NENs.
498 Further, our bioinformatic analyses and immunofluorescence analyses of select MENs markers
499 helped identify MENs in publicly available murine dataset generated by May-Zhang et al[56], and
500 in transcriptomic data from the human gut cell atlas[59], thus extending the validity of our observa-
501 tions to other published data. While May-Zhang-et al. did not further interrogate the develop-

502 mental origins of the „mesenchymal" enteric neurons to establish the etiology of their distinct
503 transcriptomic signature, identification and correct annotation of a population of cells as MENs
504 in other murine and human datasets would not have been possible since these were performed
505 either exclusively on neural crest-derived ENS cells[46], or when done in a more agnostic manner,
506 only applied known canonical neural markers (such as Ret and Snap25, now known to be spe-
507 cific to NENs) to identify the ENS population[47,59,82]. Along with our data, the lack of SNAP-25
508 expression in a large population of hippocampal neurons[83] shows the limitations of using it as a
509 pan-neuronal marker. Importantly, we were also able to confirm the presence of cells express-
510 ing MENs and neuronal markers in human scRNAseq data, and the expression of MENs mark-
511 ers MHCst, MET and SLC17A9 in many enteric neurons in adult humans, suggesting that the
512 mesoderm-derived ENS may be a feature common to mice and humans alike. MENs in both
513 species can readily be identified by their expression of MENs-specific markers, thus providing a
514 convenient tool to further discriminate and study these neurons.

515 While the co-expression of pan-neuronal markers such as Elavl2, Pde10a, Tubb2b, Stmn2,
516 Vsnl1, and Stx3 establishes the neuronal nature of MENs, the differential expression of set of
517 key genes between the two neuronal populations (MENs versus NENs) suggests putative spe-
518 cialized functional roles of these subpopulations when they co-exist in adults. These include the
519 expression of genes associated with sensory (Calcb)[84], neuromodulatory (Ntf3)[85], secretory
520 (Cftr)[86], immunomodulatory (Il18)[2], and motility-regulating roles (Slc17a9 or VNUT)[87]. These
521 MEN-enriched or MEN-specific expression profiles suggest that MENs perform various roles in
522 the regulation of diverse gastrointestinal functions. While the current scRNAseq data is restrict-
523 ed in providing meaningful cell clusters that can inform the true functional diversity of MENs, fu-
524 ture work will provide detailed analyses and functional characterization of MENs.

525 The presence of small population of MENs in the gut at the post-natal age day 10 and their ex-
526 pansion during maturation suggests that key timepoints in their development correspond with

527 the post-natal development of the ENS. A recent study by Parathan et al.[88] highlighted important
528 neuronal and neurochemical changes during this time. Further studies on ENS maturation thus
529 need to be performed in the context of the two neuronal lineages to truly understand the nature
530 of the adult ENS. A crucial aspect of this work will require identifying the cellular population that
531 serves as the progenitor for MENs. Our earlier work showed that Nestin-expressing neural pro-
532 genitor cells are neural crest-derived cells that contribute to steady state neurogenesis in the
533 adult ENS[19], thus suggesting that MENs are derived from non-Nestin$^{+}$ precursor cells.

534 Since our scRNAseq data highlighted the lineage-specific nature of the expression of Ret and
535 Met, we studied whether these genes regulated the origin, expansion, and maintenance of the
536 neuronal populations that express them. While it is known that Gdnf expression in the mature
537 gut is significantly downregulated[43,62,71,89], the functional consequences of this loss have been
538 unclear[62]. We found that reduced GDNF-RET signaling drives the age-dependent loss of NENs
539 as this loss can be slowed or reversed by GDNF supplementation or accelerated by further re-
540 duction of Ret expression. In aging animals, GDNF-driven resuscitation of NENs was associat-
541 ed with a functional normalization of age-associated delay in intestinal transit. Our results identi-
542 fy a novel role for GDNF in maintaining or resuscitating the canonical NEN population, while
543 preserving overall enteric neuronal numbers. In the last few years, studies have focused on
544 identifying juvenile protective factors (JPFs), the loss of which correlates with or drives matura-
545 tion- and aging-associated phenotypes[90]. In this context, GDNF may therefore qualify as a JPF
546 or a *senolytic* as its presence maintains the dominance of NENs in maturing ENS, correspond-
547 ing to a juvenile phenotype; and its re-introduction promotes and resuscitates the genesis of
548 NENs in adult and aging gut to restore healthy gut function. The exact nature of the cells that
549 respond to GDNF re-introduction and generate NENs is yet unknown, but it can be hypothe-
550 sized that these may include Nestin$^{+}$ enteric neural stem cells and/or GDNF-responsive
551 Schwann cells[19,91]. In addition to its effect on resuscitating NENs, acute administration of GDNF

552 also augments peristaltic motility by increasing neuronal activity[22,92]. Since the aging gut has a
553 very small number of RET-expressing GDNF-responsive NENs, we assume that GDNF-driven
554 normalization of intestinal motility would first increase the proportions of RET-expressing NENs
555 and then augment their activation. This further emphasizes the importance of using GDNF or
556 similar RET agonists in the treatment of age-associated intestinal dysmotility.

557 The observed mutually exclusive expression of RET and MET by the two lineages of enteric
558 neurons in the mature adult ENS is consistent with an earlier study that reported that a deletion
559 of Met in the Wnt1-cre expressing NC-lineage did not alter the abundance of $MET^+$ neurons in
560 the adult ENS[43]. The immunofluorescence analyses on the basis of protein expression on the
561 mutually exclusive nature of RET and MET provided by us and by Avetisyan et al.[43] contrasts
562 with the co-expression of Ret and Met transcripts observed in the scRNAseq data on neural
563 crest-derived enteric neurons from Zeisel et al.[46], which we believe highlights the well-known
564 discrepancy between single cell/nuclear transcriptomic approaches and actual protein expres-
565 sion[93]. In this study, we also show that MENs are dependent on HGF-MET signaling in a man-
566 ner analogous to the requirement of GDNF-RET signaling by NENs. Further, Ret haploinsuffi-
567 ciency-mediated loss of the NEN lineage causes a proportional increase in the MEN lineage.
568 This suggests the presence of yet unknown quorum sensing signaling mechanisms between the
569 two lineages that reciprocally regulate their populations to maintain the structure of the post-
570 natal ENS. This again implies the existence of a yet undefined precursor cell responsible for the
571 expansion of the MEN population in a manner analogous to what we have previously described
572 for NENs[19].

573 While Avetisyan et al. showed that MET expression highly correlated with CGRP-expression in
574 the adult murine myenteric plexus[43], MET co-expression by all $MHCst^+$ human enteric neurons
575 in our data and by all $PGP9.5^+$ neurons in human enteric neurons in the earlier report by Avetis-
576 yan et al.[43] suggests that MET-expression in the human ENS may not be restricted to CGRP-

577 expressing IPANs. In addition, recent data shows that our understanding of the nature of mark-
578 ers that can correctly identify IPANs in the murine and human ENS is still evolving[56,94], suggest-
579 ing that ascribing function to neurons using a single marker may be incorrect.

580 The detection of MENs cluster in the post-natal and adult scRNAseq data in the gut cell atlas
581 generated by Elmentaite et al.[59], their increasing representation with age, and the subsequent
582 validation of the MEN-specific markers MHCst, MET and SLC17A9 in a subset of adult human
583 ENS neurons shows that our findings extend to human ENS and may be of clinical importance.
584 Many gastrointestinal motility functions are compromised with advancing age, resulting in clini-
585 cally significant disorders[95]. Although the exact mechanisms will need to be worked out, our re-
586 sults indicate that a MENs-predominant ENS is associated with significant differences in gut mo-
587 tility. The progressive nature of the change in enteric neuronal lineages with age may have
588 pathological implications for the elderly gut when the balance is overwhelmingly in favor of
589 MENs. Understanding the forces that regulate parity between these two different sources of
590 neurons and the associated processes of genesis of these neurons therefore holds the promise
591 of arresting or reverting progressive loss of gut motility with increasing age. Our results may al-
592 so have implications for the pathogenesis of disordered motility unrelated to aging, as downreg-
593 ulation of Gdnf and Ret expression has been associated with diverticular disease and obstruct-
594 ed defecation in adult patients[72,75,96]. GWAS analyses further showed that Gdnf gene was in the
595 eQTL associated with increased incidence of diverticular disease[97]. It is in this context that the
596 identification of SNAP-25 as a NENs marker gene and the transcriptomic pattern analyses of
597 patients with chronic obstructed defecation are significant. Expression of Snap25 is upregulated
598 by GDNF and is significantly downregulated in gut tissues of patients with diseases associated
599 with significant reduction in GDNF-RET signaling (diverticular disease and obstructed defeca-
600 tion)[61,72,75]. Thus, while earlier thought to be a pan-neuronal marker[47,98], establishing the identity
601 of SNAP-25 as a NEN lineage-restricted marker provides us not only with an important tool to

602 query proportions of NENs in murine and human tissue but also suggests the NENs-limited na-
603 ture of prior observations based on Snap25 transgenic animals[60,98]. Gut dysmotility disorders
604 that present with conserved ENS neuronal numbers[72] have puzzled investigators on the etiology
605 of the disease. Our results suggest an explanation based on NENs-to-MENs lineage shifts that
606 conserve overall enteric neuronal numbers with variable effects on function.

607 In conclusion, using multiple lines of evidence, we show that the ENS of the juvenile and the
608 aging mammalian gut is dominated by two different classes of neurons that have distinct on-
609 togenies and trophic factors, associated with functional differences. The shift in neuronal lineage
610 may represent a functional adaptation to changes in nutrient handling, microbiota or other phys-
611 iological factors associated with different ages. Further research in the functional differences
612 between the neuronal lineages and factors that regulate the parity between these two nervous
613 systems in humans during the lifetime will be important to advance our understanding of the
614 adult ENS and the treatment of age-related and other pathological disorders of gut motility.

## Acknowledgements

We would like to thank Dr. Chulan Kwon (JHU) for his kind gift of the Mesp1-cre mice, Dr. Jeremy Nathans (JHU) for his kind gift of the Tek-EGFP, Tek-cre and *Hprt*-tdTomato lineage-traced mice and his support, and Dr. Vanda Lennon (Mayo Clinic) for her kind gift of the ANNA1 anti-Hu antisera. We thank Dr. Akira Sawa (JHU) for his help with the *Rosa26*-EGFP mouse line. We thank Dr. Xinzhong Dong (JHU) and Dr. Mark Donowitz (JHU) for their support. Microscopy was performed on the Ross Imaging Core at the Hopkins Conte Digestive Disease Center at the Johns Hopkins University (P30DK089502) using the Olympus FV 3000rs (procured with the NIH-NIDDK S10 OD025244 grant) and we thank Dr. George McNamara for his help with confocal training and imaging. The 10X Genomics Chromium processing for scRNAseq was performed at the GRCF Core and the sequencing was performed at the CIDR core at the Johns Hopkins University. S.K. was funded through a grant from the Ludwig Foundation, a grant from the NIA (R01AG066768), a pilot award from the Hopkins Digestive Diseases Basic & Translational Research Core Center grant (P30DK089502). L.A.G was funded in part by a Johns Hopkins Catalyst Award and a grant from the NIA (R01AG066768). J.S. was funded through the Maryland Genetics, Epidemiology, and Medicine training program sponsored by the Burroughs Welcome Fund. P.J.P. was funded through the Hopkins Conte Digestive Disease Center at the Johns Hopkins University (P30DK089502), NIDDK (R01DK080920), the Maryland Stem Cell Research Foundation (MSCRF130005), and a grant from the AMOS family.

## Author contributions

S.K., and P.J.P. conceived the study; S.K., M.A., M.L, L.A.G. and P.J.P. designed the research studies; S.K. L.B, C.Z, A.S., A.B., and M.S. conducted the experiments; S.K., Z.H., M.K., J.L., L.B., S.B., E.V., J.S., S.N., M.S., G.L., and L.A.G. acquired and analyzed the data; S.K., and P.J.P drafted the manuscript.

## Methods

*Animals*:

Experimental protocols were approved by The Johns Hopkins University"s Animal Care and Use Committee in accordance with the guidelines provided by the National Institutes of Health. Presence of vaginal plug was ascertained as 0.5 days post-fertilization and this metric was used to calculate age of mice. Only male mice were used for the studies detailed in this report. The Wnt1-cre:*Rosa26*-tdTomato lineage-traced line was generated as detailed before by breeding the B6.Cg-Tg(*Wnt1-cre*) with the Ai14 transgenic mouse line (Jax #: 007914) containing the *Rosa26*- tdTomato transgene[19,99,100]. The Wnt1-cre line used in this study is the well validated line for studying neural crest derivatives previously used by us and others[18,19,22,46,101], and not the Wnt1-cre2 line used by Drokhlyansky et al.[102]. We again validated the fidelity of this line by observing whether any aberrant recombination occurred in our Wnt1-cre:*Rosa26*-tdTomato line by studying the intestinal mucosal tissue and found that the line behaved expectedly to label neural crest-derivatives and epithelial cells (Suppl. Fig 1i). Pax3-cre:*Rosa26*-tdTomato lineage-traced line was generated by breeding the Ai9 transgenic mouse line (Jax #: 007909) with the Pax3-cre transgenic mouse (Jax #: 005549). The Wnt1-cre:*Hprt*-tdTomato mouse was generated by breeding our aforementioned Wnt1-cre transgenic mouse line with the *Hprt*-tdTomato transgenic mouse line (Jax #: 021428, kind gift from Prof. Jeremy Nathans). Mesp1-cre:*Rosa26*-tdTomato mice were generated by breeding the Mesp1-cre transgenic mice[103] (gift from Dr. Chulan Kwon, JHU) with the Ai14 transgenic mice. Mesp1-cre:*Rosa26*-GFP mice were generated by breeding the Mesp1-cre transgenic mice with the *Rosa26*-EGFP transgenic mouse line (gift from Dr. Akira Sawa, JHU). Neither the *Rosa26*-tdTomato (Ai14) line nor the *Rosa26*-EGFP line showed any reporter expression in the absence of a cre driver (Suppl. Fig 1j, k). $Ret^{+/CFP}$ mice (MGI:3777556) were inter-bred to get a colony of adult $Ret^{+/+}$ and $Ret^{+/CFP}$ mice. $Ret^{CFP/CFP}$

mice died at or before term. Tek-cre:*Hprt*-tdTomato mice were generated by breeding Tek-cre transgenic mice (also known as Tie2-cre; Jax #: 004128) with the *Hprt*-tdTomato transgenic mouse line. 17-month-old male C57BL/6 mice from the aging mouse colony of the National Institute of Aging were procured for the GDNF-treatment experiment.

*Human Tissues:*

Human tissues were obtained under IRB protocol IRB00181108 that was approved by Institutional Review Board at the Johns Hopkins University. Pathological normal specimens of human duodenum and colon were obtained post-resection. Tissues were obtained from adult donors and were de-identified such that the exact age, gender, and ethnicity of the donors was unknown.

*Tissue preparation*:

Mice were anesthetized with isoflurane and sacrificed by cervical dislocation. A laparotomy was performed, and the ileum was removed and lavaged with PBS containing penicillin-streptomycin (PS; Invitrogen), then cut into 1-cm-long segments and placed over a sterile plastic rod. A superficial longitudinal incision was made along the serosal surface and the LM-MP was peeled off from the underlying tissue using a wet sterile cotton swab[19] and placed in Opti-MEM medium (Invitrogen) containing Pen-Strep (Invitrogen). The tissue was then laid flat and fixed within 30 minutes of isolation with freshly prepared ice cold 4% paraformaldehyde (PFA) solution for 45 minutes in the dark to preserve fluorescence intensity and prevent photo-bleaching. All LM-MP tissues post-isolation were fixed within 30 minutes of their isolation. After the fixation, the tissue was removed and stored in ice cold sterile PBS with Pen-Strep for immunofluorescence staining and subsequent microscopy.

For human tissues, duodenal tissue from adult human patients (n = 3 patients), who did not have any prior history of chronic intestinal dysmotility, that was removed by Whipple procedure

was obtained. A colonic sample from a pathologically normal colonic resection from an adult donor suffering from colon carcinoma who similarly did not have prior history of chronic intestinal dysmotility was also obtained. The resected tissue was placed in ice cold Opti-MEM medium (Invitrogen) containing Pen-Strep (Invitrogen). The mucosal and sub-mucosal tissue was dissected out in the medium under light microscope and the muscularis layer containing myenteric plexus tissue was obtained. The tissue was laid out between two glass slides and fixed overnight in ice cold 4% PFA after which it was removed and stored in ice cold sterile PBS with Pen-Strep for immunofluorescence staining, optical clarification, and subsequent microscopy.

*Immunohistochemistry*:

For murine tissue: The fixed LM-MP tissue was washed twice in ice-cold PBS in the dark at 16 °C. The tissue was then incubated in blocking-permeabilizing buffer (BPB; 5% normal goat serum with 0.3% Triton-X) for 1 hour. While staining for antibodies that were mouse monoclonal, 5% normal mouse serum was added to the BPB. The tissue was then removed from the BPB and was incubated with the appropriate primary antibody at the listed concentration (Suppl. Table 1) for 48 h at 16 °C in the dark with shaking at 55 rpm. Following incubation with primary antibody, the tissue was washed three times (15-min wash each) in PBS at room temperature in the dark. The tissue was then incubated in the appropriate secondary antibody at room temperature for 1 hour while on a rotary shaker (65 rpm). The tissue was again washed three times in PBS at room temperature, counterstained with DAPI to stain the nuclei, overlaid with Prolong Antifade Gold mounting medium, cover-slipped, and imaged.

Colchicine treatment: For CGRP immunostaining, mice were injected with Colchicine at a concentration of 5 mg/Kg body weight 16 hours (overnight) before they were sacrificed. The mice were housed singly during this time and adequate gel packs were provided. Food and water were provided *ad libitum*. On the following day, the mice were sacrificed, and their LM-MP tissues were harvested as detailed above.

712 For human tissue: The fixed muscularis layer containing myenteric plexus tissue was removed
713 from ice cold PBS and incubated in blocking-permeabilizing buffer (BPB; 5% normal goat se-
714 rum, 5% normal mouse serum with 0.3% Triton-X) for 4 hours. The tissue was then removed
715 from the BPB and was incubated with the appropriate primary antibody at the listed concentra-
716 tion (Suppl. Table 1) for 5 days at 16°C in the dark with shaking at 55 rpm. Following incubation
717 with primary antibody, the tissue was washed five times (15-min wash each) in PBS at room
718 temperature in the dark. The tissue was then incubated in the appropriate secondary antibody at
719 16°C in the dark with shaking at 55 rpm for 2 days. The tissue was again washed in dark for five
720 times in PBS that contained DAPI at room temperature. After the final wash, the tissue was
721 suspended in tissue clarification buffer CUBIC[104] for 1 hour at 4°C in the dark after which it was
722 overlaid with Prolong Antifade Gold mounting medium, cover-slipped, and imaged. Briefly, the
723 CUBIC optical clarification buffer was made by mixing 2.5 g of urea 25 by wt , 2.5 g of N, N,
724 N ,N -tetrakis (2-hydroxy-propyl) ethylenediamine (25% by wt), 1.5 g of Triton X-100 (15% by
725 wt) in 35 ml of Distilled Water. The solution was shaken till the ingredients were dissolved and
726 yielded a clear viscous solution.

727 *Microscopy*:

728 Imaging was done by using the oil immersion 63X objective on the Leica SP8 confocal micro-
729 scope and by using the oil immersion 40X objective on the Olympus Fluoview 3000rs confocal
730 microscope with resonance scanning mode. For thick tissues, such as human tissues, the Gal-
731 vano mode of the Olympus Fluoview 3000rs microscope that enabled higher resolution imaging
732 and averaging was used. Images obtained were then analyzed using Fiji (https://fiji.sc/).

733 Live tissue imaging of the mouse gut tissue was performed by harvesting small intestinal tissue
734 from an adult Wnt1-cre:*Rosa26*-tdTomato mouse and immediately putting it in OptiMEM solu-
735 tion. The tissue was then immediately put on a chamber slide containing OptiMEM and imaged
736 in live tissue culture conditions of the EVOS M7000 microscope under the 20X objective.

*Enumeration of neurons*:

Enumeration of tdTomato$^{+}$ and tdTomato$^{-}$ neurons was performed on tissue with native tdTomato fluorescence. The native tdTomato fluorescence in fixed tissue was intense, thus there was no need to increase fluorescent signal using anti-RFP/tdTomato antibodies.

Enumeration of enteric neurons to study alterations to ENS neuronal numbers was performed by following the well-established protocol[105-108] of counting the numbers of neurons in myenteric ganglia and comparing them between animals for statistically significant differences. Identification of myenteric ganglia was performed according to our pre-determined method published earlier[19]. Briefly, contiguous clusters of neurons were defined as a ganglia and the total numbers of neurons within these clusters were enumerated as numbers of myenteric neurons per ganglion. As a rule, clusters of 3 neurons or more were deemed to consist a ganglion and our enumeration strategy did not count extra-ganglionic neurons. We imaged ~10 ganglia per tissue for our enumeration and each group studied had n ≥ 3 mice. Identification and enumeration of neurons and detection of co-localization was performed manually by trained laboratory personnel. Fig 1d comprises of the data from 6 P60 mice, which includes data from the 3 mice that were used for the development experiment presented in Fig 8c.

*Protein isolation and detection:*

After the LM-MP tissue was isolated, it was weighed and placed in a sterile 1.5 ml microfuge tube. 1X RIPA buffer (Cell Signaling Technology) with Halt Protease Inhibitor Cocktail (Thermo Scientific) at 5X concentration, Phosphatase Inhibitor Cocktails II and III (Sigma-Aldrich) at 2X concentrations were added to the tissue lysate buffer. Tissue was disrupted using 1.0 mm silica beads in Bullet Blender 24 (Next Advance) for 5 mins at highest setting. The lysate was incubated at 4°C with shaking for 30 mins, centrifuged at 14,000rpm for 20 mins and the supernatant was taken and stored in -80°C in aliquots. Protein concentration was estimated using Brad-

ford assay solution (Biorad) following the manufacturer‟s protocol. For immunoblotting, 40 µg of protein was loaded per well of 4%-20% gradient denaturing gel (Biorad). Protein marker used was Precision Plus Dual Color standards (Biorad). After fractionating the proteins, they were blotted onto ImmunBlot PVDF membrane (Biorad) overnight at 4°C at 17V for 12-16 hours. After blotting, membrane was blocked with Odyssey TBS blocking buffer (Li-Cor) for 1 hour at room temperature with shaking. Incubation with primary antibodies were carried out at 4°C with shaking for 24 hours. Following binding, the blot was washed 4 times with TBS-T (Tris Buffered Saline with 0.5% Tween) for 15 mins each with shaking at room temperature. Secondary antibody incubation was carried out in dark at room temperature for 1.5 hours with shaking. The blot was then washed 4 times for 15 mins each and imaged on Odyssey CLx system (Li-Cor).

Antibody used to detect RET was a well validated antibody used previously for detecting RET in ENS[109] and was further validated by us using a western blot on total proteins isolated from murine small intestinal LM-MP (Suppl. Fig 8e). Antibodies used are detailed in the Supplementary Table 1.

*RNA isolation and quantitative detection of specific transcripts:*

The isolated tissue was stored in RNALater Solution (Ambion). RNA was isolated using RNeasy Mini Kit Qiagen following manufacturer‟s protocol. RNA quantification was carried out using Epoch Microplate Spectrophotometer (BioTek). cDNA synthesis was carried by SuperScript IV VILO Master Mix (Invitrogen). Quantitative Real-time PCR was carried out using Taqman Gene Expression Master Mix (Applied Biosystems) and Roto-Gene Q (Qiagen). The probes used are listed in Supplementary Table 1.

*Single Cell RNA sequencing and analyses:*

Single cell preparation from adult murine ileal tissues: Ileal tissues from two 6-month old adult male littermate C57/BL6 wildtype mice were isolated by peeling as previously described. The

785 tissues were then dissociated in Digestion Buffer containing 1 mg/ml Liberase (Sigma-Aldrich) in
786 OptiMEM. Tissues from mouse 1 were dissociated in the Digestion buffer containing Liberase
787 TH and tissues from mouse 2 were dissociated in the Digestion buffer containing Liberase TL.
788 Dissociation was performed at 37°C for 30 minutes on a rotary shaker, after which the cells
789 were centrifuged at 200g for 7 minutes, and the pellet was resuspended in ice cold sterile PBS.
790 The cell suspension was passed through a 40 µm cell sieve and the resulting filtered cell sus-
791 pension was again centrifuged at 200g for 7 minutes. This process of cell centrifugation and fil-
792 tration was repeated two more times, after which the cells were resuspended in 1 ml ice cold
793 sterile PBS. The repeated steps of serial cell washes and filtration removed clumps and debris
794 and the viability of the resulting cell suspension was estimated to be >90% using Trypan Blue
795 dye test. The cells were then processed through 10X Genomics Chromium V2.0 system accord-
796 ing to the manufacturer"s suggested workflow. The processing was done at the GRCF Core Fa-
797 cility at the Johns Hopkins University. The pooled libraries were sequenced on an Illumina HiS-
798 eq 2500 to an average depth of $3.125 \times 10^8$ reads per sample library. The sequencing was per-
799 formed at the CIDR core facility at the Johns Hopkins University.

800 Pre-processing of FASTQs to Expression Matrices: FASTQ sequence files were processed fol-
801 lowing a Kallisto Bustools workflow compatible with downstream RNA velocity[110]. References
802 required for pseudo-alignment of transcripts were obtained using the get_velocity_files (func-
803 tionality of BUSpaRSE (https://github.com/BUStools/BUSpaRse)), with "L=98" for 10X Ge-
804 nomics v2.0 sequencing chemistry. Reads were pseudo-aligned to an index built from Ensembl
805 97 transcriptome annotation (Gencode vM22; GRCm38). Across two samples processed, a total
806 of 578,529,125 reads were successfully pseudo-aligned. Barcodes within a Hamming distance
807 of one to known 10X Genomics v2.0 barcodes were corrected. Reads were classified as
808 "spliced" or "unspliced" by their complement to the target list of intronic sequences and exonic

809 sequences, respectively, and subsequently quantified separately into expression count matri-
810 ces. Spliced counts are used for all analyses.

811 Single cell gene expression analysis: scRNA-seq count matrices were analyzed using Mono-
812 cle3. 11,123 high-quality cells were identified as meeting a 200 UMI minimum threshold with a
813 mitochondrial read ratio of less than 20%; droplets that did not meet these criteria were exclud-
814 ed from the analysis. Mitochondrial counts were determined as the sum of reads mapping to 37
815 genes annotated to the mitochondrial genome. All genes with non-zero expression were includ-
816 ed for downstream analysis. Raw counts were first scaled by a cell-size scaling factor and sub-
817 sequently log10 transformed with a pseudo-count of 1. Normalized values are used in place of
818 raw counts unless otherwise noted.

819 Prior to UMAP dimensionality reduction, batch effects between the two biological replicates
820 were assessed and corrected via the mutual nearest neighbors (MNN) algorithm as implement-
821 ed by Batchelor in Monocle3[111]. 15 clusters of cells in the UMAP embedding were identified by
822 Leiden community detection. 30 marker genes for each cluster were identified based on great-
823 est pseudo $R^2$ values and used for supervised annotation of cell types by searching UniProt,
824 Allen Cell Atlas and through literature search with Pubmed.

825 NC-derived cell clusters were identified by expression of NC markers Ret and Sox10. MEN clus-
826 ter was identified by its expression of CGRP-coding Calcb, Met, and Cdh3. The pan-MENs pro-
827 tein marker MHCst was identified by labeling with an antibody S46 which labels all members of
828 the MHCst family[40]. Since the antibody does not identify a single gene product, MHCst im-
829 munostaining could not be used to identify a specific gene marker for use in the annotation of
830 the MEN cluster. For further analysis into the MENs population, the full LM-MP dataset was
831 subset to include only the 2,223 cells annotated as MENs. These cells were re-processed as
832 above, but with a reduced PCA dimensionality of k=20 as input for the UMAP embedding. 5

clusters of cells in the UMAP embedding were identified by Leiden community detection (k= 10, resolution = 5e -4).

External datasets: Spliced and unspliced count matrices for mesenchymal subset of the Gut Cell Atlas were obtained from https://www.gutcellatlas.org/, and existing annotations were used when available. SnRNAseq counts matrices from May-Zhang et al.[56] were downloaded from GEO GSE153192. Bulk RNAseq dataset from the Human Obstructed defecation study by Kim et al.[75] was obtained from GEO GSE101968.

Pattern discovery and ProjectR analyses: Pattern discovery was utilized to identify sets of co-expressed genes that define cell-type specific transcriptional signatures. The normalized expression matrix was decomposed via non-negative matrix factorization (NMF) as implemented in the R package *NNLM*, with k=50 and default parameters. Cell weights for each pattern were grouped by assigned cell-type and represented by heatmap. Pattern vectors were hierarchically clustered by a Euclidian distance metric, implemented in ComplexHeatmap[112]. These patterns were then tested on the bulk RNA-Seq expression matrix for the Human Obstructed Defecation study[75]. The log2 expression (log2(rpkm + 1)) from this study was projected onto the NMF patterns using projectR[57]. Students" t tests were performed on the projection weights from the Control and OD groups to test for differences between them. For the projection of datasets generated by May-Zhang et al. and Elmentaite et al., log10-transformed normalized counts were projected.

**Analysis of May-Zhang et al. dataset**

Raw UMI count matrices for the single-nucleus RNA sequencing of enteric neurons performed by May-Zhang et al.[56] from the ileum of adult mice were obtained from GEO (GSE153192). The DropletUtils package (v1.10.3)[113,114] was used to compute barcode ranks, knee, and inflection point statistics for all the samples. All barcodes in the 10X genomics libraries with total UMI

857 greater than the inflection point were considered to be cell-containing droplets and retained for
858 further analysis. The inDrop libraries were filtered to retain all barcodes with UMI greater than
859 200. The filtered matrices were combined to form a SingleCellExperiment object.

860 Cell-specific scaling factors accounting for composition biases were computed using com-
861 puteSumFactors (scran v1.18.7)[115]. The raw UMI counts were then scaled using the scaling fac-
862 tors and log 2 transformed after addition of a pseudo count of 1 using logNormCounts (scater
863 v1.18.6)[116]. Batch effects between the samples were corrected using fastMNN (batchelor
864 v1.6.3)[111].

865 Unsupervised clustering was performed using a graph-based clustering technique. The graph
866 was obtained using buildSNNgraph (scran v1.18.7)[115] and the louvain algorithm implemented in
867 the igraph package (v1.2.7)[117] was used to identify communities. Differential expression testing
868 was performed between all pairs of clusters using findMarkers (scran v1.18.7)[115]. One-sided
869 Welch"s t-test was used to identify genes that were upregulated in a cluster as compared to any
870 others in the dataset. Benjamini-Hochberg method was applied (to combined p-values) to cor-
871 rect for multiple testing and the genes were ranked by significance. The top ranked genes were
872 used as marker genes for the clusters. The log fold change from the pairwise comparison with
873 the lowest p-value was used as the summary log fold change.

874 The log normalized counts from this dataset were then projected into the NMF patterns learned
875 on our scRNAseq data. This was performed using transfer learning implemented in projectR
876 (v1.6.0). The projection weights corresponding to the four MEN-specific patterns were then clus-
877 tered using graph-based clustering and visualized by UMAP (uwot v0.1.10)(
878 https://github.com/jlmelville/uwot).

879 *Whole gut transit time analyses*:

Whole-gut transit time (WGTT) for every mouse was analyzed by the method using the carmine red protocol[19]. Mice were placed in individual cages and deprived of food for 1 hour before receiving 0.3 mL 6% (wt/vol) carmine solution in 0.5% methylcellulose by oral gavage into the animal"s stomach. The time taken for each mouse to produce a red fecal pellet after the administration of carmine dye was recorded in minutes. The experiment was terminated at 210 minutes post-gavage and the WGTT of any mice that did not expel the red dye at the termination was marked at the value of 210 min. The mean difference in whole gut transit time (in minutes) between both the $Ret^{+/+}$ and $Ret^{+/-}$ mice cohorts, and the GDNF and Saline-treated Control cohorts were analyzed statistically.

*In vivo Injections:*

GDNF injection: Similar to prior report that gave sub-cutaneous injections of GDNF to post-natal mice[71], we took 6 littermate 10 day old (P10) male Wnt1-cre:*Rosa26*-tdTomato mice and divided into two subgroups, GDNF and Control. Each mouse in the GDNF group was injected subcutaneously with 50 µl of 2mg/ml of GDNF (Peprotech Catalogue #: 450-44) every other day, while the Control group was injected with 50 µl of sterile saline. The mice were given 5 doses and then sacrificed on P20, after which their LM-MP tissues were isolated as detailed above. The tissues were then immunostained with antibodies against HuC/D and imaged. For studying the effect of GDNF on aging mice, two cohorts of 17-month-old male C57BL/6 mice (n=5 mice/cohort) were obtained from the aging colony of the National Institute of Aging. Before the start of dosing, the whole gut transit time was assayed. The animals were then injected daily sub-cutaneously either with 100 µl of saline (Control) or 100 µl of GDNF (500 µg/ml) for 10 consecutive days, after which the mice were sacrificed and their LM-MP tissues were isolated as detailed above. The tissues were then immunostained with appropriate antibodies and imaged.

HGF injection: Similar to prior report that gave sub-cutaneous injections of HGF to post-natal mice, we took 5 littermate 10 day old (P10) male Wnt1-cre:*Rosa26*-tdTomato mice and divided into two subgroups, HGF and Control. Each mouse in the HGF group was injected sub-cutaneously with 100 µl of 2mg/ml of HGF (Peprotech Catalogue #:315-23) every other day, while the saline group was injected with 100 µl of sterile saline. The mice were given 5 doses and then sacrificed on P20, after which their LM-MP tissues were isolated as detailed above. The tissues were then immunostained with antibodies against HuC/D and imaged.

*Statistics:*

Data was analyzed using Graphpad Prism 8.3.1 and R using Unpaired Students t-test, Simple Linear Regression, and Ordinary One-Way ANOVA.

*Data:*

All raw data are provided in Supplementary Table 2 - 4. Raw single cell RNA sequencing data is archived on the NCBI GEO server and can be accessed under the accession number GSE156146.

*Code:*

Code generated for the scRNA/snRNA analyses is available at https://github.com/jaredslosberg/6month_ENS/.

## Figures

**Fig 1: Half of all adult small intestinal myenteric neurons are derived from a non-neural crest lineage.**

**(a)** Enteric glia, labeled with GFAP (green) in the myenteric plexus from an adult Wnt1-cre:*Rosa26*-tdTomato mouse. Inset is magnified in color segregated panels, showing $GFAP^+$ glia co-expressing tdTomato (red, red arrows). Nuclei are labeled with DAPI (blue). Scale bar = 10 μm.

**(b)** 2 dimensional representation of a 3 dimensional stack of images shows enteric neurons, labeled with HuC/D (green), in the myenteric plexus from an adult Wnt1-cre:*Rosa26*-tdTomato mouse. Enteric neurons either express tdTomato (red arrow) or not (white arrows). Nuclei are labeled with DAPI (blue). Scale bar = 10 μm.

**(c)** Orthogonal views of the image **(b)** shows the lack of tdTomato expression in a particular HuC/D-immunolabeled enteric neuron.

**(d)** Quantification of $tdTomato^+$ and $tdTomato^-$ neurons in the myenteric ganglia of 6 P60 Wnt1-cre:*Rosa26*-tdTomato mice. Data represents Mean ± SEM.

**Fig 2: Mesoderm-lineage-tracing and marker expression provide evidence of the mesodermal-derivation of half of all adult small intestinal myenteric neurons.**

**(a)** Small intestinal LM-MP from adult male Tek-cre:*Hprt*-tdTomato shows the presence of Tek-derived and hence mesoderm-derived tdTomato$^+$ (red) HuC/D$^+$ (green) neurons (white arrows) and non-mesoderm-derived tdTomato$^-$ neurons (green arrows). Vascular cells depict higher fluorescence intensity (yellow arrow) than cells in the ganglia. Nuclei are labeled with DAPI. Scale bar = 10 μm.

**(b)** Cardiac tissue from heart and **(c)** small intestinal LM-MP tissue of adult male Mesp1-cre:*Rosa26*-tdTomato mice shows the presence of variable tdTomato expression in cells of these tissues. While cardiomyocytes in heart and cells within the myenteric ganglia (white arrows) exhibit lower tdTomato fluorescence, similar to the tissues from Tek-cre:*Hprt*-tdTomato mice in **(a)**, the vascular cells exhibit higher fluorescence intensity (yellow arrows). Scale bar = 10 μm.

**(d)** Small intestinal LM-MP from adult male Mesp1-cre:*Rosa26*-tdTomato mouse shows the presence of mesoderm-derived tdTomato$^+$ (red) HuC/D$^+$ (green) neurons (white arrows) and non-mesoderm-derived tdTomato$^-$ neurons (green arrows). Nuclei are labeled with DAPI. Scale bar = 10 μm.

**(e)** Small intestinal LM-MP from adult male Mesp1-cre:*Rosa26*-EGFP mouse, when immunostained with antibodies against GFP and against HuC/D, shows the presence of mesoderm-derived EGFP$^+$ (green) HuC/D$^+$ (red) neurons (white arrows) and non-mesoderm-derived EGFP$^-$ neurons (red arrows). Nuclei are labeled with DAPI. Scale bar = 10 μm.

**(f)** Quantification of tdTomato-expressing and non-expressing neurons in the myenteric ganglia of 3 P60 Mesp1-cre:*Rosa26*-tdTomato mice. Data represents Mean ± SEM.

958 MHCst immunolabeling exclusively marks all the **(g)** mesoderm-derived adult HuC/D$^+$ (green)
959 neurons in the small intestinal LM-MP of Mesp1-cre:*Rosa26*-tdTomato mice; and **(h)** all the non-
960 NC-derived neurons in the small intestinal LM-MP of Wnt1-cre:*Rosa26*-tdTomato mice (white
961 arrows). MHCst does not label tdTomato$^+$ NC-derived cells (yellow arrows). Nuclei are stained
962 with DAPI (blue). Scale bar = 10 μm.

**Fig 3: Cellular and molecular phenotyping of MENs and NENs.**

MET immunostaining (green) labels **(a)** Wnt1-cre:*Rosa26*-tdTomato$^{-}$ MENs and **(b)** a population of Mesp1-cre:*Rosa26*-tdTomato$^{+}$ MENs (white arrow) while not labeling all MENs (red arrow).

**(c)** RET immunostaining (green) only labels Wnt1-cre:*Rosa26*-tdTomato$^{+}$ NENs (green arrow) and not tdTomato$^{-}$ MENs (white arrows).

**(d)** NOS1 is expressed by both tdTomato$^{+}$ NENs (red, white arrows) and tdTomato$^{-}$ MENs (blue arrows) in an adult Wnt1-cre:*Rosa26*-tdTomato mouse, but most MENs do not express NOS1 (marked by *).

**(e)** Both tdTomato$^{+}$ (red) and tdTomato$^{-}$ neurons in the myenteric plexus of an adult Wnt1-cre:*Rosa26*-tdTomato mouse (HuC/D, green) express CGRP (blue) Inset showing a tdTomato$^{-}$ CGRP$^{+}$ neuron (white arrow) is magnified on the right.

**(f)** NEN lineage contains significantly higher proportions of NOS1$^{+}$ neurons compared to MEN lineage in Wnt1-cre:*Rosa26*-tdTomato mice. Data represent mean ± S.E.M. Student"s t-test ** $p < 0.01$.

**(g)** MEN lineage contains significantly higher proportions of CGRP$^{+}$ neurons compared to NEN lineage in Wnt1-cre:*Rosa26*-tdTomato male mice. Data represent mean ± S.E.M. Student"s t-test **** $p < 0.0001$.

**(h)** MENs express the protein P-Cadherin/CDH-3 (green; white arrows) while tdTomato$^{+}$ (red) NENs do not (blue arrows) in myenteric ganglia from adult Wnt1-cre:*Rosa26*-tdTomato mice.

Nuclei in **(b), (c), (h)** are labeled with DAPI (blue). Scale bar for all images denotes 10 μm.

**Fig 4: scRNAseq-analyses identifies the distinct transcriptomic profile of the MENs.**

**(a)** UMAP representation of 11,123 sequenced high-quality cells that were identified as meeting a 200 UMI minimum threshold with a mitochondrial read ratio of less than 20%. Clusters were annotated by markers that were found to be cell-type specific by searching UniProt, Allen Cell Atlas and Pubmed databases. Cells of the neural crest lineage were then identified as NENs by their expression of neural crest marker gene Ret and Neuroglia by their expression of Ncam1 and Sox10, or as MENs by co-expression of Calcb (CGRP), Cdh3, and Met genes.

**(b)** Visualization of expression of select MEN-specific and neuronal markers using quasi-violin plots. “Max value” represents the scale for the log-normalized expression of each gene.

**(c)** Validation of the MENs-specific marker genes discovered in the scRNAseq analyses by immunohistochemistry and confocal microscopy of small intestinal LM-MP from adult male Wnt1-cre:*Rosa26*-tdTomato mice. Expression of neuronal markers STX3, VSNL1, STMN2, HAND2, GPR88, PDE10A, ELAVL2, and TUBB2B (Gray, green arrows) was found in tdTomato$^{-}$ MENs. Immunostaining of the proteins AEBP1, CFTR, CLIC3, NT-3, SLPI, SMO, IL-18, SLC17A9, FMO2 and MYL7 (green; green arrows) was found to be localized to tdTomato$^{-}$ MENs. tdTomato$^{+}$ (red) NC-cells did not immunostain for these markers (red arrows). Panel also shows Wnt1-cre:*Rosa26*-tdTomato tissue with no primary controls (stained with AlexaFluor 488 and AlexaFluor 647 antibodies). Figures with * annotations are 2D representation of 3D stacks of images, whose orthogonal views are presented in Suppl Fig 3. Nuclei in some panels were labeled with DAPI (blue). Scale bar denotes 10 μm.

**Fig 5: Computational analyses using *Project R* identifies MENs in publicly available murine and human transcriptomic datasets.**

**(a)** Heatmap of cell weights for the patterns learned by NMF (k=50). Hierarchical clustering was calculated using Euclidean distance. Multiple clusters annotated as the same cell type are merged. The four most specific MENs patterns (16, 27, 32 and 41) are selected.

**(b)** In addition to using the four MEN-specific NMF patterns to label the MENs cluster in our scRNAseq dataset (plots in top row), two other transcriptomic datasets: May-Zhang et al."s murine ileal ENS snRNAseq dataset[56] (plots in second row), and Elmentaite et al."s gut mesenchymal scRNAseq dataset[59] (plots in third row), were projected into the defined four MEN-specific pattern space using *ProjectR*. Raw projected cell weights were visualized using previously learned UMAP embedding. The cell clusters that show high pattern usage are shown bounded by the red square. Plots in the third row shows projection of healthy post-natal mesenchymal cells from Elmentaite et al"s data into the four MEN-specific NMF patterns, which again show a population of cells showing high MEN-specific pattern utilization.

**Fig 6. Detection of MENs in human single cell RNA sequencing data.**

**(a)** UMAP representation of scRNAseq data from Elmentaite et al."s[59] healthy post-natal mesenchymal cells from the human gut.

**(b)** Breakdown for previously published annotated features of the post-natal health subset of the gut cell atlas as presented in Elmentaite et al.

**(c)** Expression of neuronal marker genes Slc17a9, Stx3, Uchl1, Tubb2b, Pde10a, and Hand2 in the UMAP representation of healthy post-natal data from Elmentaite et al., which was annotated as clusters of mesenchymal cells.

**Fig 7: Validation of SNAP-25 as a NENs marker and detection of MENs in human tissues**

**(a)** SNAP-25 expression is restricted to the neural crest lineage in the adult myenteric ganglia. SNAP-25 expression (green) co-localizes with tdTomato (red) but not with the MENs marker MHCst (cyan) as observed in 2D and orthogonal views of a myenteric ganglia from a Wnt1-cre:*Rosa26*-tdTomato mouse that was immunolabeled with antibodies against MHCst and SNAP-25. Nuclei were labeled with DAPI (blue). Scale bar denotes 10 μm.

**(b)** Putative human MENs (red arrows) and NENs (green arrows) identified by presence or absence of the murine MENs markers, MET (blue) and MHCst (red) in subpopulations of HuC/D$^{+}$ (green) small intestinal myenteric neurons from normal human duodenal tissue. Scale bar denotes 10 μm.

**(c)** MENs marker SLC17A9 expression (green, green arrows) in a subset of MHCst-expressing (red) neurons. Subset of MHCst-expressing cells do not express SLC17A9 (red arrow). Nuclei are labeled with DAPI (blue) in the normal human duodenal tissue. Scale bar denotes 10 μm.

**Fig 8: GDNF and HGF signaling regulate age-dependent changes in NENs and MENs proportions.**

**(a, b)** Immunostaining myenteric plexus tissue from juvenile and aging Wnt1-cre:*Rosa26*-tdTomato mice with antibodies against the pan-neuronal marker HuC/D (green).

**(c)** Age-associated loss of NENs and gain of MENs in the small intestinal LM-MP of maturing and aging Wnt1-cre:*Rosa26*-tdTomato mice. Data represent mean ± S.E.M.

**(d)** Mean ± SEM of the four MEN-specific pattern weights in the human mesenchymal cell populations from Elmentaite et al.[59], wherein data from age ranges of 4 – 12 years was clubbed together as Juvenile (Juv), data from age ranges of 20 – 50 years was clubbed together as Adult (Ad), and data from age ranges of 60 – 75 years was clubbed together as Aged (Ag). Every datapoint refers to mean projected pattern weight for cells within a defined age or age range, where Juv data comprise of ages 4, 6, 9, 10, 12 years; Ad data comprise of age ranges 20 - 25, 25 – 30, and 45-50 years; and finally Ag data comprise of age ranges 60 – 65, 65 – 70, and 70 – 75 years. One-way ANOVA ** = $p < 0.01$).

**(e)** Western blot analyses of GDNF (green) and the house-keeping protein β-actin (red) expression in LM-MP tissues from mice of ages P10, P30, and P90. (n = 3 mice per group; each sample is a biological replicate). Fluorescent intensities of the two bands of GDNF (that correspond to ~25 kD bands of protein marker) were quantified together. The lower band of GDNF is present only in the P10 tissues and disappears in P30 and P90 adult murine tissues.

**(f)** Western blot analyses of HGF (green) and the house-keeping protein β-Actin (red) expression in LM-MP tissues from mice of ages P10, P30, and P90. (n = 3 mice per group; each sample is a biological replicate). Fluorescent intensities of the two bands of HGF (that are between 50 kD and 37 kD bands of the protein marker) were quantified together.

1063 **(g)** The normalized fluorescent intensity of GDNF protein to house-keeping protein β-Actin com-
1064 pared between the three age groups. GDNF presence was highest in P10 group and was signif-
1065 icantly reduced in P30 and P90 groups. Data represent mean ± S.E.M. One-way ANOVA **** p
1066 < 0.001.

1067 **(h)** Age-dependent decrease in Gdnf mRNA transcript expression (normalized to the house-
1068 keeping gene Hprt) in the myenteric plexuses of P30 and P90 old mice. Data represent mean ±
1069 S.E.M. Student"s t-test *p < 0.05.

1070 **(i)** The normalized fluorescent intensity of HGF protein to house-keeping protein β-Actin was
1071 compared between the three age groups. HGF expression significantly increased from P10
1072 through P90. Data represent mean ± S.E.M. One-way ANOVA *p < 0.05.

1073 **(j)** Age-dependent increase in Hgf mRNA transcript expression (normalized to the house-
1074 keeping gene Hprt) in the myenteric plexuses of P10, P30, and P90 old mice. Data represent
1075 mean ± S.E.M. One-way ANOVA * p < 0.05, *** p < 0.01, **** p < 0.001.

1076 **(k)** Percent proportions of tdTomato$^{-}$ MENs and mean HuC/D$^{+}$ neurons/ganglia in LM-MP of
1077 cohorts of Wnt1-cre:*Rosa26*-tdTomato mice that were dosed with GDNF or Saline from P10 to
1078 P20 age. Data represent mean ± S.E.M. Student"s t-test ** p < 0.01.

1079 **(l)** Percent proportions of tdTomato$^{-}$ MENs and mean HuC/D$^{+}$ neurons/ganglia in LM-MP of co-
1080 horts of Wnt1-cre:*Rosa26*-tdTomato mice that were dosed with HGF or Saline from P10 to P20
1081 age. Data represent mean ± S.E.M. Student"s t-test * p < 0.05.

1082

**Fig 9: Reduced RET signaling accelerates ENS aging to cause pathology**

**(a)** HuC/D immunostaining (green) LM-MP tissues from 16-week-old $Ret^{+/CFP}$ ($Ret^{+/-}$) mouse shows mutually exclusive expression of Ret-CFP (cyan, green arrow) and MHCst (red, red arrow) MENs. Nuclei are stained with DAPI (blue). Scale bar = 10 μm.

**(b)** Quantification of Ret-$CFP^{+}$ neurons from 9- and 16-week-old $Ret^{+/-}$ mice show age-associated loss of Ret-$CFP^{+}$ neurons. Data represent mean ± S.E.M. Student"s t-test * $p < 0.05$.

**(c)** Quantification of $MHCst^{+}$ MENs shows significant increase in their proportions in $Ret^{+/-}$ mice but not in $Ret^{+/+}$ mice with age. Data represent mean ± S.E.M. One way ANOVA * $p < 0.05$, ** $p < 0.01$, *** $p < 0.001$).

**(d)** Measures of whole gut transit time (WGTT) in cohorts of $Ret^{+/-}$ and $Ret^{+/+}$ mice MENs show significant slowing of whole gut transit of $Ret^{+/-}$ but not $Ret^{+/+}$ mice with age. Data represent mean ± S.E.M. One way ANOVA * = $p < 0.05$.

**Fig 10: GDNF normalizes altered intestinal motility by increasing NENs proportions in the aging gut.**

**(a)** Measures of whole gut transit time (WGTT) in GDNF (treated with GDNF) and Control (treated with Saline) cohorts of 17-month-old mice taken before the start of treatments and after the end of 10 consecutive days of treatment shows that the two groups are matched in their transit times before treatment, but GDNF treatment significant decreases average transit times when compared to the control cohort. Data represent mean ± S.E.M. Student"s t-test *** = $p < 0.001$.

**(b)** Quantification of percent MHCst$^{+}$ MENs per HuC/D-labeled neurons in myenteric ganglia in the GDNF and Control cohorts shows significant decrease in their proportions in GDNF-treated cohort but not in saline-treated control cohort. Data represent mean ± S.E.M. Student"s t-test ** $p < 0.01$.

**(c)** Quantification of numbers of RET$^{+}$ NENs per 40X field views of myenteric ganglia shows significant increase in their numbers in GDNF cohort mice when compared with Control cohort mice. Data represent mean ± S.E.M. Student"s t-test * $p < 0.05$.

**Fig 11: Patients with chronic gut dysmotility show significant shifts in their normal proportions of the two neuronal lineages.**

**(a)** *ProjectR*-based projection of bulkRNAseq data from intestinal specimens of patients with normal motility (controls) and patients with obstructive defecation (OD), a chronic condition of intestinal dysmotility, into the 50 different NMF patterns learnt earlier, shows that the MEN-specific NMF patterns 32 and 41 were significantly upregulated in bulk-RNAseq of OD patients compared to controls. Data represent mean ± S.E.M. One way ANOVA. Data mined from raw data generated by Kim et al.[75]

**(b)** OD patients show a significant decrease in the expression of important NENs-associated genes such as Ret, Gdnf, Snap-25, Nos1, Klhl1, and Chat, while showing a significant increase in the expression of important MENs-specific genes such as Clic3, Upk3a, Cdh3, Slpi, and Slc17a9. Data taken from Kim et al.[75]

**Suppl. Figure 1: Presence and absence of tdTomato reporter expression in the myenteric ganglia of adult neural crest lineage-traced mice**

**(a)** HuC/D immunostained Wnt1-cre:*Rosa26*-tdTomato LM-MP tissue, where tdTomato-expression (red) marks neural crest-derived cells, and HuC/D (green) labels myenteric neurons, we observed the presence of higher intensity fluorescence (red arrows) and lower intensity fluorescence (orange arrows) in various tdTomato$^{+}$ neurons. The myenteric ganglia also contained HuC/D$^{+}$ neurons that did not express tdTomato (green arrow) and these neurons alone were deemed to be non-neural crest-derived neurons. Scale bar denotes 10 µm.

**(b)** Reporter non-expressing HuC/D-immunolabeled neurons (green, green arrows) can be observed both through the expression of the tdTomato reporter (red), as well as on antibody labeling of the tdTomato reporter (gray).

**(c)** Freshly harvested small intestinal tissue from Wnt1-cre:*Rosa26*-tdTomato mice when imaged under 20X magnification of a live tissue fluorescence microscope shows the presence of cells that express tdTomato (red) and those that don't.

**(d)** Cells showing hyper-aggregation of the tdTomato reporter can be found in freshly harvested full-thickness small intestinal myenteric plexus in tissues imaged under 20X magnification of a live tissue fluorescence microscope.

**(e)** Myenteric ganglia from fixed LM-MP tissue of adult Wnt1-cre:*Rosa26*-tdTomato mice show show hyper-aggregation of tdTomato (white arrow) when imaged using a confocal microscope. Nuclei are stained with nuclear marker DAPI (blue). Scale bar denotes 10 µm.

**(f)** Cells showing hyper-aggregation of tdTomato (red, red arrow) show no detectable nuclear labeling with DAPI (blue) or of pan-neuronal marker HuC/D (green, green arrow). Scale bar denotes 10 µm.

In addition, interrogation of two other neural crest-specific lineage-traced mouse lines confirms our observations with Wnt1-cre:*Rosa26*-tdTomato mice. **(g)** In Wnt1-cre:*Hprt*-tdTomato adult male mice, tdTomato expression (red) is present only in a subset of HuC/D-immunolabeled (green) neurons (red arrows) while it is not detected in other HuC/D-expressing neurons (green). Similarly, **(h)** only a subpopulation of HuC/D$^+$ adult enteric neurons (green) is derived from the neural crest, as seen by its co-expression of tdTomato (red, red arrows) in the Pax3-cre:*Rosa26*-tdTomato mice while other neurons that do not express tdTomato (white arrows) are inferred to be not derived from the neural crest. Scale bar denotes 10 μm.

**(i)** Orthogonal views of small intestinal villus from a Wnt1-cre:*Rosa26*-tdTomato mouse that shows presence of tdTomato-expressing (red) neural crest-derived fibers inside the villus but a complete lack of tdTomato-expression by intestinal epithelial cells. Nuclei are labeled with DAPI (blue). Scale bar denotes 10 μm.

**(j)** Representational image of the myenteric plexus from a *Rosa26*-tdTomato mouse without any cre driver showing that in absence of cre recombinase to drive tdTomato expression, there is a lack of tdTomato expression in this layer. Nuclei are labeled with DAPI (blue). Scale bar denotes 10 μm.

**(k)** Representational image of the myenteric plexus from a *Rosa26*-EGFP mouse without any cre driver showing that in absence of cre recombinase to drive EGFP expression, there is a lack of EGFP expression in this layer. Nuclei are labeled with DAPI (blue). Scale bar denotes 10 μm.

**Suppl. Figure 2: Tek-expressing and Mesp1-expressing mesodermal lineage contributes to adult enteric neurons.**

**(a)** Adult small intestinal LM-MP layer from a male Tek-EGFP mouse, where EGFP expression (green) labels Tek-expressing cells was immunostained with specific antibodies against the pan-neuronal marker PGP9.5 (red) and imaged under a confocal microscope. The Tek-EGFP expression did not label any cells within the myenteric plexus marked by PGP9.5 expression showing that adult small intestinal myenteric neurons did not express Tek. Nuclei are labeled with DAPI (blue). Scale bar denotes 10 μm.

**(b)** We observed the presence of higher intensity fluorescence (red arrows) and lower intensity fluorescence (green arrow) in various tdTomato$^{+}$ cells in a section of heart tissue from a 6-month-old Mesp1-cre:*Rosa26*-tdTomato adult male mouse, where tdTomato (red) labels Mesp1-derived cells of the mesodermal lineage that includes cardiomyocytes and vasculature. Nuclei are stained by DAPI (blue). Scale bar denotes 10 μm.

**(c)** Adult small intestinal LM-MP layer from a 6-month-old male Mesp1-cre:*Rosa26*-tdTomato mouse, where tdTomato (red) cells are mesoderm-derived cells, was immunostained with specific antibodies against the pan-neuronal marker HuC/D (green) and imaged under a confocal microscope. tdTomato-expressing cells outside the ganglia (red arrows) were brighter than tdTomato$^{+}$ neurons inside the ganglia (green arrows). Nuclei are labeled with DAPI (blue). Scale bar denotes 10 μm.

**(d)** Adult small intestinal LM-MP layer from a 2-month old male Mesp1-cre:*Rosa26*-EGFP mouse, where EGFP cells are mesoderm-derived, was immunostained with specific antibodies against the reporter EGFP (green) and the pan-neuronal marker HuC/D (red) and imaged under a confocal microscope. A population of HuC/D-immunolabeled neurons were also labeled with antibodies against EGFP (green arrows) while other neurons were not (red arrows), suggesting

1189 the derivation of EGFP$^{+}$ neurons from the Mesp1-expressing mesoderm. **(e)** No primary control
1190 for the Anti-GFP immunostaining showed very weak EGFP expression in the fixed LM-MP tis-
1191 sue from these animals. Nuclei were labeled with DAPI (blue). Scale bar = 10 μm. Consistent
1192 with the observations made with the tdTomato reporter in this transgenic line, the Mesp1-
1193 cre:*Rosa26*-EGFP animals also show a brighter reporter signal in the vasculature and a dimmer
1194 reporter signal in the myenteric neurons.

1195 **(f)** MHCst$^{+}$ (cyan) labels all tdTomato$^{+}$ (red) HuC/D$^{+}$ (green) adult neurons (white arrows) but
1196 not the tdTomato$^{-}$ neurons (yellow arrow) in the mesoderm-specific Tek-cre:*Hprt*-tdTomato line-
1197 age-traced lines. Nuclei are stained with DAPI (blue). Scale bar = 10 μm.

**Suppl. Figure 3: Validation of MENs-specific markers by immunohistochemistry and confocal microscopy.**

Small intestinal LM-MP from several adult 5-month-old male Wnt1-cre:*Rosa26*-tdTomato mice, where tdTomato-expression (red) labels neural crest-derived cells, was used to ascertain and validate the expression of the novel MENs marker and of known neuronal marker genes.

**(a)** MHCst-specific antibody S46 (green) was found to label tdTomato non-expressing cells within the myenteric ganglia as well as cells outside of the myenteric ganglia. Neural crest-derived cells within the myenteric ganglia expressed tdTomato. Nuclei are labeled with DAPI (blue). Scale bar denotes 10 µm.

The immunostaining of the MENs-markers elucidated through scRNAseq analyses: **(b)** CDH3, **(c)** AEBP1, **(d)** SLPI, **(e)** CFTR, **(f)** NT-3, **(g)** CLIC3, **(h)** FMO2, **(i)** IL-18, **(j)** MYL-7, and **(k)** SLC17A9 (all immunolabeled cells in these panels are green; green arrows) was found to be localized to or enriched in cells without tdTomato expression, while the tdTomato$^{+}$ cells were found to show not to express these MENs-specific markers (red arrow). In addition, we also immunolabeled the myenteric ganglia from this transgenic mouse line with known neuronal markers (gray) and with antibodies against the pan-neuronal marker HuC/D (green) to show that the neuronal markers Elavl2 or HuB **(l)**, GPR88 **(m)**, HAND2 **(n)**, PDE10A **(o)**, TUBB2B **(p)** and VSNL1 **(q)** were expressed by both tdTomato$^{+}$ (red arrow) and tdTomato$^{-}$ HuC/D$^{+}$ neurons. Orthogonal views of images where 3D image z-stacks were obtained are provided for better visualization of marker expression in the 3D space. Nuclei in these tissues were labeled with DAPI (blue). Scale bar denotes 10 µm.

**Suppl. Figure 4: scRNAseq metrics**

**(a)** MENs are significantly larger in size as compared to the NENs, as the mean Feret"s Diameter of the Wnt1-cre:*Rosa26*-tdTomato$^{-}$ MENs is significantly more than that of the Wnt1-cre:tdTomato$^{+}$ NENs. Data presented as mean ± SEM. Student"s t-test; ** p value < 0.01.

**(b, c)** UMAP representation of sequenced cells generated from 10X Genomics Chromium-derived libraries from the two mouse samples, taken from separate littermate adult male mice, shows similar representation of their cells across the various clusters.

**(d)** Quasi-violin plots of expressed genes provide a comparison of important MEN-specific and neuronal genes between the NENs and MENs clusters in the adult ileal May-Zhang et al[56]. dataset and the NENs, Neuroglial, and MENs clusters in our scRNAseq dataset.

**(e)** Top genes that are pattern drivers for the four MEN-specific NMF patterns along with their gene weights.

**(f)** The four MEN-specific patterns were together used to label a group of cells (True) that together showed increased usage of the MEN-specific patterns, when compared to other cell types in the adult ileal snRNAseq dataset from May-Zhang et al.

**(g)** Top-expressed genes in the group of cells **(f)** that showed higher utilization of the MEN-specific patterns, compared to other cells in the dataset.

**(h)** Representation of the four MEN-specific NMF patterns in the UMAP of our data and the projection of the May-Zhang et al murine ileal dataset and the entire gut mesenchymal single cell RNA seq dataset by Elmentaite et al[59] into the MEN-specific patterns highlights cell clusters that show higher usage of the four NMF patterns. Bottom row shows increasing usage of these patterns with age in the entire mesenchymal gut cell atlas data.

**Suppl. Figure 5: Putative mesoderm-derived enteric neurons (MENs) are present in adult human myenteric ganglia.**

**(a, b)** The mesodermal specific markers, MET and MHCst are expressed by a subpopulation of human enteric neurons. Myenteric ganglia from normal duodenal tissue of 3 different adult human subjects express the pan-neuronal marker HuC/D (green), with distinct subpopulations positive and negative for MET (blue) and MHCst (red). MET and MHCst-expressing neurons (red arrows) in the human ENS are assumed to be mesoderm-derived enteric neurons (MENs) and those not expressing these MENs markers (green arrows) are presumably NENs. Nuclei are labeled with DAPI (gray). Scale bar = 10 µm.

**(c)** Distribution of the various mesenchymal clusters of the post-natal healthy gut cell atlas data (generated by Elmentaite et al.[59]) by donor age. For the age of each donor, the proportion of cells annotated as belonging to each cluster is shown. Proportions of Cluster 1 are observed to expand with age.

**Suppl. Figure 6: Sub-clustering MENs in our dataset.**

**(a)** Sub-clustering the MENs cluster from our scRNAseq dataset into 5 distinct clusters **(b)** was found to be not based on the expression of cluster-specific marker genes.

**Suppl. Figure 7: HGF and GDNF ratios in maturing and adult murine gut.**

**(a)** Ratio of HGF:GDNF values in fluorescence intensities of their western blots (normalized to their own house-keeping protein β-Actin) from the small intestinal LM-MP of post-natal mice at different ages during their maturation.

**(b)** Ratio of HGF:GDNF expression values from the full thickness small intestinal tissue of adult mice taken from the Tabula muris database[69].

**(c)** Analyses of human plasma proteome from 1,025 individuals was performed by Sathyan et al.[70] and the correlation of various plasma proteomes with aging was calculated. Of the genes that showed significant correlation with age ($p < 0.05$), we found that the HGF levels in human plasma correlated positively with age (above 0), while the levels of GDNF and RET correlated negatively with age (below 0).

**Suppl. Figure 8: RET-CFP mice and the effect of GDNF treatment on MHCst-expressing MENs and RET-expressing NENs in aging mice**

Representative image of MHCst (red) and HuC/D (green)-immunostained myenteric ganglia of **(a)** saline-treated control and **(b)**. GDNF-treated 17-month-old mice show MHCst$^{+}$ (yellow arrows) and MHCst$^{-}$ neurons. Note the reduction in MHCst-immunostaining on inter-ganglionic fibers in the 17-month-old mice when treated with GDNF, compared to control mice. Nuclei are stained with DAPI (blue). Scale bar indicates 10 µm.

Representative image of RET-immunostained (green) myenteric ganglia of **(c)** saline-treated control and **(d)** GDNF-treated 17-month-old mice. Nuclei are stained with DAPI (blue). Scale bar indicates 10 µm.

**(e)** Western blot image of a 4-20% gel performed using the RET antibody on total protein lysate from small intestinal LM-MP layer from post-natal mice shows the expected band between150 and 250 kDa of RET protein.

**Suppl. Figure 9: Projection of the bulk RNA sequencing data of intestinal tissue from Control and Patients with Obstructed Defecation into our murine scRNAseq-derived NMF patterns using *projectR*.**

Transcriptomic data from intestinal tissues of patients with normal intestinal motility and those with obstructed defecation (OD) was procured from GEO (GSE101968). Non-negative matrix factorization (NMF), as implemented in the R package *NNLM* (https://github.com/linxihui/NNLM), was performed on the murine scRNAseq data using k=50 and default parameters; and cell weights for each pattern were grouped. Using projectR, the log2 expression (log2(rpkm + 1)) from the human bulk RNA sequencing data from control and OD patients were projected into the murine scRNAseq-derived NMF patterns. The mean projection weights from Control and OD groups were tested for statistically significant differences using Students" t tests.

## References


1 Kulkarni, S. *et al.* Advances in Enteric Neurobiology: The "Brain" in the Gut in Health and Disease. *J Neurosci* **38**, 9346-9354, doi:10.1523/JNEUROSCI.1663-18.2018 (2018).

2 Jarret, A. *et al.* Enteric Nervous System-Derived IL-18 Orchestrates Mucosal Barrier Immunity. *Cell* **180**, 50-63 e12, doi:10.1016/j.cell.2019.12.016 (2020).

3 Uesaka, T., Young, H. M., Pachnis, V. & Enomoto, H. Development of the intrinsic and extrinsic innervation of the gut. *Dev Biol* **417**, 158-167, doi:10.1016/j.ydbio.2016.04.016 (2016).

4 Obermayr, F., Hotta, R., Enomoto, H. & Young, H. M. Development and developmental disorders of the enteric nervous system. *Nat Rev Gastroenterol Hepatol* **10**, 43-57, doi:10.1038/nrgastro.2012.234 (2013).

5 Hao, M. M. & Young, H. M. Development of enteric neuron diversity. *J Cell Mol Med* **13**, 1193-1210, doi:10.1111/j.1582-4934.2009.00813.x (2009).

6 Anderson, R. B., Newgreen, D. F. & Young, H. M. Neural crest and the development of the enteric nervous system. *Adv Exp Med Biol* **589**, 181-196, doi:10.1007/978-0-387-46954-6_11 (2006).

7 Young, H. M. & Newgreen, D. Enteric neural crest-derived cells: origin, identification, migration, and differentiation. *Anat Rec* **262**, 1-15, doi:10.1002/1097-0185(20010101)262:1<1::AID-AR1006>3.0.CO;2-2 (2001).

8 Young, H. M., Hearn, C. J. & Newgreen, D. F. Embryology and development of the enteric nervous system. *Gut* **47 Suppl 4**, iv12-14; discussion iv26, doi:10.1136/gut.47.suppl_4.iv12 (2000).

9 Bergner, A. J. *et al.* Birthdating of myenteric neuron subtypes in the small intestine of the mouse. *J Comp Neurol* **522**, 514-527, doi:10.1002/cne.23423 (2014).

10 Uesaka, T., Nagashimada, M. & Enomoto, H. Neuronal Differentiation in Schwann Cell Lineage Underlies Postnatal Neurogenesis in the Enteric Nervous System. *J Neurosci* **35**, 9879-9888, doi:10.1523/JNEUROSCI.1239-15.2015 (2015).

11 Espinosa-Medina, I. *et al.* Dual origin of enteric neurons in vagal Schwann cell precursors and the sympathetic neural crest. *Proc Natl Acad Sci U S A* **114**, 11980-11985, doi:10.1073/pnas.1710308114 (2017).

12 Burns, A. J. Migration of neural crest-derived enteric nervous system precursor cells to and within the gastrointestinal tract. *Int J Dev Biol* **49**, 143-150, doi:10.1387/ijdb.041935ab (2005).

13 Laranjeira, C. *et al.* Glial cells in the mouse enteric nervous system can undergo neurogenesis in response to injury. *J Clin Invest* **121**, 3412-3424, doi:10.1172/JCI58200 (2011).

14 Brokhman, I. *et al.* Dual embryonic origin of the mammalian enteric nervous system. *Dev Biol* **445**, 256-270, doi:10.1016/j.ydbio.2018.11.014 (2019).

15 Sohal, G. S., Ali, M. M. & Farooqui, F. A. A second source of precursor cells for the developing enteric nervous system and interstitial cells of Cajal. *Int J Dev Neurosci* **20**, 619-626 (2002).

16 Habeck, M. VENT cells--a load of hot air? *Drug Discov Today* **8**, 332-333, doi:10.1016/s1359-6446(03)02663-1 (2003).

17 Saffrey, M. J. Cellular changes in the enteric nervous system during ageing. *Dev Biol* **382**, 344-355, doi:10.1016/j.ydbio.2013.03.015 (2013).

18 Becker, L., Kulkarni, S., Tiwari, G., Micci, M. A. & Pasricha, P. J. Divergent fate and origin of neurosphere-like bodies from different layers of the gut. *Am J Physiol Gastrointest Liver Physiol* **302**, G958-965, doi:10.1152/ajpgi.00511.2011 (2012).

19 Kulkarni, S. *et al.* Adult enteric nervous system in health is maintained by a dynamic balance between neuronal apoptosis and neurogenesis. *Proc Natl Acad Sci U S A* **114**, E3709-E3718, doi:10.1073/pnas.1619406114 (2017).

20 Antal, M., Beneduce, B. M. & Regehr, W. G. The substantia nigra conveys target-dependent excitatory and inhibitory outputs from the basal ganglia to the thalamus. *J Neurosci* **34**, 8032-8042, doi:10.1523/JNEUROSCI.0236-14.2014 (2014).

21 Freyer, L., Aggarwal, V. & Morrow, B. E. Dual embryonic origin of the mammalian otic vesicle forming the inner ear. *Development* **138**, 5403-5414, doi:10.1242/dev.069849 (2011).

22 Wright, C. M. *et al.* scRNA-Seq Reveals New Enteric Nervous System Roles for GDNF, NRTN, and TBX3. *Cell Mol Gastroenterol Hepatol* **11**, 1548-1592 e1541, doi:10.1016/j.jcmgh.2020.12.014 (2021).

23 Honig, G., Liou, A., Berger, M., German, M. S. & Tecott, L. H. Precise pattern of recombination in serotonergic and hypothalamic neurons in a Pdx1-cre transgenic mouse line. *J Biomed Sci* **17**, 82, doi:10.1186/1423-0127-17-82 (2010).

24 Bardot, E. *et al.* Foxa2 identifies a cardiac progenitor population with ventricular differentiation potential. *Nat Commun* **8**, 14428, doi:10.1038/ncomms14428 (2017).

25 Burtscher, I., Barkey, W., Schwarzfischer, M., Theis, F. J. & Lickert, H. The Sox17-mCherry fusion mouse line allows visualization of endoderm and vascular endothelial development. *genesis* **50**, 496-505, doi:10.1002/dvg.20829 (2012).

26 Wilm, B., Ipenberg, A., Hastie, N. D., Burch, J. B. & Bader, D. M. The serosal mesothelium is a major source of smooth muscle cells of the gut vasculature. *Development* **132**, 5317-5328, doi:10.1242/dev.02141 (2005).

27 Kawaguchi, M., Bader, D. M. & Wilm, B. Serosal mesothelium retains vasculogenic potential. *Dev Dyn* **236**, 2973-2979, doi:10.1002/dvdy.21334 (2007).

28 Herrick, S. E. & Mutsaers, S. E. Mesothelial progenitor cells and their potential in tissue engineering. *Int J Biochem Cell Biol* **36**, 621-642, doi:10.1016/j.biocel.2003.11.002 (2004).

29 Chan, Sunny S.-K. *et al.* Mesp1 Patterns Mesoderm into Cardiac, Hematopoietic, or Skeletal Myogenic Progenitors in a Context-Dependent Manner. *Cell Stem Cell* **12**, 587-601, doi:10.1016/j.stem.2013.03.004 (2013).

30 Devine, W. P., Wythe, J. D., George, M., Koshiba-Takeuchi, K. & Bruneau, B. G. Early patterning and specification of cardiac progenitors in gastrulating mesoderm. *Elife* **3**, doi:10.7554/eLife.03848 (2014).

31 Lescroart, F. *et al.* Early lineage restriction in temporally distinct populations of Mesp1 progenitors during mammalian heart development. *Nat Cell Biol* **16**, 829-840, doi:10.1038/ncb3024 (2014).

32 Klotz, L. *et al.* Cardiac lymphatics are heterogeneous in origin and respond to injury. *Nature* **522**, 62-67, doi:10.1038/nature14483 (2015).

33 Chan, S. S. *et al.* Mesp1 patterns mesoderm into cardiac, hematopoietic, or skeletal myogenic progenitors in a context-dependent manner. *Cell Stem Cell* **12**, 587-601, doi:10.1016/j.stem.2013.03.004 (2013).

34 Baup, D., Moser, M., Schurmans, S. & Leo, O. Developmental regulation of the composite CAG promoter activity in the murine T lymphocyte cell lineage. *Genesis* **47**, 799-804, doi:10.1002/dvg.20569 (2009).

35 Alexopoulou, A. N., Couchman, J. R. & Whiteford, J. R. The CMV early enhancer/chicken beta actin (CAG) promoter can be used to drive transgene expression during the differentiation of murine embryonic stem cells into vascular progenitors. *BMC Cell Biol* **9**, 2, doi:10.1186/1471-2121-9-2 (2008).

36 Hu, X. *et al.* Reprogramming progressive cells display low CAG promoter activity. *Stem Cells* **39**, 43-54, doi:10.1002/stem.3295 (2021).

37 Akagi, Y. *et al.* Transcriptional activation of a hybrid promoter composed of cytomegalovirus enhancer and beta-actin/beta-globin gene in glomerular epithelial cells in vivo. *Kidney Int* **51**, 1265-1269, doi:10.1038/ki.1997.172 (1997).

38 Agah, R. *et al.* Gene recombination in postmitotic cells. Targeted expression of Cre recombinase provokes cardiac-restricted, site-specific rearrangement in adult ventricular muscle in vivo. *J Clin Invest* **100**, 169-179, doi:10.1172/JCI119509 (1997).

39 Sokoloff, A. J., Li, H. & Burkholder, T. J. Limited expression of slow tonic myosin heavy chain in human cranial muscles. *Muscle Nerve* **36**, 183-189, doi:10.1002/mus.20797 (2007).

40 Stockdale, F. E. & Miller, J. B. The cellular basis of myosin heavy chain isoform expression during development of avian skeletal muscles. *Dev Biol* **123**, 1-9, doi:10.1016/0012-1606(87)90420-9 (1987).

41 Miller, J. B., Crow, M. T. & Stockdale, F. E. Slow and fast myosin heavy chain content defines three types of myotubes in early muscle cell cultures. *J Cell Biol* **101**, 1643-1650, doi:10.1083/jcb.101.5.1643 (1985).

42 Vaughan, S. K., Stanley, O. L. & Valdez, G. Impact of Aging on Proprioceptive Sensory Neurons and Intrafusal Muscle Fibers in Mice. *J Gerontol A Biol Sci Med Sci* **72**, 771-779, doi:10.1093/gerona/glw175 (2017).

43 Avetisyan, M. *et al.* Hepatocyte Growth Factor and MET Support Mouse Enteric Nervous System Development, the Peristaltic Response, and Intestinal Epithelial Proliferation in Response to Injury. *J Neurosci* **35**, 11543-11558, doi:10.1523/JNEUROSCI.5267-14.2015 (2015).

44 Rappolee, D. A., Iyer, A. & Patel, Y. Hepatocyte growth factor and its receptor are expressed in cardiac myocytes during early cardiogenesis. *Circ Res* **78**, 1028-1036, doi:10.1161/01.res.78.6.1028 (1996).

45 Abraira, V. E. *et al.* The Cellular and Synaptic Architecture of the Mechanosensory Dorsal Horn. *Cell* **168**, 295-310 e219, doi:10.1016/j.cell.2016.12.010 (2017).

46 Zeisel, A. *et al.* Molecular Architecture of the Mouse Nervous System. *Cell* **174**, 999-1014 e1022, doi:10.1016/j.cell.2018.06.021 (2018).

47 Drokhlyansky, E. *et al.* The Human and Mouse Enteric Nervous System at Single-Cell Resolution. *Cell* **182**, 1606-1622, doi:10.1016/j.cell.2020.08.00310.1101/746743 (2020).

48 Heanue, T. A. & Pachnis, V. Expression profiling the developing mammalian enteric nervous system identifies marker and candidate Hirschsprung disease genes. *Proceedings of the National Academy of Sciences* **103**, 6919, doi:10.1073/pnas.0602152103 (2006).

49 D'Autreaux, F., Morikawa, Y., Cserjesi, P. & Gershon, M. D. Hand2 is necessary for terminal differentiation of enteric neurons from crest-derived precursors but not for their migration into the gut or for formation of glia. *Development* **134**, 2237-2249, doi:10.1242/dev.003814 (2007).

50 Strick, C. A. *et al.* Alterations in gene regulation following inhibition of the striatum-enriched phosphodiesterase, PDE10A. *Neuropharmacology* **58**, 444-451, doi:10.1016/j.neuropharm.2009.09.008 (2010).

51 Bernstein, H. G. *et al.* Hippocampal expression of the calcium sensor protein visinin-like protein-1 in schizophrenia. *Neuroreport* **13**, 393-396, doi:10.1097/00001756-200203250-00006 (2002).

52 Massart, R., Guilloux, J. P., Mignon, V., Sokoloff, P. & Diaz, J. Striatal GPR88 expression is confined to the whole projection neuron population and is regulated by dopaminergic and glutamatergic afferents. *Eur J Neurosci* **30**, 397-414, doi:10.1111/j.1460-9568.2009.06842.x (2009).

53 Soo Hoo, L. *et al.* The SNARE Protein Syntaxin 3 Confers Specificity for Polarized Axonal Trafficking in Neurons. *PLoS One* **11**, e0163671, doi:10.1371/journal.pone.0163671 (2016).

54 Breuss, M. *et al.* The Expression of Tubb2b Undergoes a Developmental Transition in Murine Cortical Neurons. *J Comp Neurol* **523**, 2161-2186, doi:10.1002/cne.23836 (2015).

55 De Giorgio, R., Arakawa, J., Wetmore, C. J. & Sternini, C. Neurotrophin-3 and neurotrophin receptor immunoreactivity in peptidergic enteric neurons. *Peptides* **21**, 1421-1426, doi:10.1016/s0196-9781(00)00286-2 (2000).

56 May-Zhang, A. A. *et al.* Combinatorial Transcriptional Profiling of Mouse and Human Enteric Neurons Identifies Shared and Disparate Subtypes In Situ. *Gastroenterology*, doi:10.1053/j.gastro.2020.09.032 (2020).

57 Stein-O'Brien, G. L. *et al.* Decomposing Cell Identity for Transfer Learning across Cellular Measurements, Platforms, Tissues, and Species. *Cell Syst* **8**, 395-411 e398, doi:10.1016/j.cels.2019.04.004 (2019).

58 Stein-O'Brien, G. L. *et al.* Enter the Matrix: Factorization Uncovers Knowledge from Omics. *Trends Genet* **34**, 790-805, doi:10.1016/j.tig.2018.07.003 (2018).

59 Elmentaite, R. *et al.* Cells of the human intestinal tract mapped across space and time. *Nature* **597**, 250-255, doi:10.1038/s41586-021-03852-1 (2021).

60 Matheis, F. *et al.* Adrenergic Signaling in Muscularis Macrophages Limits Infection-Induced Neuronal Loss. *Cell* **180**, 64-78 e16, doi:10.1016/j.cell.2019.12.002 (2020).

61 Barrenschee, M. *et al.* SNAP-25 is abundantly expressed in enteric neuronal networks and upregulated by the neurotrophic factor GDNF. *Histochem Cell Biol* **143**, 611-623, doi:10.1007/s00418-015-1310-x (2015).

62 Gianino, S., Grider, J. R., Cresswell, J., Enomoto, H. & Heuckeroth, R. O. GDNF availability determines enteric neuron number by controlling precursor proliferation. *Development* **130**, 2187-2198, doi:10.1242/dev.00433 (2003).
63 Natarajan, D., Marcos-Gutierrez, C., Pachnis, V. & de Graaff, E. Requirement of signalling by receptor tyrosine kinase RET for the directed migration of enteric nervous system progenitor cells during mammalian embryogenesis. *Development* **129**, 5151-5160 (2002).
64 Taraviras, S. *et al.* Signalling by the RET receptor tyrosine kinase and its role in the development of the mammalian enteric nervous system. *Development* **126**, 2785-2797 (1999).
65 Rodrigues, D. M., Li, A. Y., Nair, D. G. & Blennerhassett, M. G. Glial cell line-derived neurotrophic factor is a key neurotrophin in the postnatal enteric nervous system. *Neurogastroenterol Motil* **23**, e44-56, doi:10.1111/j.1365-2982.2010.01626.x (2011).
66 Amano, O. *et al.* Hepatocyte growth factor is essential for migration of myogenic cells and promotes their proliferation during the early periods of tongue morphogenesis in mouse embryos. *Dev Dyn* **223**, 169-179, doi:10.1002/dvdy.1228 (2002).
67 Brun, P. *et al.* Toll-like receptor 2 regulates intestinal inflammation by controlling integrity of the enteric nervous system. *Gastroenterology* **145**, 1323-1333, doi:10.1053/j.gastro.2013.08.047 (2013).
68 Jangphattananont, N. *et al.* Distinct Localization of Mature HGF from its Precursor Form in Developing and Repairing the Stomach. *Int J Mol Sci* **20**, doi:10.3390/ijms20122955 (2019).
69 Almanzar, N. *et al.* A single-cell transcriptomic atlas characterizes ageing tissues in the mouse. *Nature* **583**, 590-595, doi:10.1038/s41586-020-2496-1 (2020).
70 Sathyan, S. *et al.* Plasma proteomic profile of age, health span, and all-cause mortality in older adults. *Aging Cell* **n/a**, e13250, doi:10.1111/acel.13250.
71 Wang, H. *et al.* The timing and location of glial cell line-derived neurotrophic factor expression determine enteric nervous system structure and function. *J Neurosci* **30**, 1523-1538, doi:10.1523/JNEUROSCI.3861-09.2010 (2010).
72 Barrenschee, M. *et al.* No neuronal loss, but alterations of the GDNF system in asymptomatic diverticulosis. *PLoS One* **12**, e0171416, doi:10.1371/journal.pone.0171416 (2017).
73 Rossi, V. *et al.* Chronic intestinal pseudo-obstruction in a child harboring a founder Hirschsprung RET mutation. *Am J Med Genet A* **170**, 2400-2403, doi:10.1002/ajmg.a.37787 (2016).
74 Uesaka, T., Nagashimada, M., Yonemura, S. & Enomoto, H. Diminished Ret expression compromises neuronal survival in the colon and causes intestinal aganglionosis in mice. *J Clin Invest* **118**, 1890-1898, doi:10.1172/JCI34425 (2008).
75 Kim, M. *et al.* Obstructed defecation-an enteric neuropathy? An exploratory study of patient samples. *Int J Colorectal Dis* **34**, 193-196, doi:10.1007/s00384-018-3160-1 (2019).
76 Sun, T. *et al.* Aging-dependent decrease in the numbers of enteric neurons, interstitial cells of Cajal and expression of connexin43 in various regions of gastrointestinal tract. *Aging (Albany NY)* **10**, 3851-3865, doi:10.18632/aging.101677 (2018).

77 Becker, L. *et al.* Age-dependent shift in macrophage polarisation causes inflammation-mediated degeneration of enteric nervous system. *Gut* **67**, 827-836, doi:10.1136/gutjnl-2016-312940 (2018).

78 Sharma, G., Colantuoni, C., Goff, L. A., Fertig, E. J. & Stein-O'Brien, G. projectR: an R/Bioconductor package for transfer learning via PCA, NMF, correlation and clustering. *Bioinformatics* **36**, 3592-3593, doi:10.1093/bioinformatics/btaa183 (2020).

79 Young, H. M. & Newgreen, D. Enteric neural crest-derived cells: Origin, identification, migration, and differentiation. *The Anatomical Record* **262**, 1-15, doi:10.1002/1097-0185(20010101)262:1<1::AID-AR1006>3.0.CO;2-2 (2001).

80 Prummel, K. D., Nieuwenhuize, S. & Mosimann, C. The lateral plate mesoderm. *Development* **147**, dev175059, doi:10.1242/dev.175059 (2020).

81 Xue, R. *et al.* Expression of Cystic Fibrosis Transmembrane Conductance Regulator in Ganglia of Human Gastrointestinal Tract. *Sci Rep* **6**, 30926, doi:10.1038/srep30926 (2016).

82 Morarach, K. *et al.* Diversification of molecularly defined myenteric neuron classes revealed by single cell RNA-sequencing. *bioRxiv*, 2020.2003.2002.955757, doi:10.1101/2020.03.02.955757 (2020).

83 Frassoni, C. *et al.* Analysis of SNAP-25 immunoreactivity in hippocampal inhibitory neurons during development in culture and in situ. *Neuroscience* **131**, 813-823, doi:10.1016/j.neuroscience.2004.11.042 (2005).

84 Wang, W. *et al.* Selective Expression of a SNARE-Cleaving Protease in Peripheral Sensory Neurons Attenuates Pain-Related Gene Transcription and Neuropeptide Release. *Int J Mol Sci* **22**, doi:10.3390/ijms22168826 (2021).

85 Tender, G. C., Kaye, A. D., Li, Y. Y. & Cui, J. G. Neurotrophin-3 and tyrosine kinase C have modulatory effects on neuropathic pain in the rat dorsal root ganglia. *Neurosurgery* **68**, 1048-1055; discussion 1055, doi:10.1227/NEU.0b013e318208f9c4 (2011).

86 de Jonge, H. R., Ardelean, M. C., Bijvelds, M. J. C. & Vergani, P. Strategies for cystic fibrosis transmembrane conductance regulator inhibition: from molecular mechanisms to treatment for secretory diarrhoeas. *FEBS Lett* **594**, 4085-4108, doi:10.1002/1873-3468.13971 (2020).

87 Chaudhury, A., Dendi, V. S. & Mirza, W. Colligative Property of ATP: Implications for Enteric Purinergic Neuromuscular Neurotransmission. *Front Physiol* **7**, 500, doi:10.3389/fphys.2016.00500 (2016).

88 Parathan, P., Wang, Y., Leembruggen, A. J., Bornstein, J. C. & Foong, J. P. The enteric nervous system undergoes significant chemical and synaptic maturation during adolescence in mice. *Dev Biol* **458**, 75-87, doi:10.1016/j.ydbio.2019.10.011 (2020).

89 Golden, J. P., DeMaro, J. A., Osborne, P. A., Milbrandt, J. & Johnson, E. M., Jr. Expression of neurturin, GDNF, and GDNF family-receptor mRNA in the developing and mature mouse. *Exp Neurol* **158**, 504-528, doi:10.1006/exnr.1999.7127 (1999).

90 Papaconstantinou, J. *et al.* Attenuation of p38alpha MAPK stress response signaling delays the in vivo aging of skeletal muscle myofibers and progenitor cells. *Aging (Albany NY)* **7**, 718-733, doi:10.18632/aging.100802 (2015).

91 Soret, R. *et al.* Glial Cell-Derived Neurotrophic Factor Induces Enteric Neurogenesis and Improves Colon Structure and Function in Mouse Models of Hirschsprung Disease. *Gastroenterology* **159**, 1824-1838 e1817, doi:10.1053/j.gastro.2020.07.018 (2020).

92 Grider, J. R., Heuckeroth, R. O., Kuemmerle, J. F. & Murthy, K. S. Augmentation of the ascending component of the peristaltic reflex and substance P release by glial cell line-derived neurotrophic factor. *Neurogastroenterol Motil* **22**, 779-786, doi:10.1111/j.1365-2982.2010.01489.x (2010).

93 Li, J., Zhang, Y., Yang, C. & Rong, R. Discrepant mRNA and Protein Expression in Immune Cells. *Curr Genomics* **21**, 560-563, doi:10.2174/1389202921999200716103758 (2020).

94 Melo, C. G. S. *et al.* Identification of intrinsic primary afferent neurons in mouse jejunum. *Neurogastroenterol Motil* **32**, e13989, doi:10.1111/nmo.13989 (2020).

95 Saffrey, M. J. Aging of the mammalian gastrointestinal tract: a complex organ system. *Age (Dordr)* **36**, 9603, doi:10.1007/s11357-013-9603-2 (2014).

96 Cossais, F. *et al.* Altered enteric expression of the homeobox transcription factor Phox2b in patients with diverticular disease. *United European Gastroenterology Journal* **7**, 349-357, doi:10.1177/2050640618824913 (2019).

97 Schafmayer, C. *et al.* Genome-wide association analysis of diverticular disease points towards neuromuscular, connective tissue and epithelial pathomechanisms. *Gut* **68**, 854, doi:10.1136/gutjnl-2018-317619 (2019).

98 Muller, P. A. *et al.* Microbiota-modulated CART(+) enteric neurons autonomously regulate blood glucose. *Science* **370**, 314-321, doi:10.1126/science.abd6176 (2020).

99 Becker, L., Kulkarni, S., Tiwari, G., Micci, M.-A. & Pasricha, P. J. Divergent fate and origin of neurosphere-like bodies from different layers of the gut. *American Journal of Physiology-Gastrointestinal and Liver Physiology* **302**, G958-G965, doi:10.1152/ajpgi.00511.2011 (2012).

100 Becker, L., Peterson, J., Kulkarni, S. & Pasricha, P. J. Ex vivo neurogenesis within enteric ganglia occurs in a PTEN dependent manner. *PLoS One* **8**, e59452 (2013).

101 Becker, L., Peterson, J., Kulkarni, S. & Pasricha, P. J. Ex vivo neurogenesis within enteric ganglia occurs in a PTEN dependent manner. *PLoS One* **8**, e59452, doi:10.1371/journal.pone.0059452 (2013).

102 Drokhlyansky, E. *et al.* The Human and Mouse Enteric Nervous System at Single-Cell Resolution. *Cell* **182**, 1606-1622 e1623, doi:10.1016/j.cell.2020.08.003 (2020).

103 Shenje, L. T. *et al.* Precardiac deletion of Numb and Numblike reveals renewal of cardiac progenitors. *Elife* **3**, e02164, doi:10.7554/eLife.02164 (2014).

104 Susaki, E. A. *et al.* Whole-brain imaging with single-cell resolution using chemical cocktails and computational analysis. *Cell* **157**, 726-739, doi:10.1016/j.cell.2014.03.042 (2014).

105 Young, H. M., Furness, J. B., Sewell, P., Burcher, E. F. & Kandiah, C. J. Total numbers of neurons in myenteric ganglia of the guinea-pig small intestine. *Cell Tissue Res* **272**, 197-200, doi:10.1007/BF00323587 (1993).

106 Zhou, Y. *et al.* Enteric nervous system abnormalities are present in human necrotizing enterocolitis: potential neurotransplantation therapy. *Stem Cell Res Ther* **4**, 157, doi:10.1186/scrt387 (2013).

107 Hosie, S. *et al.* Gastrointestinal dysfunction in patients and mice expressing the autism-associated R451C mutation in neuroligin-3. *Autism Res* **12**, 1043-1056, doi:10.1002/aur.2127 (2019).

108 Lefevre, C. *et al.* Enteric Nervous System Remodeling in a Rat Model of Spinal Cord Injury: A Pilot Study. *Neurotrauma Rep* **1**, 125-136, doi:10.1089/neur.2020.0041 (2020).

109 Qiu, X. *et al.* NEDL2 regulates enteric nervous system and kidney development in its Nedd8 ligase activity-dependent manner. *Oncotarget* **7**, 31440-31453, doi:10.18632/oncotarget.8951 (2016).

110 Bray, N. L., Pimentel, H., Melsted, P. & Pachter, L. Near-optimal probabilistic RNA-seq quantification. *Nat Biotechnol* **34**, 525-527, doi:10.1038/nbt.3519 (2016).

111 Haghverdi, L., Lun, A. T. L., Morgan, M. D. & Marioni, J. C. Batch effects in single-cell RNA-sequencing data are corrected by matching mutual nearest neighbors. *Nat Biotechnol* **36**, 421-427, doi:10.1038/nbt.4091 (2018).

112 Gu, Z., Eils, R. & Schlesner, M. Complex heatmaps reveal patterns and correlations in multidimensional genomic data. *Bioinformatics* **32**, 2847-2849, doi:10.1093/bioinformatics/btw313 (2016).

113 Lun, A. T. L. *et al.* EmptyDrops: distinguishing cells from empty droplets in droplet-based single-cell RNA sequencing data. *Genome Biol* **20**, 63, doi:10.1186/s13059-019-1662-y (2019).

114 Griffiths, J. A., Richard, A. C., Bach, K., Lun, A. T. L. & Marioni, J. C. Detection and removal of barcode swapping in single-cell RNA-seq data. *Nat Commun* **9**, 2667, doi:10.1038/s41467-018-05083-x (2018).

115 Lun, A. T., McCarthy, D. J. & Marioni, J. C. A step-by-step workflow for low-level analysis of single-cell RNA-seq data with Bioconductor. *F1000Res* **5**, 2122, doi:10.12688/f1000research.9501.2 (2016).

116 McCarthy, D. J., Campbell, K. R., Lun, A. T. & Wills, Q. F. Scater: pre-processing, quality control, normalization and visualization of single-cell RNA-seq data in R. *Bioinformatics* **33**, 1179-1186, doi:10.1093/bioinformatics/btw777 (2017).

117 Csárdi, G. & Nepusz, T.

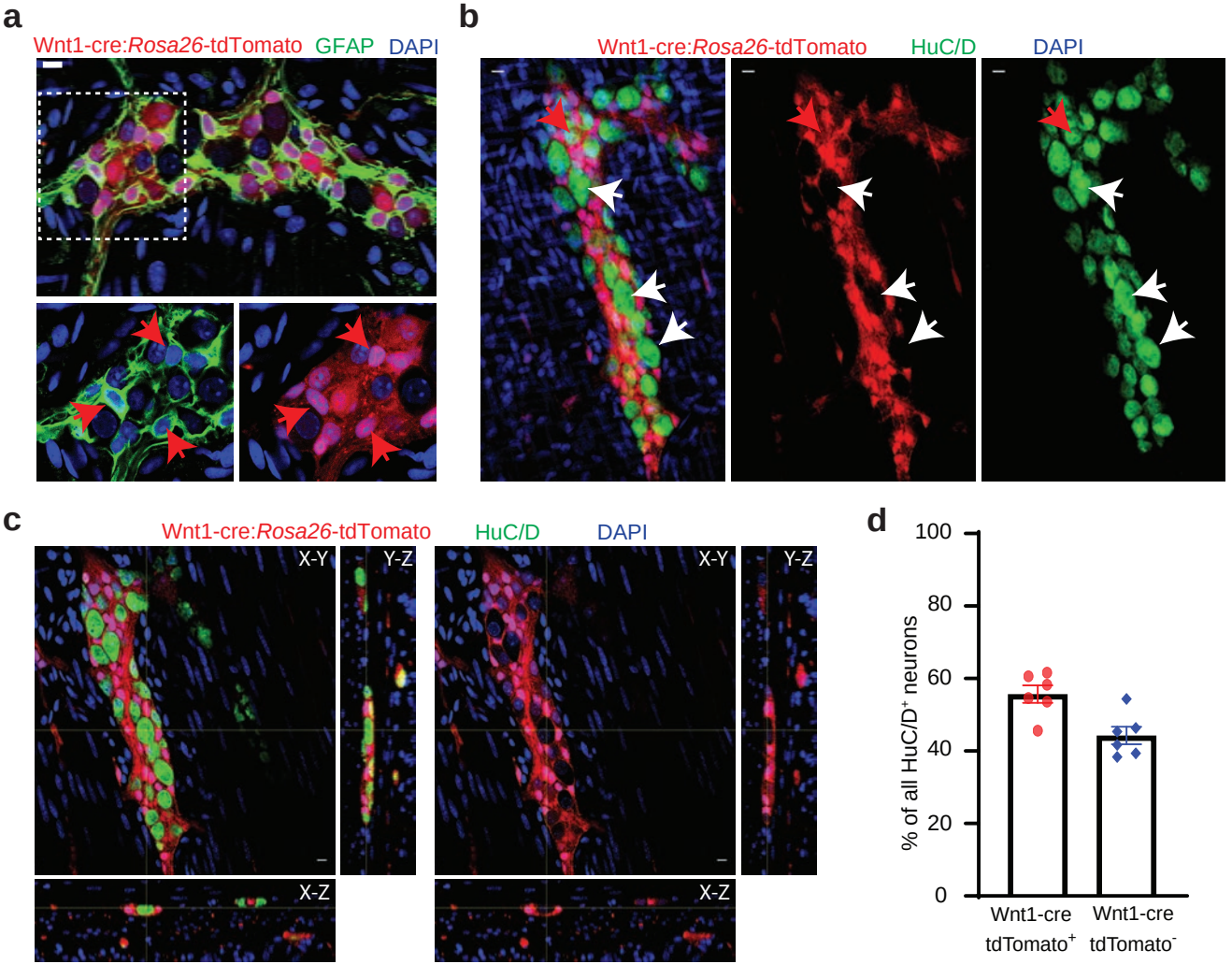
a
Wnt1-cre:Rosa26-tdTomato
GFAP
DAPI
b
Wnt1-cre:Rosa26-tdTomato
HuC/D
DAPI
c
Wnt1-cre:Rosa26-tdTomato
HuC/D
DAPI
X-Y
Y-Z
X-Z
d
% of all HuC/D+ neurons
100
80
60
40
20
0
Wnt1-cre tdTomato+
Wnt1-cre tdTomato-

Figure 1

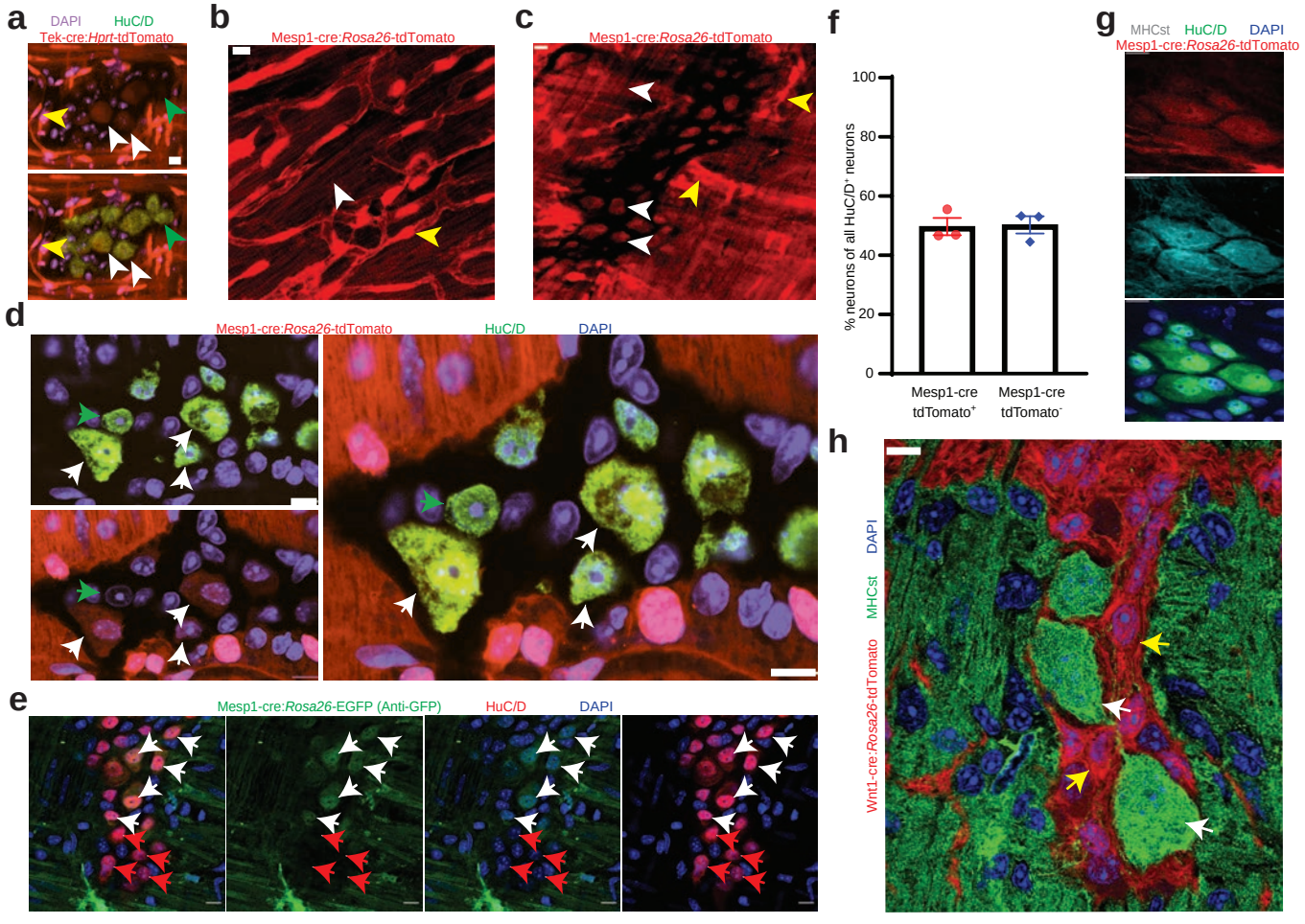
a
DAPI
HuC/D
Tek-cre:Hprt-tdTomato
b
Mesp1-cre:Rosa26-tdTomato
c
Mesp1-cre:Rosa26-tdTomato
d
Mesp1-cre:Rosa26-tdTomato
HuC/D
DAPI
e
Mesp1-cre:Rosa26-EGFP (Anti-GFP)
HuC/D
DAPI
f
% neurons of all HuC/D+ neurons
100
80
60
40
20
0
Mesp1-cre tdTomato+
Mesp1-cre tdTomato-
g
MHCst
HuC/D
DAPI
Mesp1-cre:Rosa26-tdTomato
h
DAPI
MHCst
Wnt1-cre:Rosa26-tdTomato

Figure 2

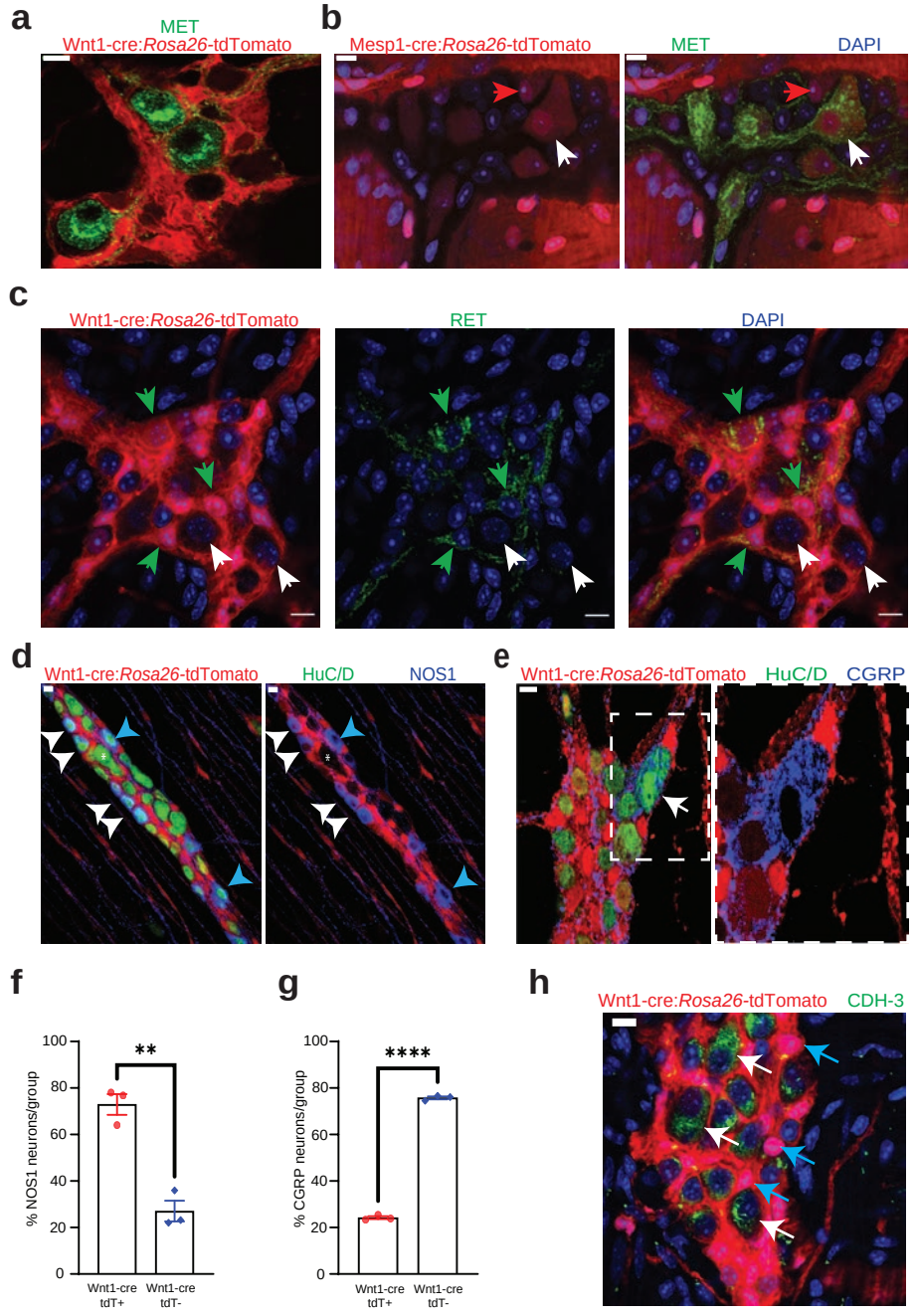
a
MET
Wnt1-cre:Rosa26-tdTomato
b
Mesp1-cre:Rosa26-tdTomato
MET
DAPI
c
Wnt1-cre:Rosa26-tdTomato
RET
DAPI
d
Wnt1-cre:Rosa26-tdTomato
HuC/D
NOS1
e
Wnt1-cre:Rosa26-tdTomato
HuC/D
CGRP
f
% NOS1 neurons/group
100
80
60
40
20
0
**
Wnt1-cre tdT+
Wnt1-cre tdT-
g
% CGRP neurons/group
100
80
60
40
20
0
****
Wnt1-cre tdT+
Wnt1-cre tdT-
h
Wnt1-cre:Rosa26-tdTomato
CDH-3

Figure 3

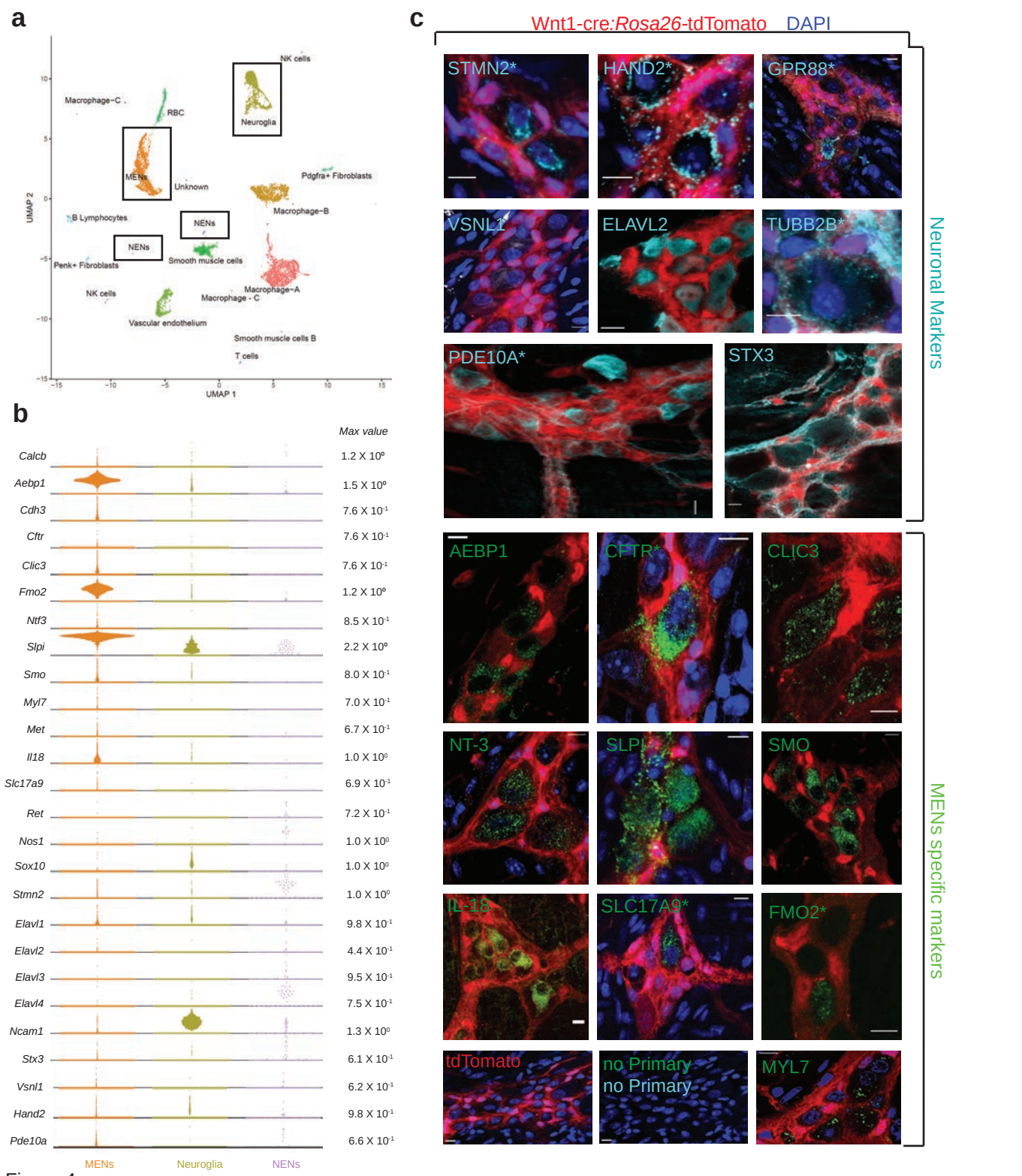
a
NK cells
Macrophage−C
RBC
Neuroglia
MENs
Unknown
Pdgfra+ Fibroblasts
Macrophage−B
B Lymphocytes
NENs
NENs
Penk+ Fibroblasts
Smooth muscle cells
NK cells
Macrophage−A
Macrophage - C
Vascular endothelium
Smooth muscle cells B
T cells
UMAP 2
UMAP 1
b
Max value
Calcb 1.2 X 10⁰
Aebp1 1.5 X 10⁰
Cdh3 7.6 X 10⁻¹
Cftr 7.6 X 10⁻¹
Clic3 7.6 X 10⁻¹
Fmo2 1.2 X 10⁰
Ntf3 8.5 X 10⁻¹
Slpi 2.2 X 10⁰
Smo 8.0 X 10⁻¹
Myl7 7.0 X 10⁻¹
Met 6.7 X 10⁻¹
Il18 1.0 X 10⁰
Slc17a9 6.9 X 10⁻¹
Ret 7.2 X 10⁻¹
Nos1 1.0 X 10⁰
Sox10 1.0 X 10⁰
Stmn2 1.0 X 10⁰
Elavl1 9.8 X 10⁻¹
Elavl2 4.4 X 10⁻¹
Elavl3 9.5 X 10⁻¹
Elavl4 7.5 X 10⁻¹
Ncam1 1.3 X 10⁰
Stx3 6.1 X 10⁻¹
Vsnl1 6.2 X 10⁻¹
Hand2 9.8 X 10⁻¹
Pde10a 6.6 X 10⁻¹
MENs
Neuroglia
NENs
c
Wnt1-cre:Rosa26-tdTomato DAPI
STMN2*
HAND2*
GPR88*
VSNL1
ELAVL2
TUBB2B*
PDE10A*
STX3
Neuronal Markers
AEBP1
CFTR*
CLIC3
NT-3
SLPI
SMO
IL-18
SLC17A9*
FMO2*
tdTomato
no Primary
no Primary
MYL7
MENs specific markers

Figure 4

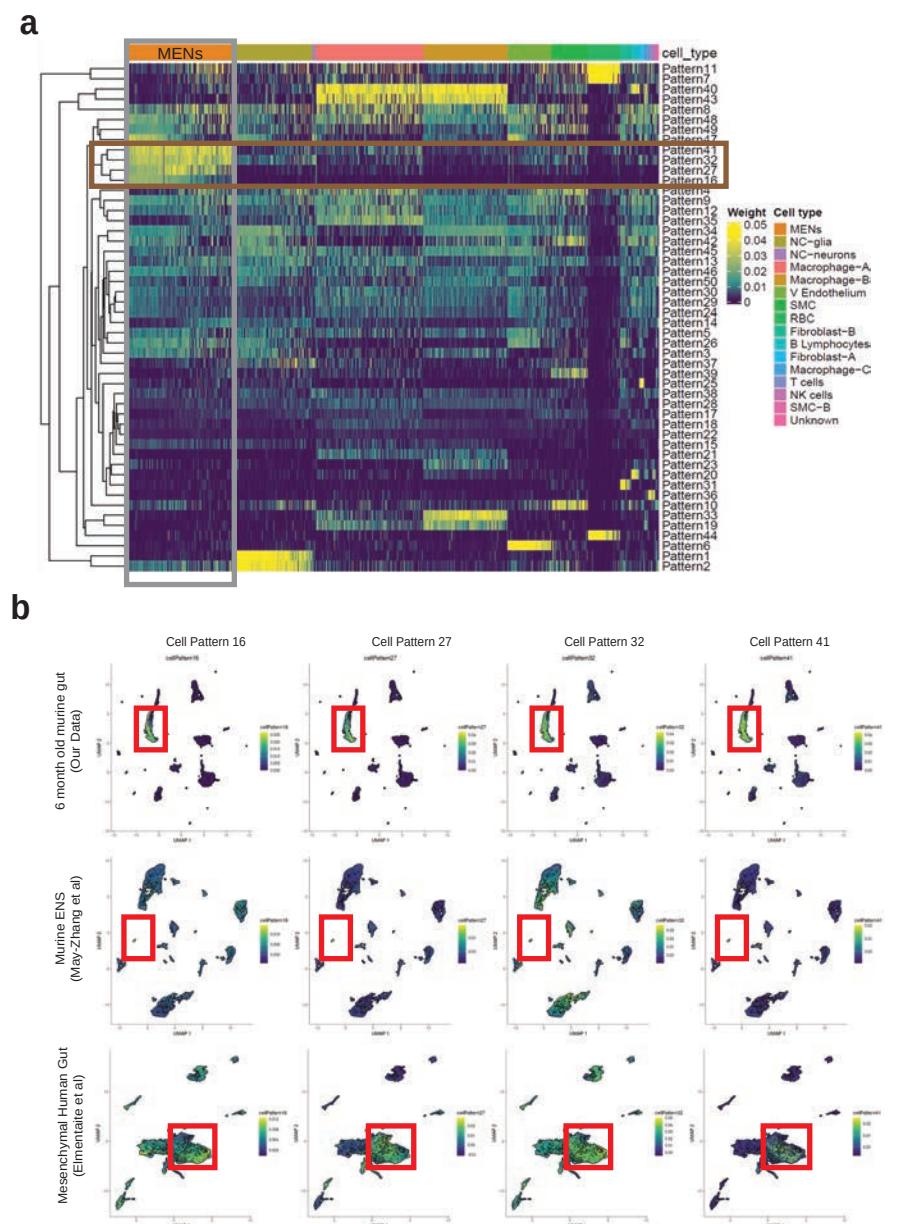
a
MENs
cell_type
Pattern11
Pattern7
Pattern40
Pattern43
Pattern8
Pattern48
Pattern49
Pattern41
Pattern32
Pattern27
Pattern16
Pattern4
Pattern9
Pattern12
Pattern35
Pattern34
Pattern42
Pattern45
Pattern13
Pattern46
Pattern50
Pattern30
Pattern29
Pattern24
Pattern14
Pattern5
Pattern26
Pattern3
Pattern37
Pattern39
Pattern25
Pattern38
Pattern28
Pattern17
Pattern18
Pattern22
Pattern15
Pattern21
Pattern23
Pattern20
Pattern31
Pattern36
Pattern10
Pattern33
Pattern19
Pattern44
Pattern6
Pattern1
Pattern2
Weight
0.05
0.04
0.03
0.02
0.01
0
Cell type
MENs
NC−glia
NC−neurons
Macrophage−A
Macrophage−B
V Endothelium
SMC
RBC
Fibroblast−B
B Lymphocytes
Fibroblast−A
Macrophage−C
T cells
NK cells
SMC−B
Unknown
b
Cell Pattern 16
Cell Pattern 27
Cell Pattern 32
Cell Pattern 41
6 month old murine gut
(Our Data)
Murine ENS
(May-Zhang et al)
Mesenchymal Human Gut
(Elmentaite et al)

Figure 5

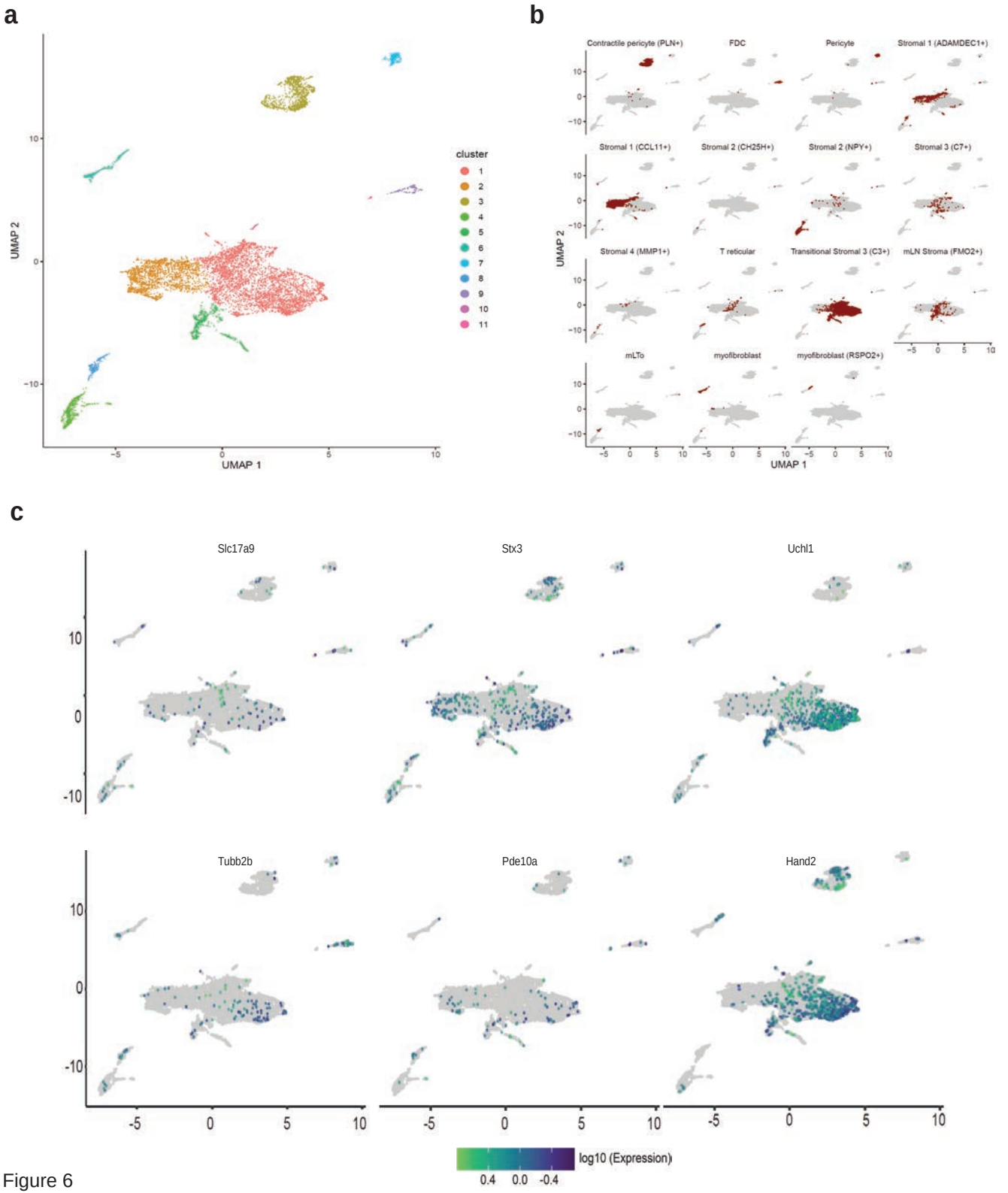
a
UMAP 2
UMAP 1
cluster
1
2
3
4
5
6
7
8
9
10
11
b
Contractile pericyte (PLN+)
FDC
Pericyte
Stromal 1 (ADAMDEC1+)
Stromal 1 (CCL11+)
Stromal 2 (CH25H+)
Stromal 2 (NPY+)
Stromal 3 (C7+)
Stromal 4 (MMP1+)
T reticular
Transitional Stromal 3 (C3+)
mLN Stroma (FMO2+)
mLTo
myofibroblast
myofibroblast (RSPO2+)
UMAP 2
UMAP 1
c
Slc17a9
Stx3
Uchl1
Tubb2b
Pde10a
Hand2
log10 (Expression)
0.4
0.0
-0.4

Figure 6

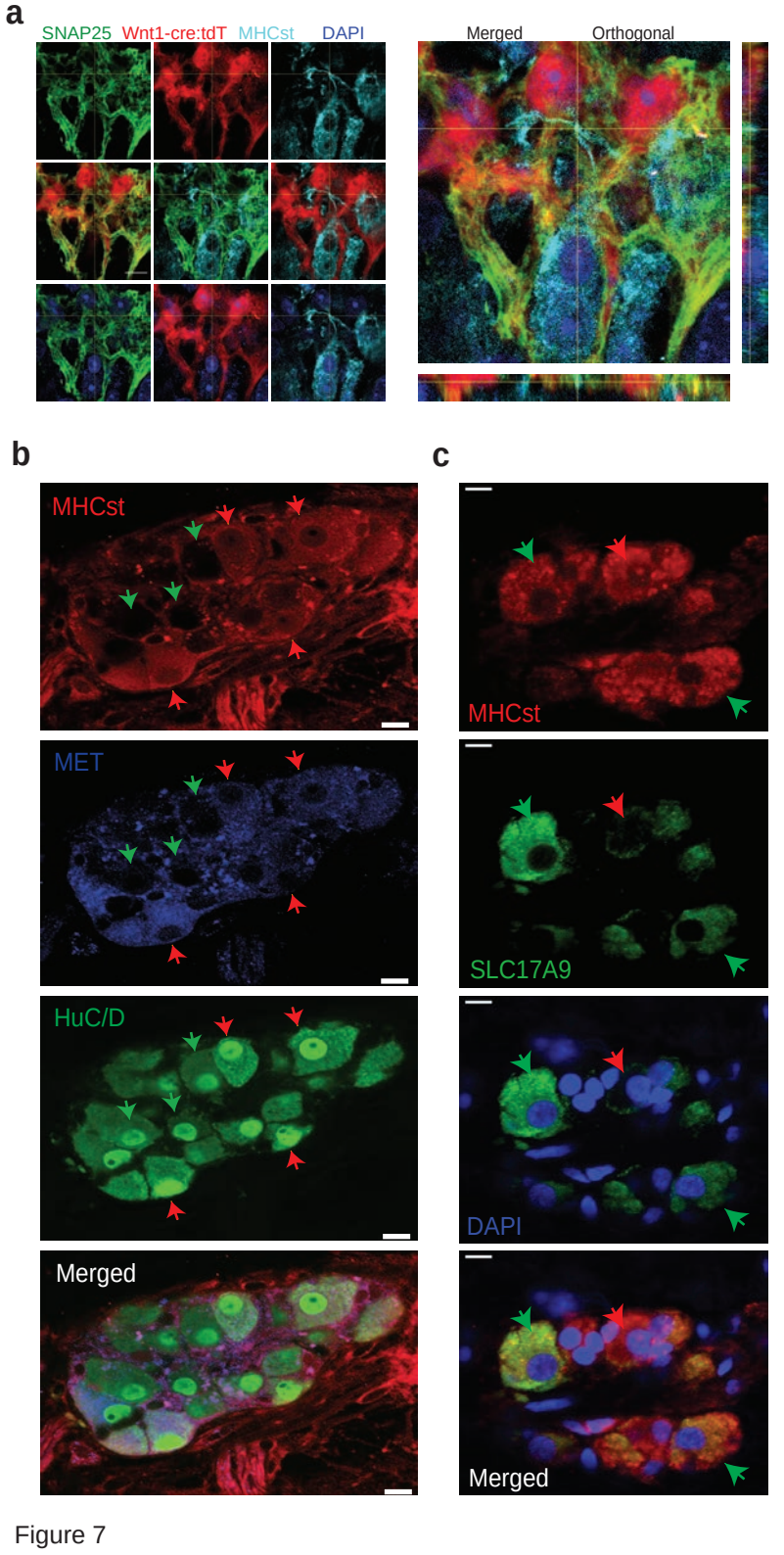
a
SNAP25
Wnt1-cre:tdT
MHCst
DAPI
Merged
Orthogonal
b
MHCst
MET
HuC/D
Merged
c
MHCst
SLC17A9
DAPI
Merged

Figure 7

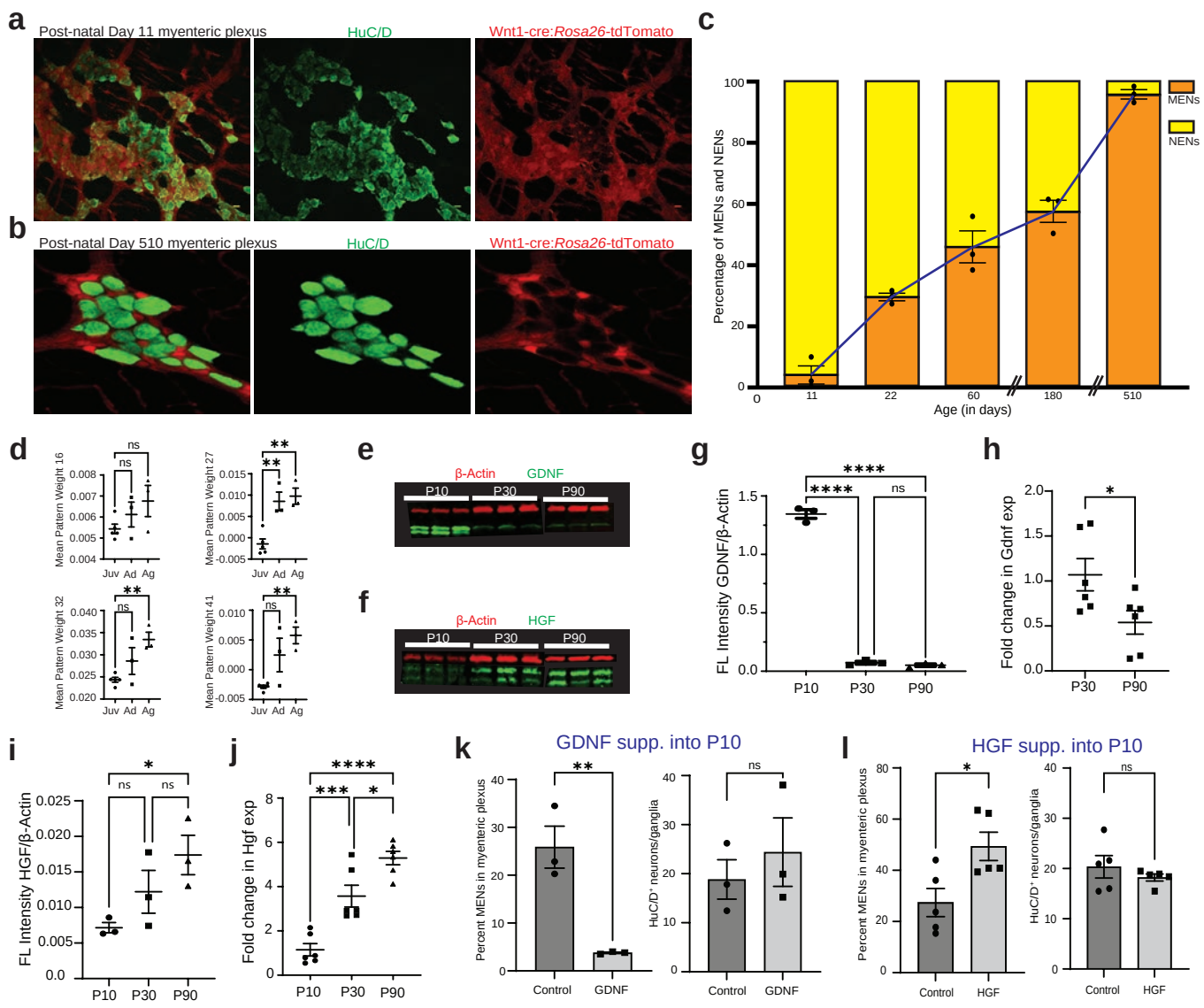
a
Post-natal Day 11 myenteric plexus
HuC/D
Wnt1-cre:Rosa26-tdTomato
b
Post-natal Day 510 myenteric plexus
HuC/D
Wnt1-cre:Rosa26-tdTomato
c
Percentage of MENs and NENs
Age (in days)
MENs
NENs
d
Mean Pattern Weight 16
Mean Pattern Weight 27
Mean Pattern Weight 32
Mean Pattern Weight 41
Juv Ad Ag
e
β-Actin GDNF
P10 P30 P90
f
β-Actin HGF
P10 P30 P90
g
FL Intensity GDNF/β-Actin
P10 P30 P90
h
Fold change in Gdnf exp
P30 P90
i
FL Intensity HGF/β-Actin
P10 P30 P90
j
Fold change in Hgf exp
P10 P30 P90
k
GDNF supp. into P10
Percent MENs in myenteric plexus
HuC/D+ neurons/ganglia
Control GDNF
l
HGF supp. into P10
Percent MENs in myenteric plexus
HuC/D+ neurons/ganglia
Control HGF

Figure 8

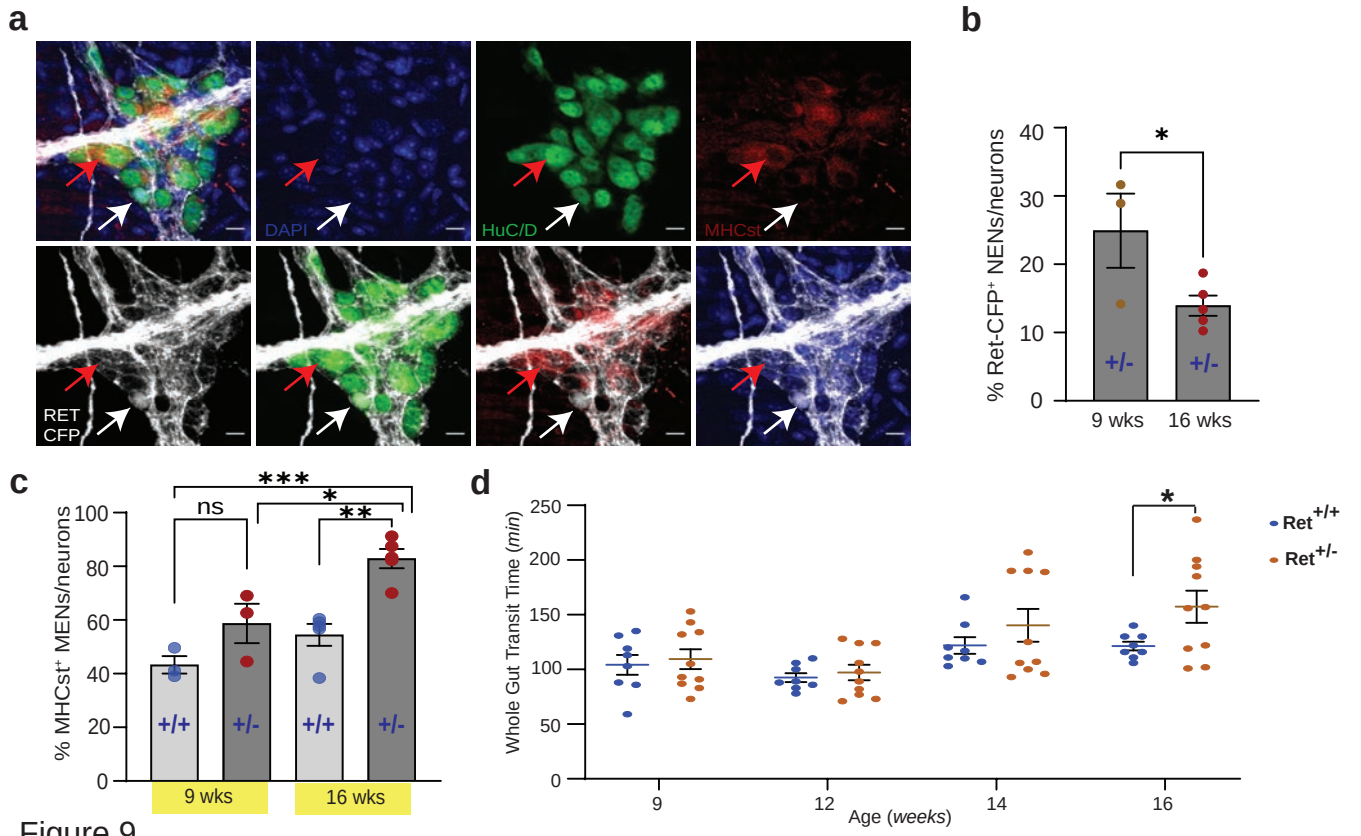
a
DAPI
HuC/D
MHCst
RET
CFP
b
% Ret-CFP+ NENs/neurons
40
30
20
10
0
*
+/-
+/-
9 wks
16 wks
c
% MHCst+ MENs/neurons
100
80
60
40
20
0
***
ns
*
**
+/+
+/-
+/+
+/-
9 wks
16 wks
d
Whole Gut Transit Time (min)
250
200
150
100
50
0
*
Ret+/+
Ret+/-
9
12
14
16
Age (weeks)

Figure 9

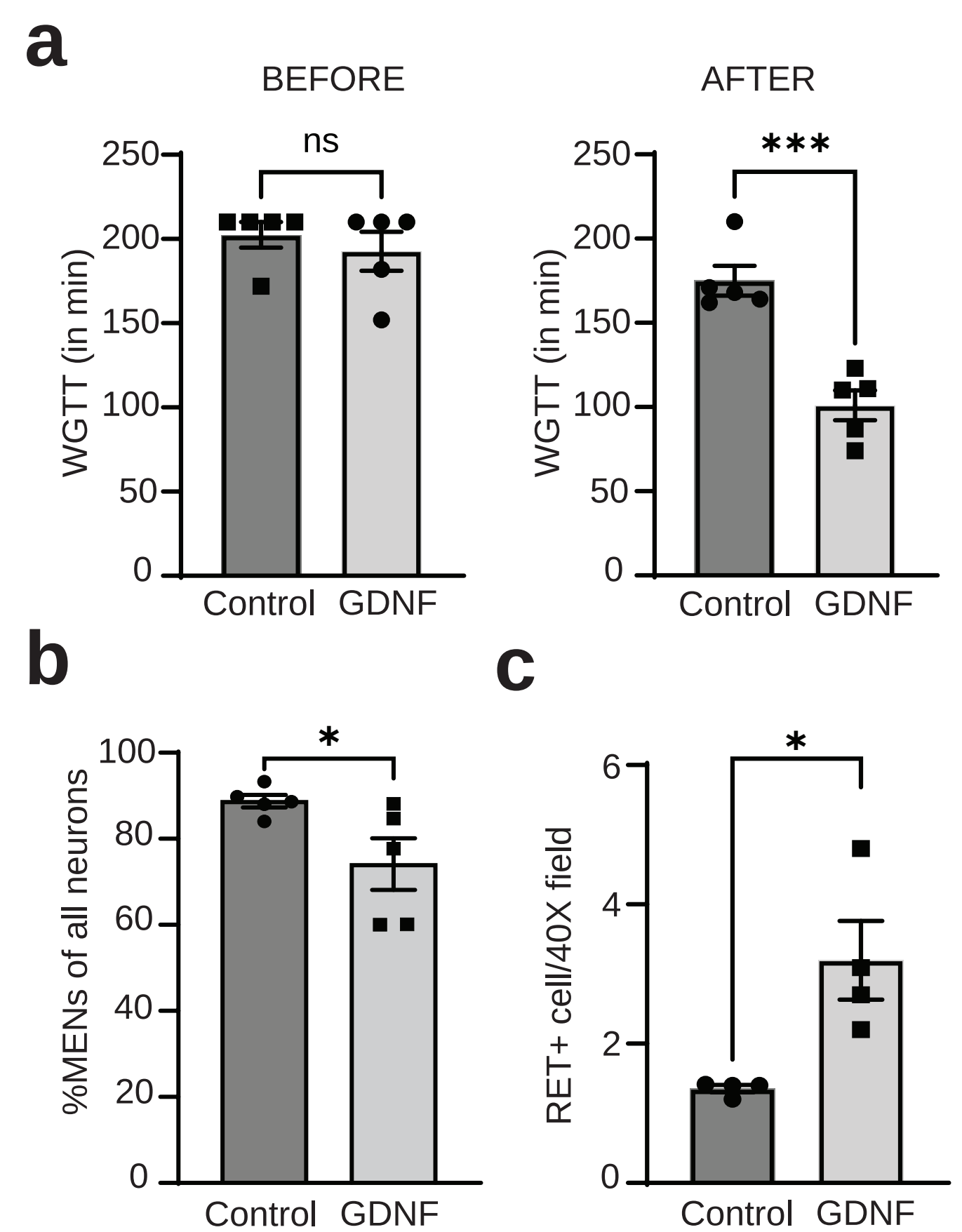
a
BEFORE
AFTER
ns
***
WGTT (in min)
250
200
150
100
50
0
Control
GDNF
b
%MENs of all neurons
100
80
60
40
20
0
*
c
RET+ cell/40X field
6
4
2
0
*

# Figure 10

**a**

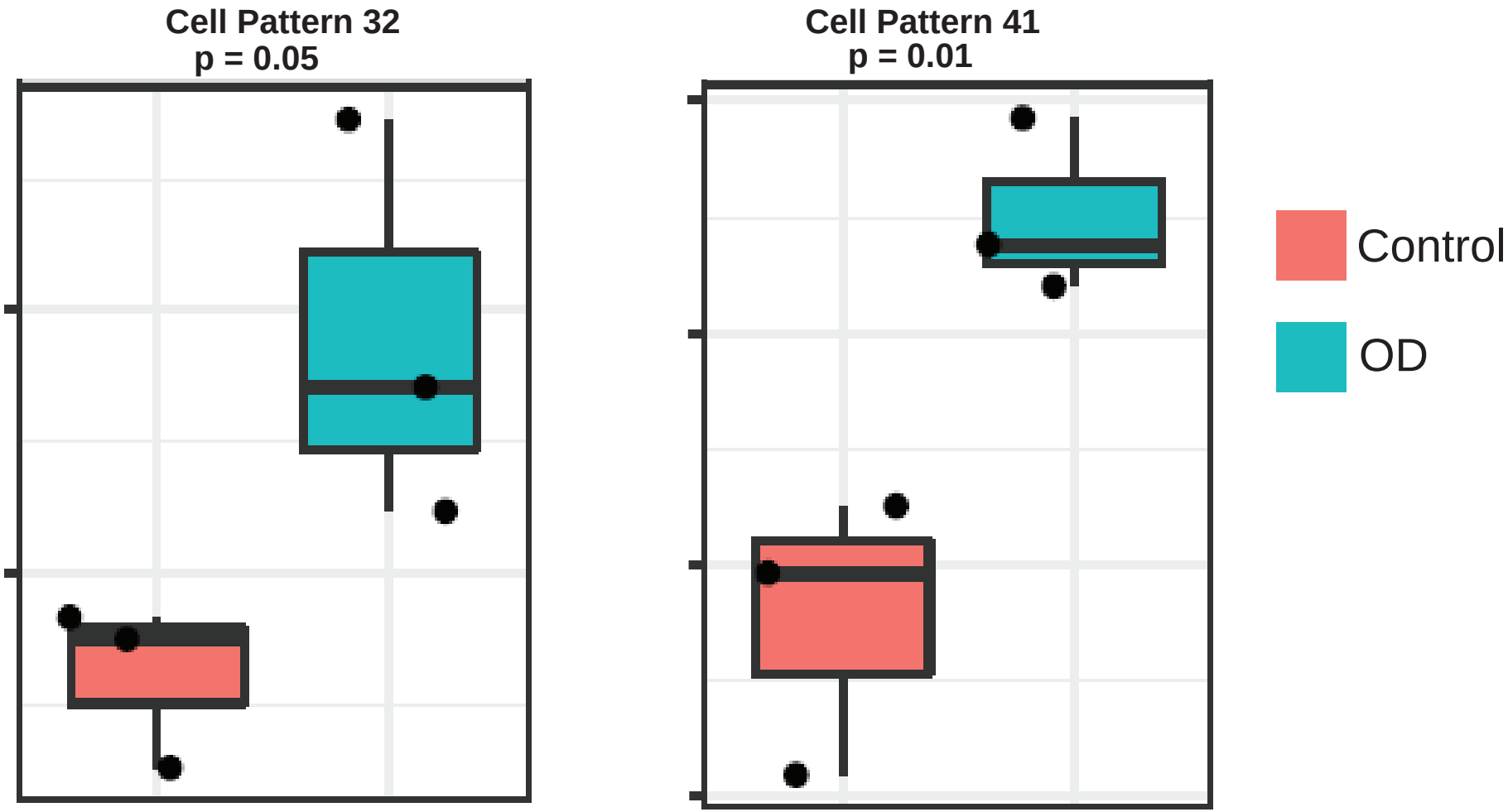


**b**

| HGNC Symbol | Direction | Gene type | Description | Coding | Mean RC | log FC | P-value | Adj. P-value |
|---|---|---|---|---|---|---|---|---|
| SNAP25 | Reduced in OD | protein_coding | synaptosomal-associated protein, 25kDa [Source:HGNC Symbol;Acc:11132] | yes | 419 | -3.56 | 2.68E-15 | 1.25E-12 |
| KLHL1 | Reduced in OD | protein_coding | kelch-like family member 1 [Source:HGNC Symbol;Acc:6352] | yes | 5 | -2.92 | 2.43E-06 | 7.07E-05 |
| NOS1 | Reduced in OD | protein_coding | nitric oxide synthase 1 (neuronal) [Source:HGNC Symbol;Acc:7872] | yes | 775 | -2.91 | 3.29E-06 | 9.06E-05 |
| CHAT | Reduced in OD | protein_coding | choline O-acetyltransferase [Source:HGNC Symbol;Acc:1912] | yes | 17 | -2.78 | 2.00E-07 | 9.34E-06 |
| GDNF | Reduced in OD | protein_coding | glial cell derived neurotrophic factor [Source:HGNC Symbol;Acc:4232] | yes | 649 | -2.75 | 2.27E-10 | 2.98E-08 |
| RET | Reduced in OD | protein_coding | ret proto-oncogene [Source:HGNC Symbol;Acc:9967] | yes | 474 | -2.59 | 6.38E-18 | 5.29E-15 |
| CLIC3 | Increased in OD | protein_coding | chloride intracellular channel 3 [Source:HGNC Symbol;Acc:2064] | yes | 98 | 2.95 | 1.74E-12 | 4.54E-10 |
| UPK3A | Increased in OD | protein_coding | uroplakin 3A [Source:HGNC Symbol;Acc:12580] | yes | 49 | 2.93 | 1.47E-06 | 4.68E-05 |
| CDH3 | Increased in OD | protein_coding | cadherin 3, type 1, P-cadherin (placental) [Source:HGNC Symbol;Acc:1762] | yes | 252 | 2.66 | 9.87E-06 | 2.20E-04 |
| SLPI | Increased in OD | protein_coding | secretory leukocyte peptidase inhibitor [Source:HGNC Symbol;Acc:11092] | yes | 1,924 | 2.56 | 9.84E-06 | 2.20E-04 |
| SLC17A9 | Increased in OD | protein_coding | solute carrier family 17 (Vesicular nucleotide transporter). [Source: HGNC] | yes | 1,997 | 2.15 | 9.67E-06 | 2.17E-07 |

Figure 11

**Table 1:** Top expressed genes by the Calcb-expressing clusters and the putative MENs cluster in data from May-Zhang et al, along with top-expressed genes in the MENs cluster in our data. Highlighted genes between MENs clusters from our data and data from May-Zhang et al show similar gene expression profiles between the two clusters.

**Calcb+ cluster corresponding to Ileum cluster in May-Zhang et al. which expresses Calcb, Calb2, Nmu, Pcdh10, Cysltr2**

| Gene | FDR | summary.logFC |
|---|---|---|
| Zfp804a | 0 | 5.314372906 |
| Pcdh10 | 0 | 2.727131014 |
| Gpr149 | 0 | 2.928565459 |
| Necab1 | 0 | 3.126115371 |
| Grin3a | 0 | 2.477871618 |
| Fam19a1 | 0 | 4.658451729 |
| Ano2 | 0 | 3.443066822 |
| Ntrk3 | 0 | 4.380099903 |
| Cntn5 | 0 | 6.308342607 |
| Ccbe1 | 0 | 3.076522552 |
| Zbtb7c | 0 | 2.656109043 |
| Astn2 | 0 | 3.366649926 |
| Dapk2 | 0 | 1.703870376 |
| Nrxn3 | 0 | 5.160806272 |
| Dgkg | 0 | 4.15397884 |
| Galr1 | 0 | 1.673088209 |
| Nmu | 0 | 3.521779106 |
| Hspb8 | 1.42E-236 | 1.244433448 |
| Cpne4 | 0 | 4.163433255 |
| Tmeff2 | 0 | 3.49539549 |
| Myl1 | 0 | 3.653772641 |
| Calcb | 0 | 3.200679451 |
| Cysltr2 | 0 | 2.487957211 |
| Clstn2 | 0 | 2.655215539 |
| Robo1 | 1.98E-297 | 1.9960685 |
| Hunk | 0 | 1.918886092 |
| Snhg11 | 0 | 2.098574269 |
| Aff2 | 0 | 2.087576143 |
| Otud7a | 3.38E-263 | 2.545208984 |
| Pcdh9 | 0 | 4.216229123 |
| Htr3b | 0 | 1.553388667 |
| Scn11a | 0 | 1.908976823 |
| Iqgap2 | 0 | 1.75599309 |
| Rbfox1 | 0 | 4.70241843 |
| Tcf7l2 | 0 | 2.84136652 |
| Tbx2 | 0 | 1.871954414 |
| Robo2 | 0 | 4.088780154 |
| Kcnt2 | 0 | 3.926721104 |
| Srrm4 | 2.23E-261 | 2.303709088 |
| Plxna4 | 0 | 3.31892195 |
| Sgcz | 0 | 4.739595343 |
| 9530059O14 | 0 | 3.600146025 |
| Sox4 | 7.89E-259 | 1.211156367 |
| Hcn1 | 8.40016528 | 1.861283774 |
| Scube1 | 0 | 2.077291022 |
| Boc | 5.82E-199 | 0.854637195 |
| Cbln2 | 0 | 2.229769856 |
| Kcnn3 | 0 | 1.899022238 |
| Rph3a | 0 | 1.741082515 |
| Cpne8 | 0 | 2.360533782 |
| Calcrl | 1.12695240 | 1.788279732 |
| Lingo2 | 0 | 4.714175039 |
| Slc4a4 | 0 | 2.575716085 |
| Cux2 | 0 | 2.614397251 |
| Chat | 1.62E-252 | 1.075493057 |
| Htr3a | 0 | 1.82434275 |
| Hs3st2 | 1.18369186 | 1.564650584 |
| Cdh8 | 0.00E+00 | 2.544193879 |
| Gm45881 | 0 | 2.045509731 |
| Cdh6 | 0 | 2.996825969 |
| Gm21847 | 9.83E-301 | 2.668713923 |
| Frmd4b | 0 | 2.260822381 |
| Ndrg4 | 5.28E-172 | 1.033574626 |
| Efr3a | 0 | 2.922824682 |
| Syt2 | 0 | 1.996197662 |
| Pak7 | 2.65E-280 | 1.50563649 |
| Lhfpl2 | 0 | 1.681014338 |
| Adgrg6 | 0 | 3.290333725 |
| Spock3 | 0 | 3.61350554 |
| Smad6 | 3.00E-194 | 0.829179685 |
| Zeb2 | 1.58E-304 | 2.305509194 |
| Hs3st5 | 0 | 2.356357004 |
| Kcnh1 | 1.71E-232 | 1.145753317 |
| Scn9a | 0 | 1.985971133 |
| Ppp3ca | 0 | 2.635476275 |
| Agrn | 0 | 2.149338255 |
| Cntnap2 | 0 | 3.976062671 |
| Ngfr | 0 | 2.251817207 |
| Tnr | 0 | 2.255094218 |
| Mcf2l | 6.65E-174 | 0.813444301 |
| Kcnb2 | 0 | 4.170860912 |
| Gpr85 | 0 | 1.49922453 |
| Nell1 | 0 | 2.464621478 |
| Arhgef3 | 0 | 1.961289599 |
| Syt15 | 3.73E-275 | 1.216092892 |
| Lsamp | 7.25E-253 | 2.548136091 |
| 5330434G04 | 4.84E-185 | 2.358912068 |
| Ptger3 | 1.23E-256 | 1.370213397 |
| 1700111E14 | 4.26E-258 | 1.561674061 |
| Mgat4c | 0 | 3.086139006 |
| Fgf14 | 0 | 3.456636428 |
| Mafg | 2.98E-74 | 1.352690002 |
| Kif26b | 0 | 2.174461286 |
| Plppr5 | 1.60E-265 | 1.61715395 |
| Srrm3 | 5.65E-165 | 1.711562875 |
| Hmbox1 | 7.78E-79 | 0.6148506 |
| Rbfox3 | 1.95E-259 | 1.230611205 |
| Ncam2 | 0 | 2.906633451 |
| Slc8a1 | 0 | 2.937485628 |

**Calcb+ cluster corresponding to Ileum cluster in May-Zhang et al. which expresses Calcb, Calb2, Sst**

| Gene | FDR | summary.logFC |
|---|---|---|
| Nlgn1 | 1.56E-227 | 4.503778932 |
| Plxna4 | 5.40E-170 | 3.513261638 |
| Pcdh15 | 6.75E-269 | 4.552606891 |
| Nrg3 | 9.23E-246 | 4.051012028 |
| Eml6 | 1.02E-166 | 3.739252675 |
| Ryr2 | 4.15E-122 | 2.724692337 |
| Nrxn3 | 1.20E-156 | 4.845162261 |
| Rbfox1 | 0.00E+00 | 4.833341666 |
| Sst | 6.45E-135 | 5.862426929 |
| Chsy3 | 4.53E-122 | 3.602794203 |
| Gria2 | 3.32E-126 | 3.083755369 |
| Ptprd | 3.17E-139 | 2.906173926 |
| Pde4b | 3.69E-210 | 3.947198917 |
| Fam19a2 | 8.41E-100 | 3.227261386 |
| Mdga2 | 2.01E-132 | 3.667573403 |
| Snhg11 | 6.24E-112 | 4.344115315 |
| Ralyl | 1.59E-128 | 3.809356707 |
| Bnc2 | 1.58E-137 | 3.131344621 |
| Robo1 | 8.43E-84 | 2.405353602 |
| Nrxn1 | 1.51E-150 | 4.662080188 |
| Pcsk2 | 5.79E-169 | 3.258681935 |
| Syn2 | 1.17E-132 | 3.619085064 |
| Ntrk3 | 1.05E-108 | 2.657539356 |
| Scube1 | 1.03E-95 | 2.265338351 |
| Man2a1 | 9.20E-139 | 3.375536511 |
| Kcnn2 | 7.39E-85 | 2.418320757 |
| Fam19a1 | 1.79E-147 | 3.622699285 |
| Nell1 | 3.21E-100 | 2.793128177 |
| Galntl6 | 1.72E-109 | 3.815091788 |
| Sgcd | 5.24E-120 | 2.88253651 |
| Pde4d | 1.18E-97 | 2.285404689 |
| Slc8a1 | 1.08E-180 | 3.289543486 |
| Tcf4 | 1.52E-159 | 2.592805317 |
| Pak3 | 2.89E-91 | 2.580345128 |
| Kcnma1 | 1.27E-136 | 2.945051283 |
| Adgrb3 | 5.63E-143 | 4.396153392 |
| Unc5c | 2.09E-114 | 3.291001111 |
| Cpne4 | 4.42E-81 | 2.730862875 |
| Meg3 | 7.04E-124 | 4.308953415 |
| Snap25 | 4.22E-135 | 3.917101813 |
| Syt1 | 7.05E-140 | 4.346683131 |
| Grik4 | 8.53E-115 | 2.35016852 |
| Ptprn2 | 1.75E-115 | 3.282060606 |
| Arhgap26 | 1.46E-133 | 2.381300441 |
| Bcl2 | 1.53E-91 | 2.27434062 |
| Ppm1h | 6.46E-139 | 3.466729684 |
| Fgf14 | 3.30E-126 | 4.330212767 |
| Gm12216 | 9.54E-78 | 1.937925878 |
| Camk2a | 1.73E-88 | 2.352765766 |
| Fgf13 | 5.32E-123 | 3.932808506 |
| Ppp3ca | 1.96E-101 | 2.03501536 |
| Adamts9 | 1.24E-60 | 1.993937158 |
| Calcb | 4.08E-76 | 2.288867891 |
| Pcbp3 | 1.17E-136 | 3.893280923 |
| Dlgap2 | 1.21E-96 | 2.470978745 |
| Nkain2 | 1.01E-107 | 2.761261609 |
| Chat | 2.41E-66 | 1.619335139 |
| Gfra2 | 4.04E-106 | 2.379843878 |
| Pde10a | 7.37E-115 | 2.924056301 |
| Ptprr | 1.01E-130 | 3.346248491 |
| Plod2 | 7.61E-111 | 2.338515945 |
| Hs6st3 | 2.71E-78 | 3.027568338 |
| Rbms3 | 2.24E-117 | 1.826125797 |
| Ccbe1 | 2.81E-69 | 1.972703173 |
| Trpm3 | 3.63E-112 | 3.250658339 |
| Frmd4a | 4.22E-106 | 3.509014084 |
| Galnt17 | 5.29E-90 | 2.14675017 |
| Itpr1 | 1.09E-85 | 2.066072139 |
| Srrm4 | 1.17E-82 | 2.302220849 |
| Slc7a14 | 2.27E-93 | 2.415887276 |
| Sema6d | 4.44E-99 | 2.246929266 |
| Pcdh7 | 8.46E-105 | 3.303407952 |
| Nwd2 | 6.48E-47 | 1.597139988 |
| Slit3 | 2.09E-90 | 2.828190275 |
| Asic2 | 3.26E-63 | 3.678490279 |
| Stxbp5l | 1.22E-98 | 2.855884955 |
| Smarca2 | 2.65E-97 | 2.286413106 |
| Ptprt | 3.14E-93 | 2.816471863 |
| Dpyd | 1.72E-91 | 3.059193551 |
| Tln2 | 1.49E-97 | 2.183191767 |
| Satb2 | 1.74E-60 | 2.016803391 |
| Tshz2 | 5.54E-95 | 2.764995869 |
| Plcxd3 | 4.17E-89 | 2.590078205 |
| Tcf7l2 | 1.76E-95 | 2.141154837 |
| Caln1 | 9.30E-64 | 2.04008457 |
| Dgki | 6.15E-121 | 3.238923425 |
| Syt17 | 5.83E-76 | 1.809205079 |
| 9530059O14 | 5.05E-74 | 2.430525524 |
| Unc79 | 7.38E-102 | 2.530692527 |
| Pvt1 | 8.90E-90 | 2.163637608 |
| Mirg | 4.73E-63 | 1.711809423 |
| Ret | 1.04E-68 | 1.699484732 |
| Nrg1 | 5.72E-62 | 3.678288908 |
| Myt1l | 1.56E-120 | 3.008757293 |
| Mapk10 | 9.27E-117 | 2.871225578 |
| Gm15398 | 4.78E-73 | 2.683512094 |
| Arhgef28 | 5.64E-99 | 2.170007537 |
| Zbtb20 | 6.81E-94 | 1.566902687 |
| Dscam | 2.70E-101 | 2.808126988 |

**MENs-like cluster corresponding to Ileum cluster in May-Zhang et al. which expresses Upk3b and Igfbp6**

| Gene | FDR | summary.logFC |
|---|---|---|
| Abi1 | 4.98E-36 | 3.316005072 |
| Dcn | 2.08E-52 | 5.091738535 |
| Col3a1 | 7.95E-31 | 3.039859427 |
| C3 | 1.11E-38 | 4.827731701 |
| Slpi | 2.75E-31 | 4.598725251 |
| Lrrn4 | 7.45E-21 | 2.797813295 |
| S100a6 | 9.36E-29 | 3.230324987 |
| Upk3b | 1.90E-26 | 3.101085936 |
| Gpm6a | 1.13E-24 | 3.730157809 |
| Sparc | 1.37E-28 | 3.316214748 |
| Meg3 | 3.89E-23 | 2.952545493 |
| Igfbp6 | 4.99E-26 | 3.61531349 |
| Agap1 | 4.03E-21 | 2.507795342 |
| Pbx1 | 4.47E-25 | 2.530783608 |
| Efemp1 | 2.67E-22 | 2.915648257 |
| Gas6 | 2.54E-20 | 2.742900314 |
| Muc16 | 2.43E-21 | 3.168081514 |
| Gas1 | 2.13E-23 | 2.708510446 |
| Dpp4 | 4.03E-21 | 2.876742349 |
| Cobll1 | 1.10E-20 | 2.231586143 |
| Rarres2 | 1.64E-20 | 3.226437143 |
| Myo1d | 6.05E-21 | 2.158327438 |
| Tbce | 1.69E-12 | 3.139158995 |
| Il6st | 6.05E-21 | 2.339891442 |
| Nfib | 7.62E-23 | 2.57202827 |
| Crip1 | 7.17E-19 | 2.764477578 |
| Sema5a | 1.97E-19 | 2.852546212 |
| Fmo2 | 1.80E-18 | 3.253371192 |
| Ezr | 2.84E-20 | 2.166036039 |
| Ahnak | 6.05E-21 | 2.714253195 |
| Bnc2 | 6.54E-20 | 3.061680372 |
| Krt19 | 6.15E-20 | 2.380492921 |
| Crim1 | 3.00E-20 | 2.434254471 |
| Plxna4 | 2.07E-19 | 2.707560817 |
| Sox6 | 3.93E-19 | 2.803585619 |
| Aebp1 | 1.57E-19 | 2.548178022 |
| Cfh | 9.08E-18 | 2.422456138 |
| Col1a1 | 2.72E-13 | 2.033502612 |
| Wt1 | 2.03E-17 | 2.196826568 |
| Ccdc171 | 1.09E-14 | 2.022034827 |
| Cd2ap | 2.30E-18 | 2.290803108 |
| Arhgap29 | 3.72E-18 | 2.409211927 |
| Ano1 | 2.38E-18 | 3.039709984 |
| Col1a2 | 5.02E-13 | 2.132928671 |
| Cav1 | 5.10E-18 | 2.235452113 |
| Bicc1 | 2.27E-19 | 2.486459956 |
| Msln | 2.26E-14 | 1.829701191 |
| Dlc1 | 1.57E-18 | 2.561801087 |
| Upk1b | 1.96E-17 | 1.970013811 |
| Sulf1 | 3.39E-17 | 2.542517734 |
| Vim | 1.68E-16 | 2.45290991 |
| Sema3c | 1.17E-17 | 2.547300887 |
| Ifitm3 | 6.57E-15 | 2.071790767 |
| Rspo1 | 1.96E-17 | 1.964755911 |
| Aldh1a2 | 4.16E-15 | 2.160694165 |
| Serping1 | 4.91E-14 | 2.101997058 |
| Timp2 | 8.53E-10 | 1.596556868 |
| Sdc4 | 9.47E-13 | 1.640281568 |
| Cd34 | 2.04E-10 | 1.324668078 |
| Serpinh1 | 2.72E-11 | 1.617681506 |
| Heg1 | 1.56E-17 | 1.795303412 |
| Arhgap18 | 1.69E-15 | 2.494302228 |
| Igfbp7 | 3.27E-15 | 2.01497489 |
| Wdr17 | 9.82E-15 | 3.265554301 |
| Anxa2 | 1.55E-16 | 1.783316817 |
| Celf2 | 8.01E-17 | 2.016354207 |
| Slc4a4 | 2.64E-14 | 2.058956296 |
| Mast4 | 7.11E-16 | 2.591248418 |
| Bcam | 3.45E-09 | 1.453472527 |
| Cobl | 3.19E-14 | 2.113252622 |
| Airn | 1.00E-16 | 2.159009448 |
| Rbbp8 | 1.25E-07 | 1.460802144 |
| Piezo2 | 6.47E-15 | 2.155464659 |
| Wls | 8.02E-16 | 1.68899014 |
| Pcolce | 2.35E-09 | 1.299424275 |
| Prkg1 | 6.92E-15 | 2.705845188 |
| Syne2 | 1.79E-15 | 2.085470282 |
| Zfpm2 | 7.87E-15 | 2.689571135 |
| Adamtsl1 | 1.19E-15 | 2.937092165 |
| Gm26809 | 0.0001518 | 1.800107543 |
| Chst4 | 1.09E-13 | 1.534679673 |
| Ctdspl | 1.02E-13 | 1.587097481 |
| Ptgis | 1.96E-10 | 1.436656186 |
| Kcnab1 | 4.33E-13 | 2.347466136 |
| Nav2 | 2.26E-14 | 2.852022736 |
| C1ra | 6.88E-07 | 1.318506858 |
| Wnt5a | 4.94E-12 | 1.540387353 |
| Dab2 | 2.15E-13 | 1.86057873 |
| Ankrd12 | 0.0001106 | 1.841901593 |
| Cavin2 | 6.09E-12 | 1.976778556 |
| Rnase4 | 1.39E-11 | 1.688218465 |
| Meis1 | 1.26E-13 | 1.908870378 |
| Anxa1 | 1.86E-12 | 1.531275304 |
| Ildr2 | 9.47E-13 | 1.550620875 |
| Slc9a3r1 | 1.86E-10 | 1.325162783 |
| 9530026P05 | 2.17E-13 | 2.515612487 |
| Man1a | 3.13E-12 | 1.539400492 |
| Gpc3 | 1.20E-12 | 1.790707073 |
| Col14a1 | 3.60E-11 | 2.039467045 |

**MENs Cluster (Our Data)**

| Gene | FDR | summary.logFC |
|---|---|---|
| Bcam | 0 | 1.310889756 |
| Mgst1 | 0 | 1.466554292 |
| Krt18 | 1.02E-252 | 0.722876212 |
| Igfbp6 | 0 | 4.277079428 |
| Rspo1 | 0 | 1.356888212 |
| Gpm6a | 0 | 2.007236002 |
| Upk3b | 0 | 2.136663175 |
| Aebp1 | 0 | 2.502295384 |
| Dcn | 0 | 4.082052904 |
| Slpi | 0 | 4.928306229 |
| Rarres2 | 0 | 4.202866323 |
| Efemp1 | 0 | 1.672848073 |
| Aldh1a2 | 4.60E-277 | 0.796263425 |
| Fmo2 | 0 | 1.582315372 |
| Upk1b | 0 | 1.081912196 |
| Gas1 | 0 | 1.464482623 |
| Krt7 | 0 | 1.315380677 |
| Crip1 | 0 | 4.56883561 |
| Clu | 0 | 1.502811937 |
| C3 | 0 | 3.494711523 |
| Dpp4 | 1.12E-210 | 0.556370013 |
| Lrrn4 | 1.58E-271 | 0.736486954 |
| Nkain4 | 0 | 1.298360281 |
| S100a6 | 0 | 4.128650316 |
| Krt19 | 0 | 1.900927424 |
| Cfb | 8.74E-203 | 0.608707666 |
| Gabarapl1 | 5.26E-250 | 0.709728291 |
| Lgals3 | 0 | 1.26072921 |
| Krt8 | 1.39E-245 | 0.689105423 |
| Tm4sf1 | 0 | 1.367716307 |
| Slc39a8 | 7.17E-197 | 0.489802511 |
| Sema3c | 2.63E-255 | 0.71554962 |
| Pcolce | 0 | 1.823133603 |
| Gsta4 | 1.09E-226 | 0.62733526 |
| Ezr | 0 | 1.019712533 |
| Cldn15 | 4.76E-291 | 0.798661223 |
| Serpinb6b | 2.66E-212 | 0.562587863 |
| Nbl1 | 0 | 1.239754358 |
| Slc16a1 | 2.28E-244 | 0.65901005 |
| Smim1 | 2.76E-245 | 0.659125894 |
| Snhg18 | 3.11E-181 | 0.475288967 |
| Cavin3 | 6.15E-293 | 0.855731534 |
| Gpc3 | 0 | 1.393181642 |
| Serpinb1a | 3.54E-178 | 0.472277374 |
| Chst4 | 3.42E-232 | 0.599828027 |
| Esam | 1.50E-188 | 0.47512383 |
| Ptgis | 5.59E-231 | 0.598750529 |
| Slc9a3r1 | 7.03E-265 | 0.883988091 |
| Ecm1 | 1.88E-172 | 0.514360839 |
| Igfbp7 | 0 | 2.347561986 |
| Msln | 0 | 2.266588157 |
| Gpx3 | 0 | 2.209730215 |
| Col14a1 | 1.17E-163 | 0.423875564 |
| Anxa1 | 4.24E-246 | 0.691007825 |
| Bace2 | 7.94E-223 | 0.603024779 |
| Cfh | 0 | 1.190621234 |
| Tmem176a | 1.85E-170 | 0.915766916 |
| Tmsb10 | 0 | 2.299200297 |
| Timp2 | 0 | 1.918063461 |
| Pdpn | 2.36E-252 | 0.846386263 |
| Prss23 | 0 | 0.980677037 |
| Cd151 | 2.85E-279 | 0.795276372 |
| P3h4 | 8.94E-212 | 0.512747523 |
| Cd200 | 0 | 0.975177086 |
| Ltbp4 | 1.80E-268 | 0.859534481 |
| Gstt1 | 2.26E-142 | 0.347320974 |
| Ssbp3 | 1.42903506 | 0.888557965 |
| Tmem98 | 3.90E-240 | 0.62900078 |
| Spint2 | 1.42E-186 | 0.478143896 |
| Nupr1 | 3.42E-226 | 0.705142527 |
| Basp1 | 6.06E-239 | 0.625848924 |
| C1ra | 2.06E-263 | 0.752700756 |
| Serpinh1 | 4.94065645 | 1.065045464 |
| Adamts2 | 9.08E-129 | 0.322228993 |
| Dmkn | 3.43E-187 | 0.652807485 |
| C1s1 | 2.25E-276 | 0.820741368 |
| Sparc | 0 | 1.954167099 |
| Espn | 3.75E-166 | 0.392816171 |
| Anxa2 | 0 | 1.579365041 |
| Krt14 | 6.29E-117 | 0.368125408 |
| Sdc4 | 0 | 1.913582811 |
| Serping1 | 0 | 1.802367854 |
| Pmp22 | 5.43E-232 | 0.6401978 |
| Cplx2 | 1.77E-251 | 0.917909984 |
| Il18 | 6.70E-154 | 0.396176068 |
| Il6st | 1.73E-262 | 0.71225818 |
| Meg3 | 1.02E-173 | 0.558817278 |
| Cald1 | 2.88E-262 | 0.803200156 |
| Mt2 | 1.37E-218 | 0.736087263 |
| Nenf | 7.12E-165 | 0.869917467 |
| Col6a1 | 2.61E-252 | 0.693856752 |
| Rnase4 | 0.00E+00 | 1.162670662 |
| Vim | 0 | 1.805718628 |
| F11r | 6.92E-219 | 0.535570277 |
| Fam180a | 2.29E-131 | 0.294690768 |
| Npdc1 | 2.34E-164 | 0.415479342 |
| Cd2ap | 2.16E-225 | 0.595177252 |
| Pamr1 | 3.15E-177 | 0.443000918 |
| Stk26 | 4.71E-112 | 0.258746973 |